BEHAVIOR OF A COUPLED ARCH SYSTEM

by

Tzu-Yang Yu

B.S. Department of Construction Engineering
National Yunlin University of Science and Technology 1996
M.S. Department of Civil Engineering
National Central University 1998

Submitted to the Department of Civil and Environmental Engineering in Partial Fulfillment of the Requirements for the Degree of

MASTER OF ENGINEERING IN CIVIL AND ENVIRONMENTAL ENGINEERING

at the

MASSACHUSETTS INSTITUTE OF TECHNOLOGY

June 2002

Signature of Author:_____
Tzu-Yang Yu
Department of Civil and Environmental Engineering
May 10, 2002

Certified by:_____
Jerome J. Connor
Professor, Department of Civil and Environmental Engineering
Thesis Supervisor

Accepted by:_____
Oral Buyukozturk
Chairman, Departmental Committee on Graduate Study

BEHAVIOR OF A COUPLED ARCH SYSTEM

Tzu-Yang Yu

Submitted to the Department of Civil and Environmental Engineering
On May 15, 2002 in partial fulfillment of the requirements for the degree of
Master of Engineering in Civil and Environmental Engineering

Abstract

The arch is one of the most frequently used structures in civil engineering. By taking advantage of its shape, engineers can establish a system that allows the utilization of the space below it. A space arch system has been proposed. It consists of two space parabolic arches leaning toward each other with brace members between them. A pair of leaning arches is more stable than a single arch because of the additional lateral stiffness due to the geometrical orientation. An investigation of the behavior is performed through numerical analysis using the finite element method (FEM). Several characteristic parameters are defined and investigated to find their influence on the load-carrying capacity of the system. The buckling behavior of the system is also discussed.

Keywords: Parabolic arch, pair of leaning arches, brace member, finite element method, buckling, stability.

Thesis Supervisor: Dr. Jerome J. Connor
Title: Professor, Department of Civil and Environmental Engineering

Acknowledgements

I would like to express my gratitude to my advisor Professor Jerome J. Connor for his guidance and encouragement. Professor Connor is always available for questions and very dedicated to his students. His advice also inspires me on solving problems.

I would also like to thank Lisa Grebner for her useful suggestion to the thesis.

I would like to thank many of my classmates for their warm and true friendship: Marc, Jason, Luca, Neeraj, Koji, and Chin-Huei.

Finally, I want to dedicate this thesis to my family and my girl friend, San-San. Their support and encouragement motivate my study at MIT.

Table of Contents

Symbols and Abbreviations

Symbols

a	Distance of twin arch ribs
$\hat{a}$	Reciprocal of α
$\overline{b}$	Mean hourly wind speed factor
$\hat{b}$	3-second gust speed factor
A	Area of cross section
A_0	Total area of openings in a wall that receives positive external pressure, in ft^2
A_f	Projected area normal to the wind except where C_f is specified for the actual surface area
A_g	Gross area of that wall in which A_0 is identified, in ft^2
c	Turbulence intensity factor
C_f	Net force coefficient
d	Thickness at cross section of angle ϕ from crown.
d_0, d_c	Thickness of arch at crown
d_k	Thickness of arch at distance kL from crown
D	Depth of the arch system
e	Structural efficiency
E	Young's modulus (modulus of elasticity)
h	Rise of arch
g_Q	Peak factor for background response
g_R	Peak factor for resonant response
g_v	Peak factor for wind response
G	Arch constant (Ch.2), Gust effect factor (Ch.3)
H, H_0	Horizontal reaction
H_{cr}	Critical intensity of the uniform load
I	Moment of inertia at cross section of angle ϕ from crow (Except Ch.3)
I	Importance factor (Ch.3)
I_c	Moment of inertia of cross section at crown
I_z	Intensity of turbulence
k	Portion of position of load to entire span
k_N, k_H	Effective length factors
K	Effective length factor

K_d	Wind directionality factor
K_z	Velocity pressure exposure coefficient
K_{zt}	Topographic factor
l	Integral length scale factor
L	Span of arch
L_d	Leaning distance between two arches at crown
L_r	Reduced length of column
L_z	Integral length scale of turbulence
M_0	Bending moment at support
m_L, m_R	Bending moment on left and right half of arch, respectively
n	Number of sections
$N_{cr,s}$	Critical axial force at the quarter point of span length under symmetric loading
N_x	Axial force in an arch member
P	Concentrated load
P_{cr}	Buckling load of a column
q'	Correction quantity due to geometry
q_z	Velocity pressure evaluated at height z of the centroid of area A_f, lb/ft^2
Q	Background response
Q_x	Shear force of an arch acting at the section defined by the horizontal distance x.
r	Radius of gyration
R	Resonant response factor
S	Length of arch
t	Change in temperature in degrees
V	Basic wind speed
V_0	Vertical reaction
w, W	Uniform load
w_L	Live load in pounds per square foot
x, y, z	Cartesian coordinates
z_g	Nominal height of the atmospheric boundary layer
z_{min}	Exposure constant
α	3-second gust speed power law exponent
α_{arch}	Arch analogy coefficient
β	Ratio of braced length to entire span, projected on x-y plane
ε	Coefficient of thermal deformation (Ch.2), ratio of solid area to gross area of

	one structure face for segment under consideration
θ	Tilt angle of arch with respect to vertical plane
θ_k	Angle between tangent to arch-axis and horizontal
σ_u	Ultimate stress
σ_y	Yield stress
κ	Buckling coefficient
λ	Slenderness ratio of arch
φ	Angle of inclination of member's axis, at the considered section
ϕ	Angle from crown for circular arch
Φ	Reduction factor

Abbreviations

LTD	Leaning-to-depth ratio
RTS	Rise-to-span ratio
SAP	Structural Analysis Program

List of Figures

List of Tables

Chapter 1 Introduction

1.1 Overview

The arch is one of the oldest forms of architecture and civil engineering. After the appearance of the first prototype of arch about 5000 years ago in Middle-East area (Ur, Bagdad) it seems that the mechanical efficiency of arch has been noticed and applied by ancient people, even though they did not understand its principles.

In architecture, the application of arch is focused on connection between two columns and the support of the roof above. Many ancient religious buildings displayed the characteristic aesthetic appeal of the arch on their exterior (Figures 1.1, 1.2, 1.3, 1.4, and 1.5). Nevertheless, the importance of the arch had been demonstrated even before its appearance in civil engineering applications (Figures 1.6, 1.7, and 1.8), especially on bridges (Figures 1.9, 1.10, and 1.11).

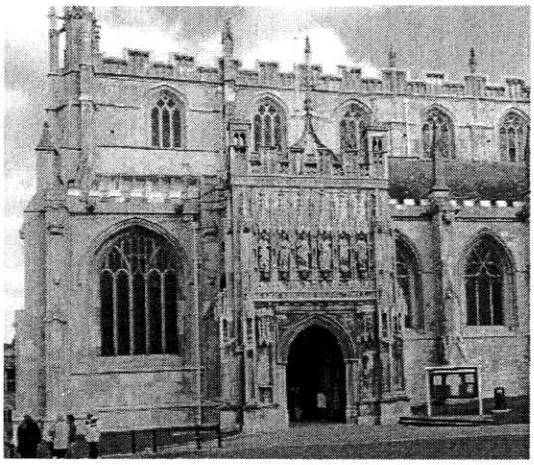

Figure 1.1 Gloucester Cathedral, Gloucester, England (~A.D.1953)

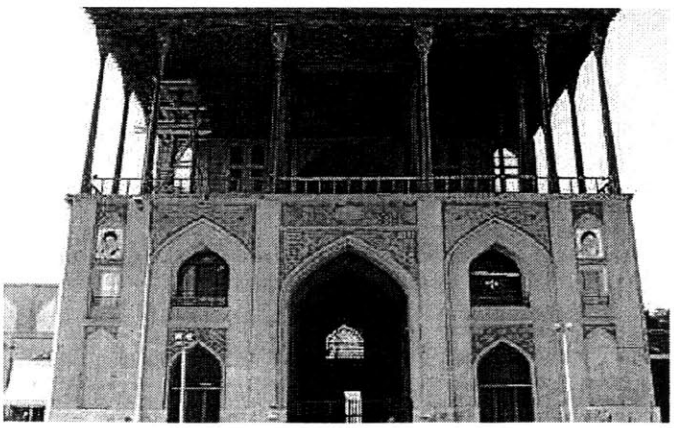

Figure 1.2 Ali Qapu (The Royal Palace), Isfahan, Iran (About A.D.1700)

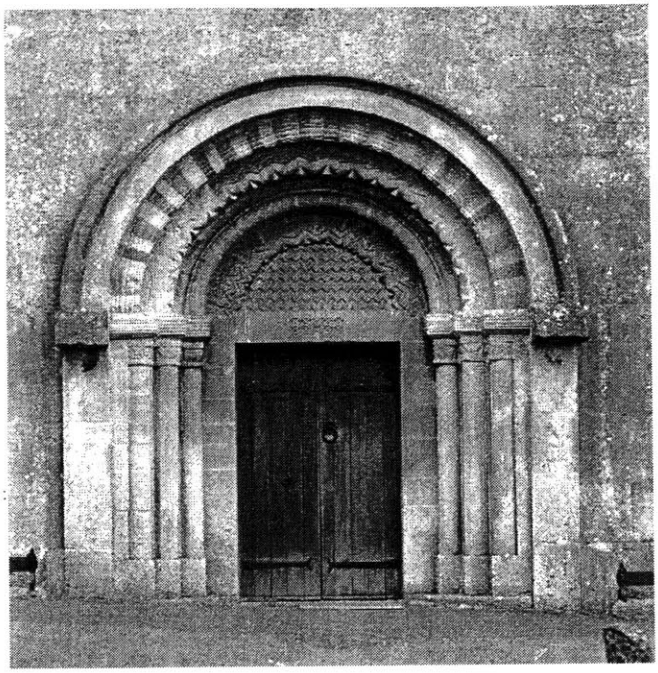

Figure 1.3 Roman Amphitheater, Nimes, France (A.D.100~A.D.200)(left)
Figure 1.4 Temple Guiting Church, Gloucestershire, England (A.D.1873)(right)

Figure 1.5 Arc de Triomphe, Paris, France (A.D.1854)

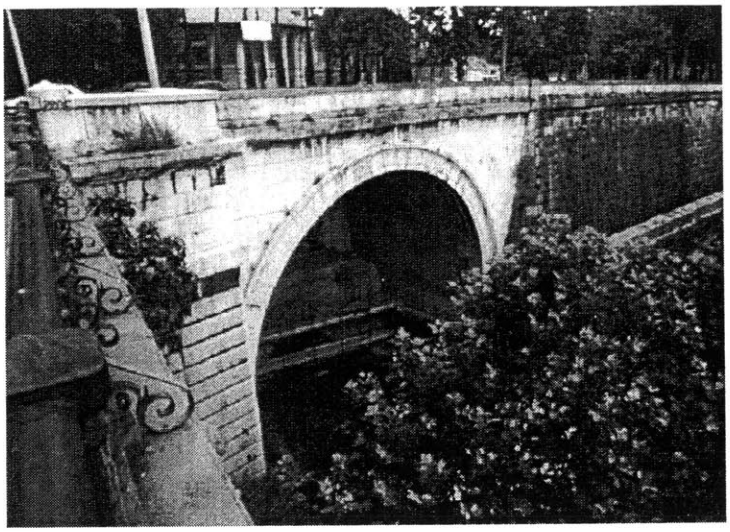

Figure 1.6 Cloaca Maxima, Rome, Italy (About B.C.600)

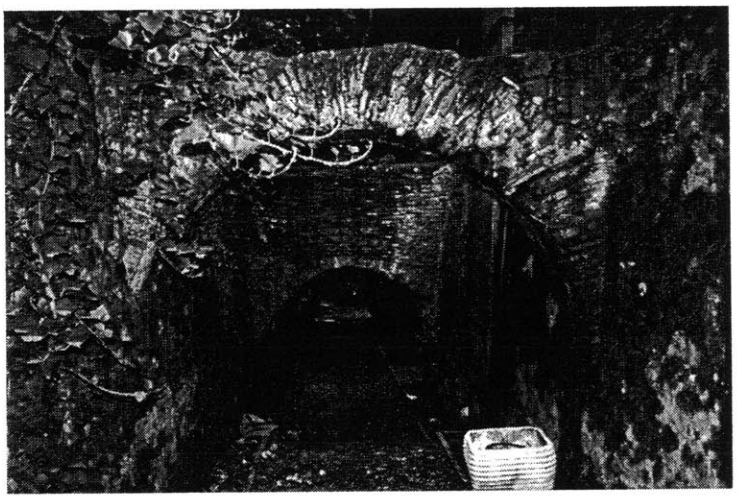

Figure 1.7 The mouth of the section of the Cloaca Maxima across from S. Giorgio in Velabro, Italy (B.C.100)

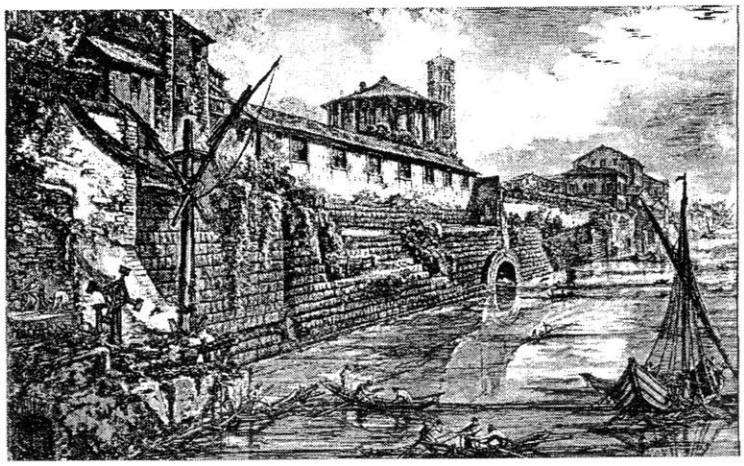

Figure 1.8 *The temple of Hercules Victor* by Giovanni Battista Piranesi (in mid 1800 A.D.) about Cloaca Maxima, Rome, Italy (About B.C.600)

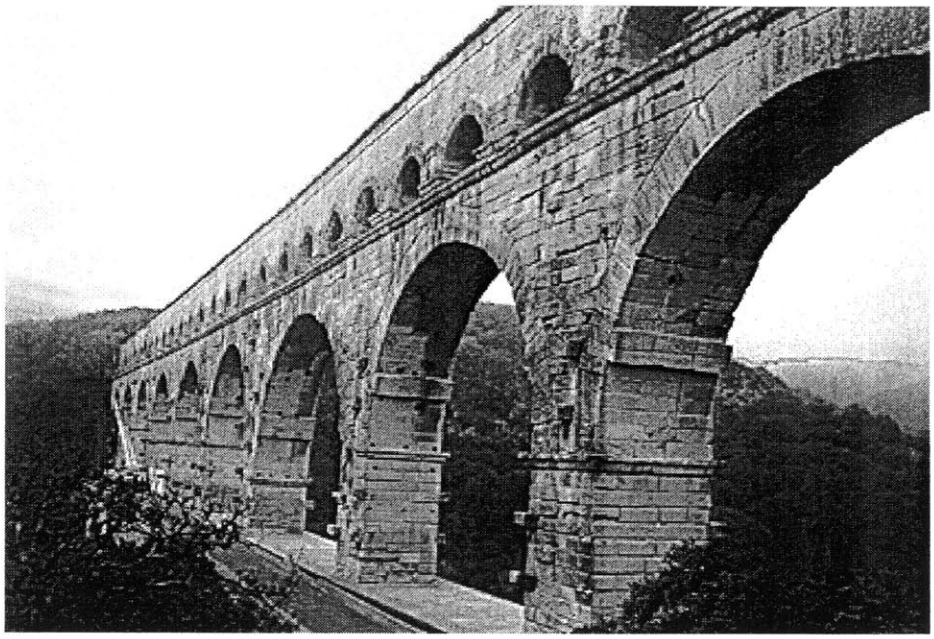

Figure 1.9 Pont du Gard, Nimes, France (B.C.19)

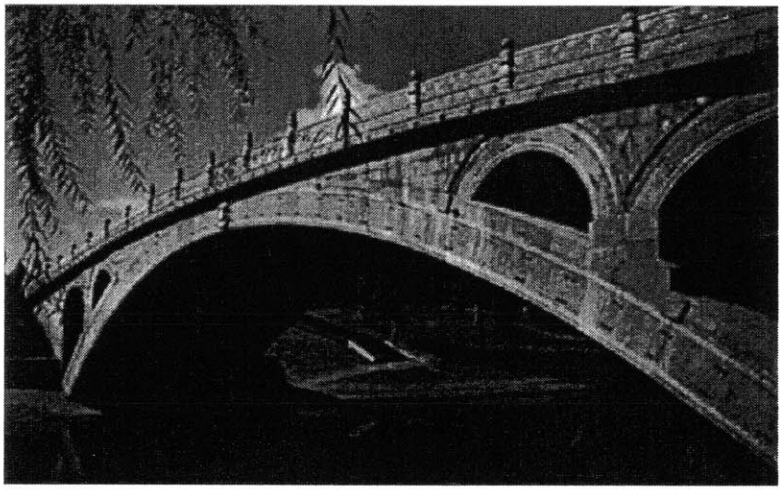

Figure 1.10 Ang-Ji Bridge, Her-Pei, China (A.D.605)

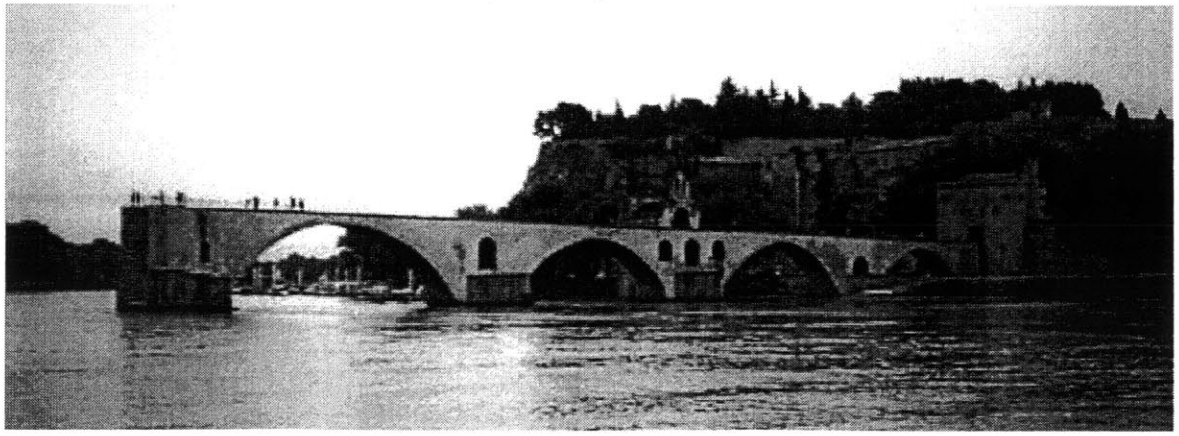

Figure 1.11 Pont d'Avignon (Bridge of Saint Benezet), Avignon, France (A.D.1187)

What ancient people knew about the arch mechanism might be that, by arranging members properly, the loading could be "guided" through members toward supports (Load Transfer) (Figure 1.12). With the aid of frictional action induced by compression between members, space would be gained below the arch (Figure 1.13).

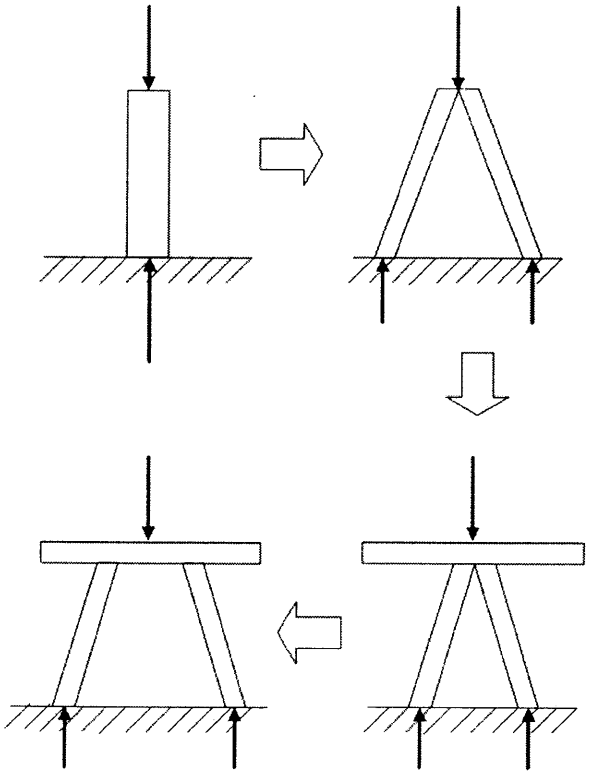

Figure 1.12 Principle of Load Transfer

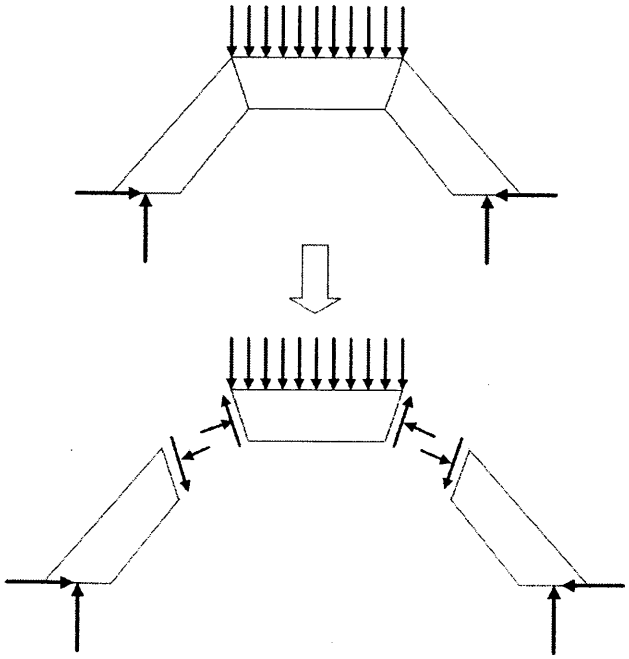

Figure 1.13 Actions between arch members

The applications of arches in bridges are more challenging than for buildings. This is because the required span of a bridge is usually large and the reserved space below the bridge is necessary for other uses. However, the applications of arches in bridges display their advantages thoroughly. Materials were the limitation of the development of arch bridges in ancient times. It was not until the emerging of new materials, such as reinforced concrete, that the spans of arch bridges could be promoted to new level.

Arches can be categorized into many types, depending on the following factors:

1) Geometrical property: a) Shape: Circular, parabolic, hyperbolic, etc.
   b) Boundary condition: Fixed, hinged, etc.
   c) Global Configuration: Two-dimensional or three-dimensional.
   d) Internal Configuration: Continuous or hinged.
2) Physical property: a) Material: Reinforced concrete, steel, stone, etc.
   b) Mechanics (Load-carrying mechanism): Carries load from top of it (through compression member, such as pillar or truss) or carries load below it (through tension member, such as hanging cable).

When designing an arch system, the following factors should be mentioned and considered with respect to the design requirements. The choice of arch type depends on:

1) Purpose of arch
2) Structural efficiency
3) Construction feasibility
4) Terrain and geology
5) Aesthetics
6) Economics (Cost)
7) Maintenance

1.2 Scope

The arch system to be considered in this thesis is a pair of leaning parabolic arches, connecting to each other with bracing member between them (Figure 1.14). It is a three-dimensional structure because it takes load and offers stiffness in three dimensions. The systems is capable of carrying loads from hanging cables attached to it and from pillars above, so as to behave like an arch bridge or an arch structure.

Numerical investigation is conducted applying finite element approach.

Commercial software is used for establishing numerical model and performing parametric analysis (SAP2000, Computers and Structures Inc., 1998).

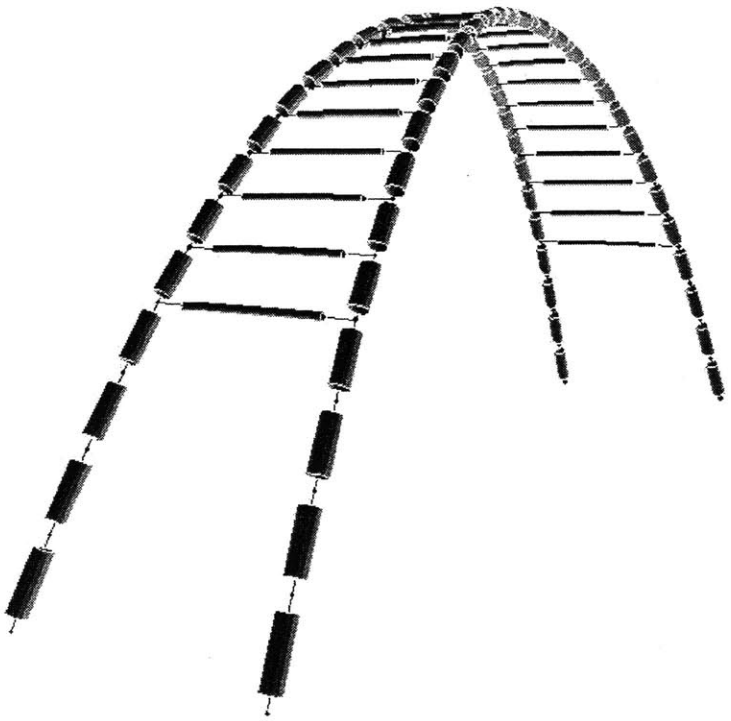

Figure 1.14 Illustration of the system

This thesis is organized in the following manner. First, the review of previous research on the topic of arch is given. Next, the configuration of arch system and description of analysis method are introduced. Finally, a pair of leaning parabolic arches is examined and investigated through parametric analysis. Stiffness and stability analyses are presented in the research.

Chapter 2 Literature Review

All theories are evolved from empirical form to analytical form, not excepting the theory of the arch. The advancement of a theory usually depends on the discovery of new phenomena and the invention of new tools for analysis.

2.1 Overview

The development of the arch theory began with geometry and then looked into mechanics. Bolarch (1755) published a book containing architectural design examples of arches. Swan (1794) introduced the work done by architects and offered design scenarios. Atwood (1801) published a dissertation on the material properties or behavioral properties of arches. Lagarrigue (1831) investigated arch geometry and pointed out that the tilt angle of an arch might be a characteristic design parameter. Nicholson (1851) collected many design examples and displayed empirical formulae based on different construction materials. Swain (1896) compared the analysis theories for different structures and mentioned the stress analysis of arch.

Melan (1915) published a book and introduced the analytical method and graphical method for arches, considering different types of boundary condition and loads. He proposed a graphical method and used the concept of influence-lines to determine the dimension of arch sections.

Timoshenko (1934) introduced the classical approach from the former Soviet Union for establishing and solving mechanical problem analytically. His several famous books on mechanics provided following researchers a clear way to obtain a universal solution.

MIT Professor Spofford (1937) described his experience with designing arch bridges in his book. He dealt with the design of continuous arch bridges of different shapes and presented analytical solutions with numerical verification.

Leontovich (1959) published a book collecting analytical solutions of arches of different shapes and considering different types of loading and boundary condition. His work provided designers a short path on evaluating the design by internal action and reaction. Leliavsky's (1982) work considered the detailed designs of components of arch

bridge. He mentioned many practical issues including long-term effect in his book.

Most of the previous works followed an analytical approach and encountered many difficulties. The main reason is geometry. When the shape of structure is irregular and can not be described by continuous mathematical function, it is not easy to formulate the relation between variables because they are geometrically dependent.

There are several ways to amend the weakness of an analytical approach. One can simplify the geometry such that the description is feasible. The disadvantage becomes the error induced by oversimplification. Or one can analogize a describable structure to the complicated structure by establishing the relationship between them. However, this strategy still requires further verification by other approach, usually numerical methods.

The goals of analysis are:

i) Stiffness

i) Critical load (Buckling load)

ii) Internal actions

iii) Deformation

Analysis is complete once the information listed above is obtained. Several analytical results for a plane parabolic arch with different boundary conditions are presented in the following sections.

2.2 Analytical Solutions for Parabolic Arch Subject to Uniform Load

Melan (1915) offered his analytical solution by graphical method for two-hinged parabolic arch subject to uniform load distributed along the projection of its entire length on horizontal axis:

$$H = \frac{\int_0^L \frac{M_b y}{I} ds}{\int_0^L \frac{y^2}{I} ds + \frac{v}{r}\int_0^L \frac{dx}{A}} \tag{2-1}$$

$$M_b = \frac{1}{2} wx(L-x) - \frac{1}{8}\frac{wL^2}{f} y$$

$$y = \frac{4f}{L^2} x(L-x) \tag{2-2}$$

where H = horizontal reaction; L = span of arch; M_b = bending moment in a simple beam; f = height (rise) of arch; I = moment of inertia of section; w = uniform load; x, y = coordinates of arch-axis; v = coordinate of the center of curvature of the arch-axis; r = radius of curvature of arch-axis at any section (only defined here); A = area of cross section. If the arch is symmetrical, the vertical reactions at two supports are half of the total load and equal to each other. In fact, Eq.(2-2) is equivalent to standard parabolic function. Its derivation is in Chapter 3.

For fixed end parabolic arch subject to uniform load,

$$H = \frac{\int_0^L \frac{M_b y}{I} ds - \frac{v}{r} q'}{\int_0^L \frac{y^2}{I} ds + \frac{v}{r} \int_0^L \frac{dx}{A}} \tag{2-3}$$

where q' = correction quantity due to geometry.

Melan also mentioned the method to determine the thickness of arch from the concept of line of resistance. In order to generate same vertical projection of section, the thickness is defined as

$$d = d_0 \sec \phi \tag{2-4}$$

where d_0 = thickness at crown; d = thickness at cross section of angle ϕ from crown. It is defined from the viewpoint of resistance capacity. Because the radius of curvature for parabolic arch and is not constant but a function of x, Eq.(2-1) and (2-3) should be modified as

$$H = \frac{\int_0^L \frac{M_b y}{I} ds}{\int_0^L \frac{y^2}{I} ds + \int_0^L \frac{v}{Ar} dx} \tag{2-1a}$$

$$H = \frac{\int_0^L \frac{M_b y}{I} ds - \sum_{i=1}^{n} \frac{v_i}{r_i} q_i'}{\int_0^L \frac{y^2}{I} ds + \int_0^L \frac{v}{Ar} dx} \tag{2-3a}$$

where n = number of sections.

Melan's graphical method contains many simplifications and definitions. His method involves the concept of line of resistance and influence. It is only applicable in the elastic

range. Some of the simplifications may induce significant error when the rise-to-span ratio (or height-to-span) of arch is large.

Spofford (1937) provided another formula for uniform load over entire structure:

$$H = \frac{\frac{1}{15}\frac{hwL^2}{EI_c} \pm \varepsilon t}{\frac{1}{AE} + \frac{8}{15}\frac{h^2}{EI_c}} \tag{2-5}$$

where H = horizontal reaction; h = rise of arch; w = uniform load; L = span of arch; EI_c = rigidity of arch; ε = coefficient of thermal deformation; t = change in temperature in degrees; A = area of cross section.

For two-hinged parabolic arch subject to concentrated load,

$$H = \frac{\frac{Ph}{3}\left(\frac{L}{I_c}\right)\left(k^4 - 2k^3 + k\right) \pm \varepsilon tE}{\frac{1}{A} + \frac{8}{15}\frac{h^2}{I_c}} \tag{2-6}$$

where P = concentrated load; k = portion of position of load to entire span.

For fixed end arch subject to any loading,

$$H_0 = \frac{1}{2}\frac{\sum m_L \frac{y}{I} + \sum m_R \frac{y}{I}}{\sum \frac{y^2}{I} + \sum \frac{1}{A}}$$

$$V_0 = \frac{1}{2}\frac{\sum m_L \frac{x}{I} + \sum m_R \frac{x}{I}}{\sum \frac{x^2}{I}}$$

$$M_0 = \frac{1}{2}\frac{\sum \frac{m_L}{I} + \sum \frac{m_R}{I}}{\sum \frac{1}{I}} \tag{2-7}$$

where H_0 = horizontal reaction; V_0 = vertical reaction; M_0 = bending moment at support. m_L, m_R = bending moment on left and right half of arch, respectively, due to applied loads, considering each half of arch to act as a cantilever fixed at left and right ends; I = moment of inertia of section.

Spofford defined the thickness of cross section in the manner of moment of inertia for two-hinged parabolic arch:

$$I = I_c \sec\phi \tag{2-8}$$

where I = moment of inertia at cross section of angle ϕ from crown; I_c = moment of inertia of cross section at crown.

For fixed end arch, the thickness is determined as

$$d_k = d_c \sqrt[6]{1+\tan^2\theta_k} \tag{2-9}$$

where d_k = thickness at distance kL from crown; d_c = thickness at crown; θ_k = angle between tangent to arch-axis and horizontal. d_c is determined as

$$d_c = \sqrt{L} + \frac{L}{10} + \frac{w_L}{200} + \frac{w_c}{400} \tag{2-10}$$

where L = span of arch; w_L = live load in pounds per square foot (50 percent to be added for impact on railroad bridge); w_c = weight of fill over crown in pounds per square foot. F.W. Weld gave this relation in 1905. Obviously it is an empirical expression.

Similar restraint applies to the formula in Professor Spofford's book, which is applicable for flat arches with small rise-to-span ratio.

Leontovich (1959) published a book collecting condensed solutions for different types of arches and frames. For vertical uniform load over entire span of two-hinged parabolic arch,

$$H = \frac{wL}{8f} \tag{2-11}$$

where H = horizontal reaction; w = uniform load; L = span of arch; f = rise of arch. The axial force in arch is computed by

$$x \le \frac{L}{2} \Rightarrow N_x = H\cos\varphi + w\left(\frac{1}{2} - \frac{x}{L}\right)\sin\varphi$$
$$x > \frac{L}{2} \Rightarrow N_x = H\cos\varphi + w\left(\frac{x}{L} - \frac{1}{2}\right)\sin\varphi \tag{2-12}$$

where x = horizontal distance from support; N_x = axial force in an arch member, acting at the section defined by the horizontal coordinate x; φ = angle between tangent to

arch-axis and horizontal.

For vertical uniform load over entire span of fixed end parabolic arch,

$$H = \frac{wL}{8f(1+G)} \tag{2-13}$$

where G is a arch constant, defined by

$$G = \frac{d_{1.5}{}^2 \tau}{f^2} \tag{2-14}$$

where $d_{1.5}$ = arch thickness at crown (in proper dimensional units); t = numerical constant. Shear force is also calculated by

$$x \le \frac{L}{2} \Rightarrow Q_x = -H\sin\varphi + w\left(\frac{1}{2} - \frac{x}{L}\right)\cos\varphi$$
$$x > \frac{L}{2} \Rightarrow Q_x = H\sin\varphi + w\left(\frac{1}{2} - \frac{x}{L}\right)\cos\varphi \tag{2-15}$$

where Q_x = shear force of an arch acting at the section defined by the horizontal distance x.

The way Leontovich determined the thickness of arch is

$$d = d_0 \sqrt[3]{\sec\varphi} \tag{2-16}$$

where φ = angle of inclination of member's axis, at the considered section.

Leontovich derived the expression of reaction and internal action from the aspect of force equilibrium. When static indeterminate structure was encountered, he integrated simplified coefficient into the expression. Other cases of different loading conditions and types of boundary condition could be referred in his book. His systematic work is helpful for evaluation of preliminary design.

2.3 Comparison of Different Formulae for Arch Length

The length of arch is essential for determining gravity load, which is the self-weight of member. When preliminary design is proceeding, a handy formula is required for evaluation with sufficient precision.

Spofford (1937) provided an approximate formula for determining the length of

parabolic arch. It is shown as below:

$$S = L\left[1+\frac{8}{3}\left(\frac{h}{L}\right)^2\right] \tag{2-17}$$

where S = length of arch.; L = span of arch; h = rise of arch. This formula was obtained by neglecting some higher terms during integration.

Leontovich (1959) offered another formula.

$$S = \frac{L}{2}\left\{\sqrt{1+\left(\frac{4h}{L}\right)^2}+\frac{L}{4h}\log\left[\frac{4h}{L}+\sqrt{1+\left(\frac{4h}{L}\right)^2}\right]\right\} \tag{2-18}$$

Definitions are the same with Eq.(2-17).

Their comparison with numerical solution is shown in Figure 2.1.

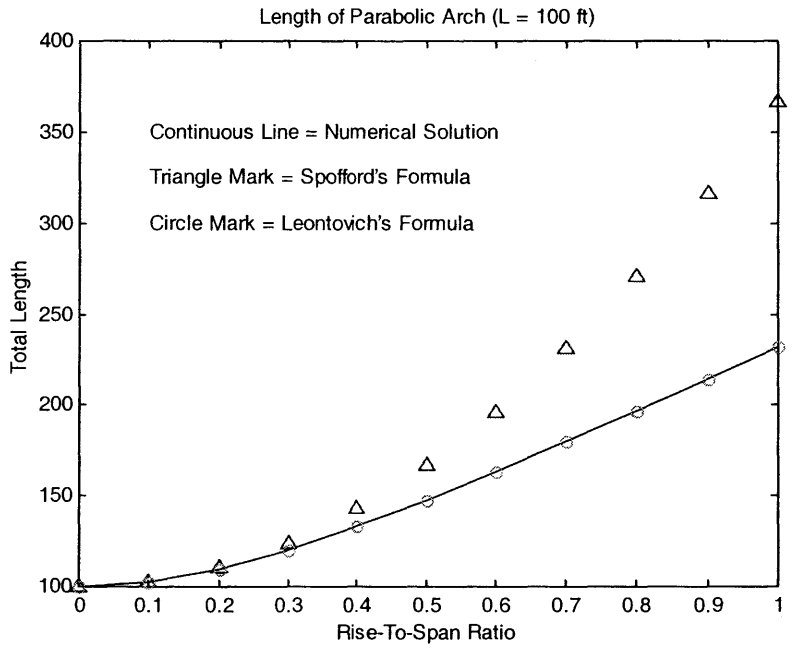

Figure 2.1 Comparison of Different Formulae

It is found that Eq.(2-17) is applicable to flat arch (rise-to-span ratio < 0.3) and not applicable when rise-to-span ratio is greater than 0.4. The difference between Eq.(2-18) and numerical solution is undetectable. Hence, when flat arch is designed, Spofford's formula is recommended. When stocky arch is designed, Leontovich's formula is recommended.

2.4 Critical Load of Single Plane Arch

Komatsu and Shinke (1977) proposed their formula for determining the ultimate strength of a plane arch subject to symmetrical loading.

$$\bar{a} \le 1 \Rightarrow N_{cr,s} = A\sigma_y\left(1 - 0.136\bar{a} - 0.3\bar{a}^{-2}\right)$$

$$\bar{a} > 1 \Rightarrow N_{cr,s} = A\sigma_y\left(\frac{1}{0.773 + \bar{a}^{-2}}\right) \qquad (2\text{-}20)$$

And

$$\bar{a} = \frac{1}{\sqrt{\left(\gamma\kappa\left(\frac{E}{\sigma_y}\right)\right)}}\frac{L}{r}$$

$$\gamma = \sqrt{\left(1 + 4\left(\frac{h}{L}\right)^2\right)} \qquad (2\text{-}21)$$

where $N_{cr,s}$ = critical axial force at the quarter point of span length under symmetric loading; A = average cross-sectional area; σ_y = yield stress; κ = Buckling coefficient given by Stussi (1935); E = Young's modulus; h = rise of arch; L = span of arch; r = radius of gyration about horizontal centroidal axis of arch cross-section.

Table 2.1 Buckling coefficient κ given by Stussi (1935)

Type	Rise-to-Span Ratio, h/L			
	0.1	**0.15**	**0.2**	**0.3**
Two-hinged arch	36.0	32.0	28.0	20.0
Fixed end arch	76.0	69.5	63.0	48.0

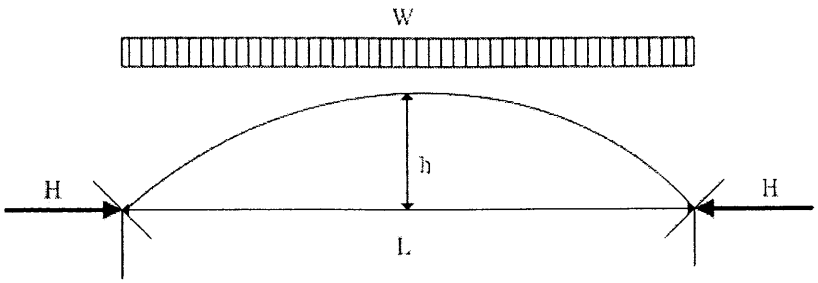

(a) Symmetric Load

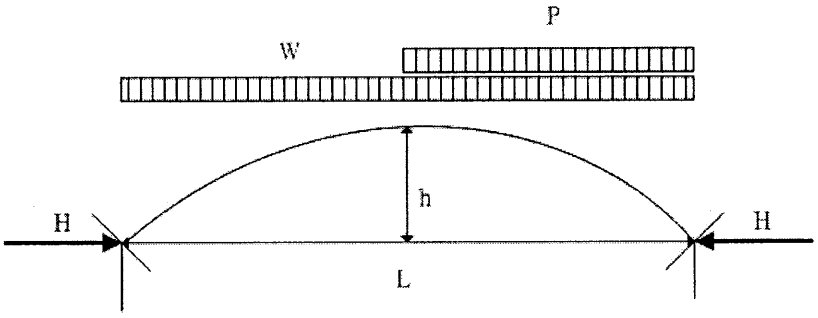

(b) Unsymmetric Load

Figure 2.2 Distribution of Load

For asymmetric loading, Komatsu (1985) modified the formula by Stussi and provided his formula:

$$N_{cr} = \Phi N_{cr,s} \tag{2-22}$$

where Φ = reduction factor. It is computed by

$$\Phi = 1 - C\sqrt{\frac{P}{W}}$$

$$C = C_1 + C_2$$

$$C_1 = 2.2\frac{h}{L} + 0.018\sqrt{\frac{E}{\sigma_y}} - 0.19$$

$$C_2 = -4\overline{K}\left(\frac{L}{r} - 6\overline{K}\sqrt{\frac{E}{\sigma_y}}\right)^2 \times 10^{-6}$$

$$\overline{K} = 1 \Rightarrow two - hinged$$

$$\overline{K} = 1.7 \Rightarrow fixed \tag{2-23}$$

where W = uniform loading over entire span of arch; P = uniform loading over half span of arch.

Sakimoto (1997) offered a formula derived from elastic linear theory for a parabolic arch subjected to uniform load and non-uniform load (Figure 2.2(b)).

The critical horizontal reaction is computed through the following formula:

$$H_{cr} = \frac{w_{cr} L^2}{8h}\left[1+\frac{1}{2}\left(\frac{P}{W}\right)\right] \tag{2-24}$$

in which H_{cr} = critical intensity of the uniform load. If define σ_{cr} as H_{cr} divided by A and divide Eq.(2-24) by σ_y, then it becomes

$$\frac{\sigma_{cr}}{\sigma_y} = \frac{w_{cr} L^2}{8hA\sigma_y}\left[1+\frac{1}{2}\left(\frac{P}{W}\right)\right] \tag{2-25}$$

where P = 0 in the case of an uniform distributed load.

Sakimoto (1997) also mentioned the effect of slenderness ratio, defined as L/r, on the critical stress. The critical stress increases as the slenderness ratio decreases, which means increasing the size of cross section or decreasing the span of arch can increase corresponding critical stress.

2.5 Critical Load of Braced Arches

Sakimoto, Yamao and Komatsu (1979) provided their formula based on the results of theoretical and experimental investigation for estimating ultimate stress σ_u, subjected only to vertical loads.

$$\sigma_u = \bar{\sigma}\sigma_y$$
$$N_u = \bar{\sigma}A\sigma_y \tag{2-26}$$

where σ_y = yield stress; N_u = ultimate axial force at springings of arch rib; A = average cross-sectional area.

$$\bar{\sigma} = 1-0.136\bar{\lambda}_y - 0.3\bar{\lambda}_y^2 \Rightarrow \bar{\lambda}_y \le 1$$
$$\bar{\sigma} = 1.276-0.888\bar{\lambda}_y + 0.176\bar{\lambda}_y^2 \Rightarrow 1 \le \bar{\lambda}_y \le 2.52$$
$$\bar{\sigma} = \frac{1}{\bar{\lambda}_y^2} \Rightarrow 2.52 \le \bar{\lambda}_y \tag{2-27}$$

And

$$\overline{\lambda}_y = \frac{1}{\pi}\sqrt{\frac{\sigma_y}{E}}\frac{KL}{r_y}$$

$$r_y = \sqrt{\frac{I_y}{A}}$$

$$K = K_e K_\beta K_l$$

$$K_e = 0.5 \Rightarrow fixed; K_e = 1.0 \Rightarrow hinged$$

$$K_\beta = 1-(1-C)\beta$$

$$C = \frac{2r_y}{K_e a}$$

$$K_l = 0.65 \Rightarrow hanger-loaded; K_l = 1.0 \Rightarrow vertical-loaded \qquad (2\text{-}28)$$

where K = effective length factor; r_y = radius of gyration about vertical centroidal axis of arch cross section; a = distance of twin arch ribs; β = ratio of the length portion to the total length of arch.

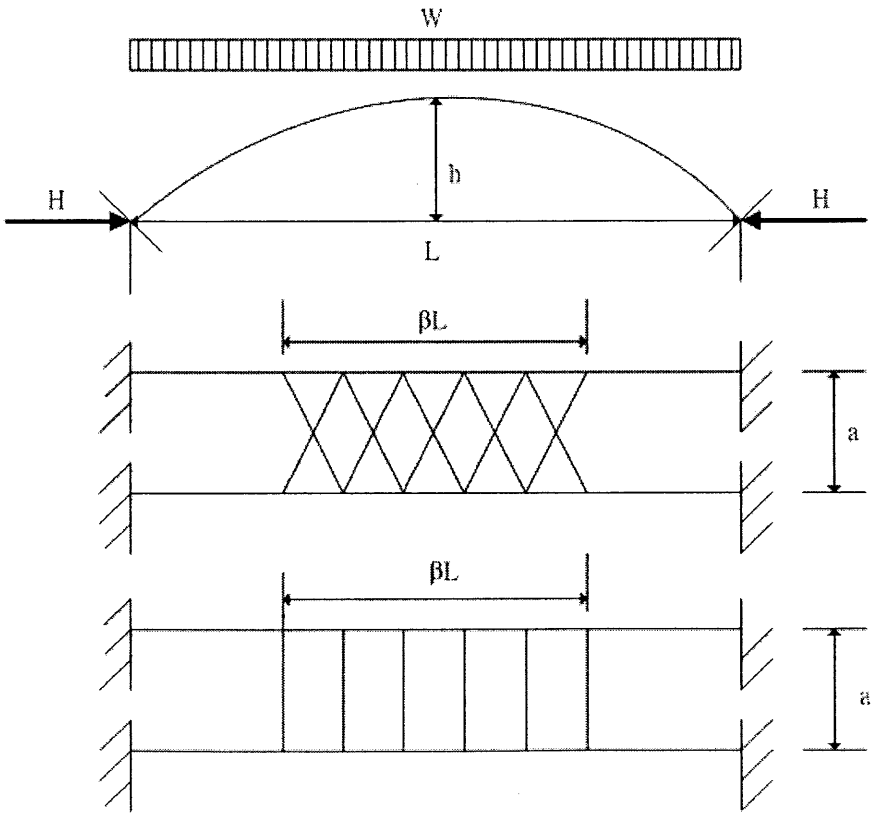

Figure 2.3 Typical Models used by Sakimoto et al. (1979)

2.6 Buckling Modes of Arches

When the load acting on an arch increases, the arch loses its stability once a certain critical value of the load is attained. In the case of elastic structures under conservative loads, the critical load corresponds to a stability limit point or a bifurcation point. When the arch configuration and the loading conditions are symmetric with respect to the crown of arch, the equilibrium path bifurcates from the original deformation mode to the buckling deformation mode. When the buckling deformation occurs in the plane of arch, it is called in-plane buckling. When it occurs out of the arch plane, it is called out-of-plane buckling.

The buckling modes are symmetric (Figure 2.4), anti-symmetric (Figure 2.5) and asymmetric (Figure 2.6). The onset of which mode depends on the type of arch.

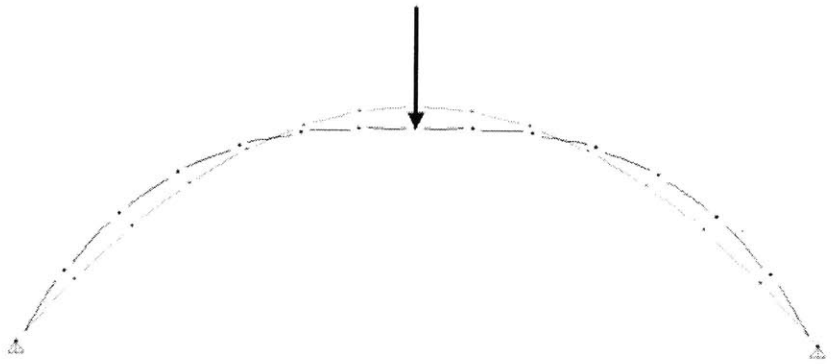

Figure 2.4 Symmetric Buckling

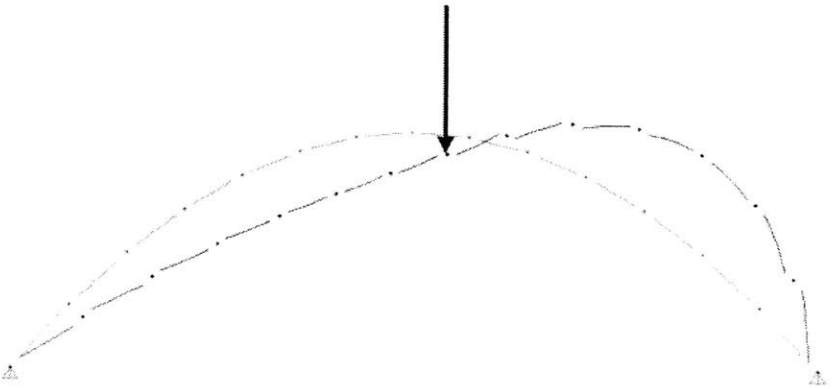

Figure 2.5 Anti-Symmetric Buckling

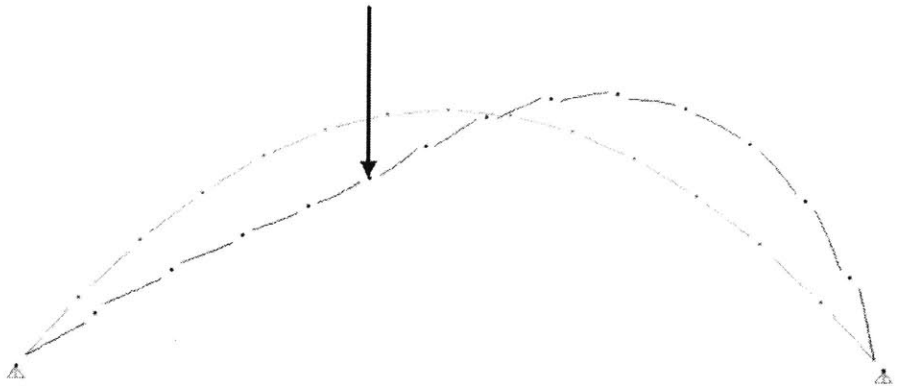

Figure 2.6 Asymmetric Buckling

In Figures 2.4 and 2.5, the concentrated load is applied at the center of arch. In Figure 2.6, the load is not applied at the canter of arch. For the in-plane problem of two-hinged arch or a stocky arch, an anti-symmetric buckling occurs under the smaller load. For the out-of-plane problem in these cases, a symmetric buckling occurs under smaller load. In the case of an asymmetric arch or a symmetric arch subjected to an asymmetric load, the load and deformation increase simultaneously until the maximum or limit load is reached.(Sakimoto and Komatsu, 1982)

2.7 A Pair of Leaning Arches System

Sakimoto et al.(1982) reported an investigation on an arch bridge system. Their arch bridge is consisted of two arches in parallel, connected with bracing system between two arches. Nevertheless, their arches are vertical, which means perpendicular to the ground (or bridge slab).

Plaut et al.(1998) performed research of a pair of leaning arches. They discussed the deflection shape, vibration modes, and the stability of a system of a pair of leaning arches. Molly et al.(1999) carried out similar research using the same model but subject to different loads. Their model consisted of two tilting arches leaning with each other. In their model, tilting angle is an essential factor for their research. However, their model does not involve bracing system between two arches. Their two arches connect with each other only at crown point.

The model to be investigated in this thesis is consisted of two arches leaning to each

other and connected with a bracing system between two arches. The tilt angle and bracing system are parameters in this research. The model is illustrated in Figures 2.7, 2.8 and 2.9.

Figure 2.7 Illustration of Model

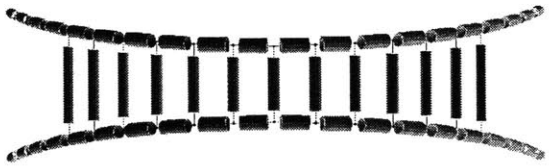

Figure 2.8 Top View of Model

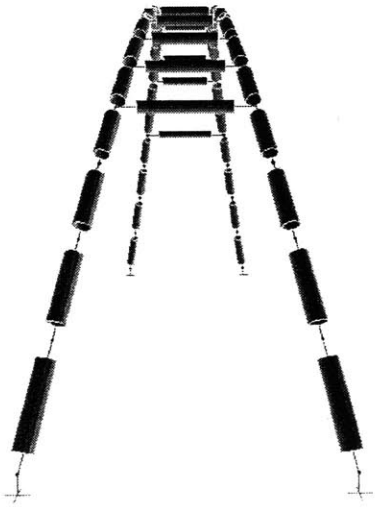

Figure 2.9 Side View of Model

Chapter 3 Methods of Analysis

3.1 Description of System

The behavior of an arch depends on two main parameters: geometrical configuration and loading condition. If an arch extends on three axes in space and is subjected to loading from any direction, its behavior is three-dimensional. If an arch can be described on a plane and is only subjected to loading on the plane, its behavior is two-dimensional. If an arch is configured on a plane but subjected to out-of-plane loading, its behavior is still three-dimensional.

Single arches possess inherent instability. It is because a single arch can only provide its out-of-plane stiffness through the bending rigidity from its supports. Once it loses its bending rigidity at support, it becomes unstable. Single arch with two-hinged support is also unstable out of plane.

A coupled arch system improves the weakness of single arch through its three-dimensional configuration. The coupled arch system discussed in this thesis is defined as "a system consisted of two arches leaning together with tilt angle and connected with bracing member between them." A coupled arch system achieves its stability by using bracing member between two arches. The main constraint to the system is whether the support should be fixed-type or the connection (between brace and arch) should be fixed-type. Another way for the system to attain its stability is to make the brace become a truss. More bracing members are required to form a truss system in that case. In this thesis, the connection between bracing member and two arches is assumed to be fixed-type, and the supports to be two-hinged-type and fixed-type.

The concept of a pair of leaning arches is an inherently stable system. Two arches, inclined toward each other in the direction perpendicular to their arch planes and connecting with another through bracing member, possess the capacity of resisting load from any direction. The illustration of such a system is shown in Figure 3.1.

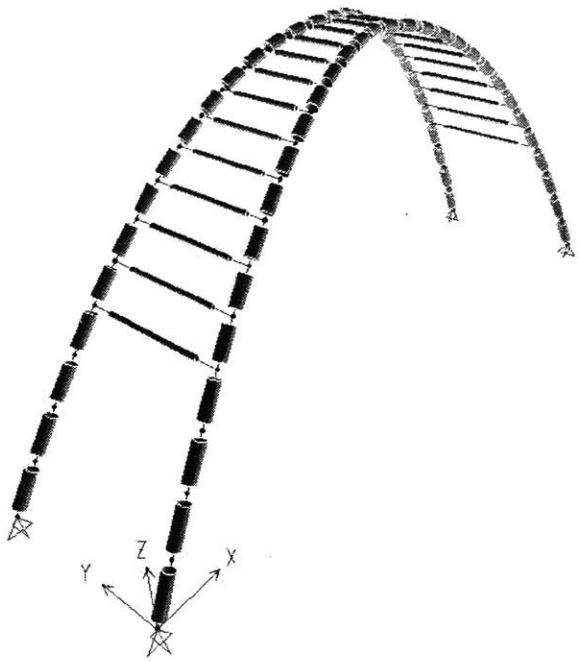

Figure 3.1 A typical pair of leaning arches system

3.1.1 Geometrical Property

The system can be defined through geometrical description. Once the shape of arch is chosen according to some regular configuration, the geometry can be determined by mathematical equation. In this paper, the shape is determined by parabolic equation. Several standard equations of the parabola are given in Cartesian coordinate.

$$(a)x^2 = 2py$$
$$(b)y^2 = 2px$$
$$(c)(y-k)^2 = 2p(x-h)$$
$$(d)(x-h)^2 = 2p(y-k) \qquad (3\text{-}1)$$

where x, y are ordinates on x-axis and y-axis, respectively; p, k, and h are all coefficients. Plot of (a) is illustrated in Figure 3.2.

The form of parabola in Polar coordinate is

$$r = \frac{p}{1-\cos\theta} \qquad (3\text{-}2)$$

where r is radius, θ is rotation angle, p is coefficient.

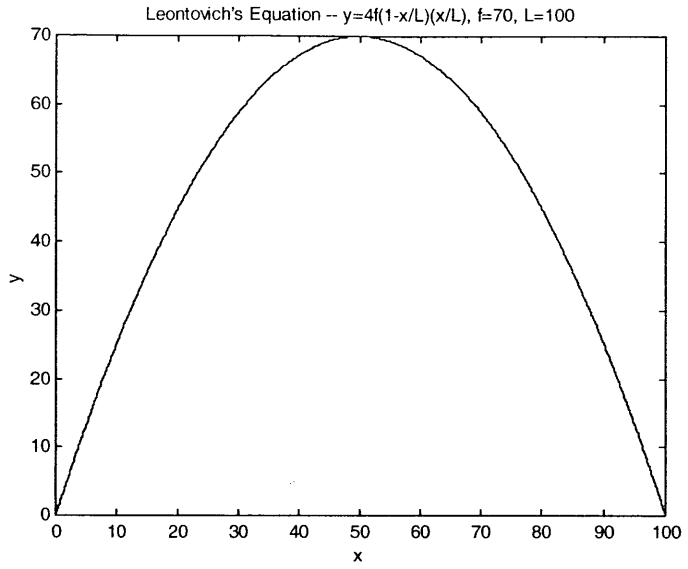

Figure 3.2 A parabola

Melan (1915) gave an equation for determining the relationship between x and y. His equation is derived from standard parabolic equation, which can be proved through the following calculation. Its form is

$$y = 4f\left(1-\frac{x}{L}\right)\frac{x}{L} \tag{3-3}$$

In Eq.(3-3), L = span of arch, f = rise of arch, x and y = coordinates of axes. Note that the origin is at left and of the member. It yields to

$$y = 4f\frac{x}{L} - 4f\left(\frac{x}{L}\right)^2 \Rightarrow y = -\left[\frac{4f}{L^2}x^2 - \frac{4f}{L}x\right]$$

$$\Rightarrow -y = \frac{4f}{L^2}\left[x^2 - 2\left(\frac{L}{2}\right)x\right] \Rightarrow -\frac{L^2}{4f}y + \left(\frac{L}{2}\right)^2 = x^2 - 2\left(\frac{L}{2}\right)x + \left(\frac{L}{2}\right)^2$$

$$\Rightarrow -\frac{L^2}{4f}(y-f) = \left(x-\frac{L}{2}\right)^2 \Rightarrow \frac{\left(x-\frac{L}{2}\right)^2}{(y-f)} = -\frac{L^2}{4f} = 2\left(-\frac{L^2}{8f}\right) \tag{3-4}$$

Comparing to (d) in Eq.(3-1), they are identical when h = L/2, k = f, p = $-L^2/(8f)$.

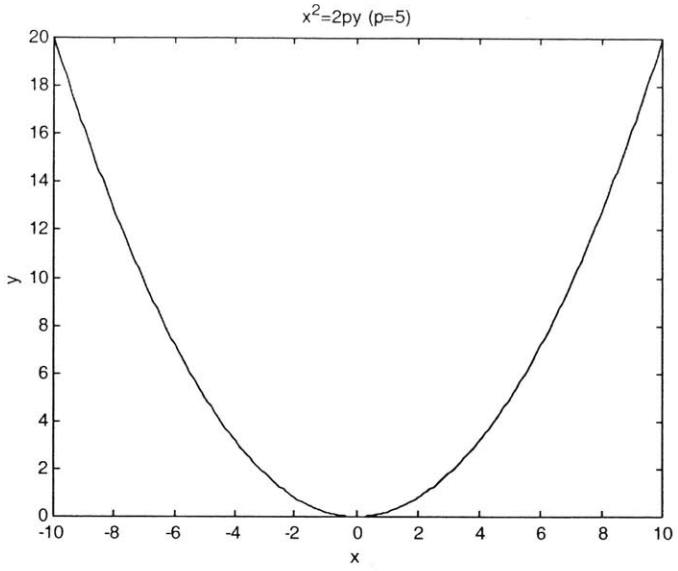

Figure 3.3 Plot of Melan's equation

Using Eq.(3-3), one can determine the coordinates on x and y axes.

The coordinate on z-axis can be defined either by a linear or nonlinear distribution. When linearly distributed on x-z plane, it means that there are two straight lines connecting the crown and two supports. When nonlinearly distributed, the lines connecting the crown and two supports are two curves. In this paper, only linearly distributed coordinate on x-z plane is considered. The front view of the system is illustrated in Figure 3.4.

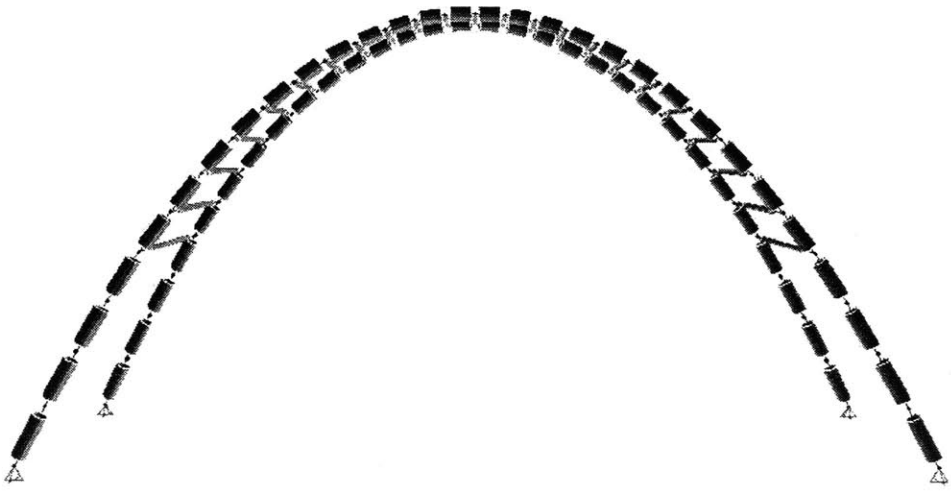

Figure 3.4 Front view of the system (x-z plane)

Plane view is also rendered in Figure 3.5.

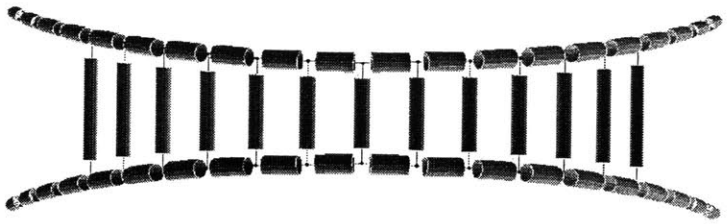

Figure 3.5 Top view of the system (x-y plane)

In order to describe the system, several geometrical parameters are defined and introduced below:

(1) Rise-to-Span Ratio, h/L

The characteristic of parabolic arch in height can be represented in terms of rise-to-span ratio, h/L. The higher the arch, the larger the ratio.

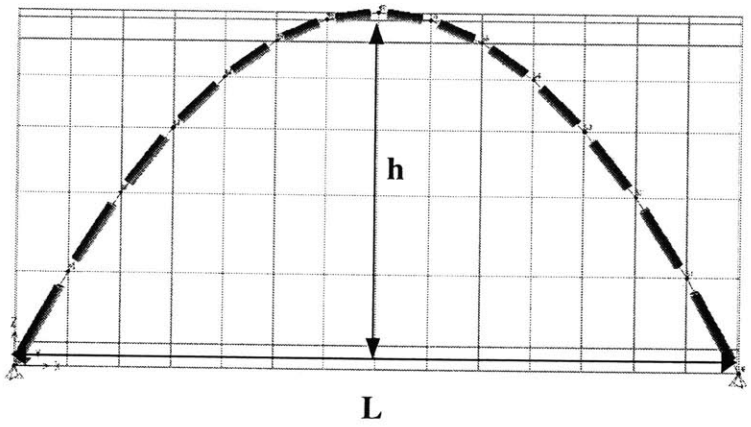

Figure 3.6 Rise-to-Span ratio, h/L

(2) Depth-to-Leaning Ratio, L_d/D

Depth-to-leaning ratio, L_d/D, is defined to be the ratio of the distance between two arches at crown to the distance at support. When L_d/D is zero, two arches are connected with each other at crown without distance. When L_d/D is unity, the lateral projection of the system will look like a typical frame with vertical columns.

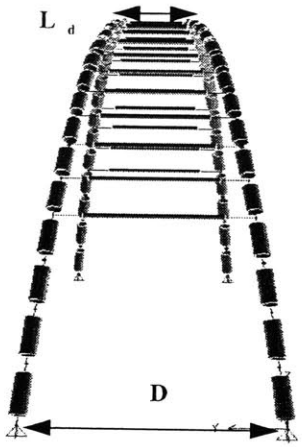

Figure 3.7 Depth-to-Leaning ratio, L_d/D

(3) Slenderness Ratio, L/r

Similar to the definition of slenderness ratio in columns, L is the span and r is the gyration radius of cross section. It is computed through Eq.(3-5).

$$\frac{L}{r} = \frac{L}{\sqrt{I_a / A_a}} = L\sqrt{\frac{A_a}{I_a}} \tag{3-5}$$

where I_a is the moment of inertia of cross section, A_a is the area of cross section.

Using the linear distribution, the coordinate on z-axis can be computed through Eq.(3-6) and (3-7). Define the arch on the right side in Figure 3.7 to be the first arch, the left to be the second, therefore,

$$FirstArch \Rightarrow z_i = \frac{i}{n}\left(\frac{D - L_d}{2}\right) \tag{3-6}$$

$$SecondArch \Rightarrow z_i = D - \frac{i}{n}\left(\frac{D - L_d}{2}\right) \tag{3-7}$$

where z_i is the coordinate on z-axis, i is the index of the coordinate starting from the support and n is half the number of total segments of an arch. An arch is simulated by 20 straight segments (n=10).

3.1.2 Boundary Conditions

Two types of boundary conditions are considered; fixed and hinged. It is not allowed to generate any displacement at support in both cases. There will be rotation in hinged case. The boundary conditions in terms of displacement and reaction are expressed in Eq.(3-8) ~ (3-11).

Displacement

Fixed Support

$$u_x|_{sup} = 0; u_y|_{sup} = 0; u_z|_{sup} = 0$$
$$\beta_x|_{sup} = 0; \beta_y|_{sup} = 0; \beta_z|_{sup} = 0 \quad (3\text{-}8)$$

Hinged Support

$$u_x|_{sup} = 0; u_y|_{sup} = 0; u_z|_{sup} = 0$$
$$\beta_x|_{sup} \neq 0; \beta_y|_{sup} \neq 0; \beta_z|_{sup} \neq 0 \quad (3\text{-}9)$$

Reaction

Fixed Support

$$\sum F_x \neq 0; \sum F_y \neq 0; \sum F_z \neq 0$$
$$\sum M_x \neq 0; \sum M_y \neq 0; \sum M_z \neq 0 \quad (3\text{-}10)$$

Hinged Support

$$\sum F_x \neq 0; \sum F_y \neq 0; \sum F_z \neq 0$$
$$\sum M_x = 0; \sum M_y = 0; \sum M_z = 0 \quad (3\text{-}11)$$

3.2 Loading Types

3.2.1 Distributed Vertical Load

The type of distributed vertical load corresponds to the weight of structure. It includes any fixed member or attached equipment, which will affect the long-term behavior of structure. Since distributed vertical load is induced by gravity and proportional to the volume of structure, the estimation of loading becomes the calculation of the volume of structure. The nature of gravity load is static, according to Newton's laws of motion, when there is no relative motion between the internal center of gravity

and the external reference axis. For this reason, gravity load is also called dead load.

Because of the configuration of arch, the distribution of dead load is not linear with respect to the span of arch. The distribution of dead load of parabolic arch is shown in Figure 3.8. The length of arch can be computed by Eq.(2-18) or by summing up the length of each segment.

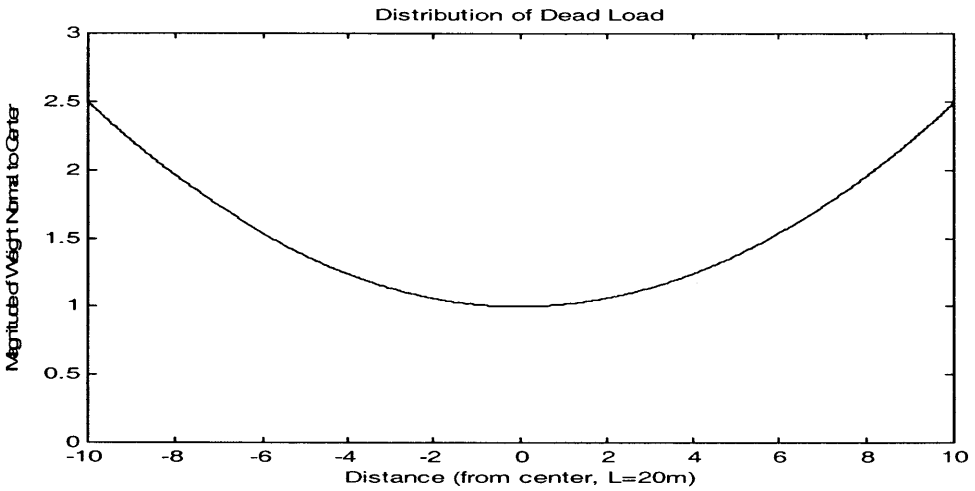

Figure 3.8 Distribution of dead load of parabolic arch

(Normalized to the value at center)

3.2.2 Distributed Horizontal Load

The type of distributed horizontal load corresponds to the pressure exerted by wind, which is called wind load. The estimation of wind loads follows the regulation by American Society of Civil Engineers (ASCE) 7-98. Three allowable methods are provided in ASCE 7-98. They are (1) Method One –Simplified Procedure; (2) Method Two – Analytical Procedure; and (3) Method Three – Wind Tunnel Procedure. Method Two is adopted in this thesis.

Design wind loads are functions of wind velocity, wind direction, terrain, exposure, structural system and exterior of system. The arch system can be considered as a frame having all walls open. This leads the arch system fall in the category of open building, which is defined as "a building having each wall at least 80% open."(Sec. 6.2, ASCE 7-98) In other words,

$$A_0 \geq 0.8A_g \tag{3-12}$$

in which A_0 = total area of openings in a wall that receives positive external

pressure, in ft^2;A_g = the gross area of that wall in which A_0 is identified, in ft^2.

Design wind force, F (lb), on open buildings and other structures is:

$$F = q_z G C_f A_f \tag{3-13}$$

where q_z = velocity pressure evaluated at height z of the centroid of area A_f, lb/ft^2, G = gust effect factor; C_f = net force coefficient and A_f = projected area normal to the wind except where C_f is specified for the actual surface area.

Velocity pressure, q_z, at height z can be computed by Eq.(3-14).

$$q_z = 0.00256 K_z K_{zt} K_d V^2 I \tag{3-14}$$

where K_z = velocity pressure exposure coefficient; K_{zt} = topographic factor; K_d = wind directionality factor; V = basic wind speed (Figure 3.9); I = importance factor.

According to the definition of exposure category, assume the location of the arch system belongs to "urban and suburban areas", which is Exposure B. By assuming Exposure B, corresponding constants are used in Eq.(3-15).

$$\alpha = 7.0; z_g = 1200(ft); \hat{a} = \frac{1}{7}; \hat{b} = \frac{1}{7};$$
$$\bar{\alpha} = \frac{1}{4}; \bar{b} = 0.45; c = 0.3; l = 320(ft); z_{\min} = 30(ft) \tag{3-15}$$

where α = 3-second gust speed power law exponent; z_g = nominal height of the atmospheric boundary layer; $\hat{a}$ = reciprocal of α; $\hat{b}$ = 3-second gust speed factor; $\bar{a}$ = mean hourly wind speed power law exponent; $\bar{b}$ = mean hourly wind speed factor; c = turbulence intensity factor; l = integral length scale factor; z_{min} = exposure constant.

For 15 ft < z < z_g, $K_z = 2.01(z/z_g)^{2/\alpha}$. At the top of arch, z = 233 ft. Thus, K_z = 1.258. From the table given by ASCE 7-98,

$$K_h = \left(\frac{233-200}{250-200}\right)(1.28-1.20)+1.20 = 1.2528 \tag{3-16}$$

For topographic factor, K_{zt},

$$K_{zt} = (1+K_1 K_2 K_3)^2 \tag{3-17}$$

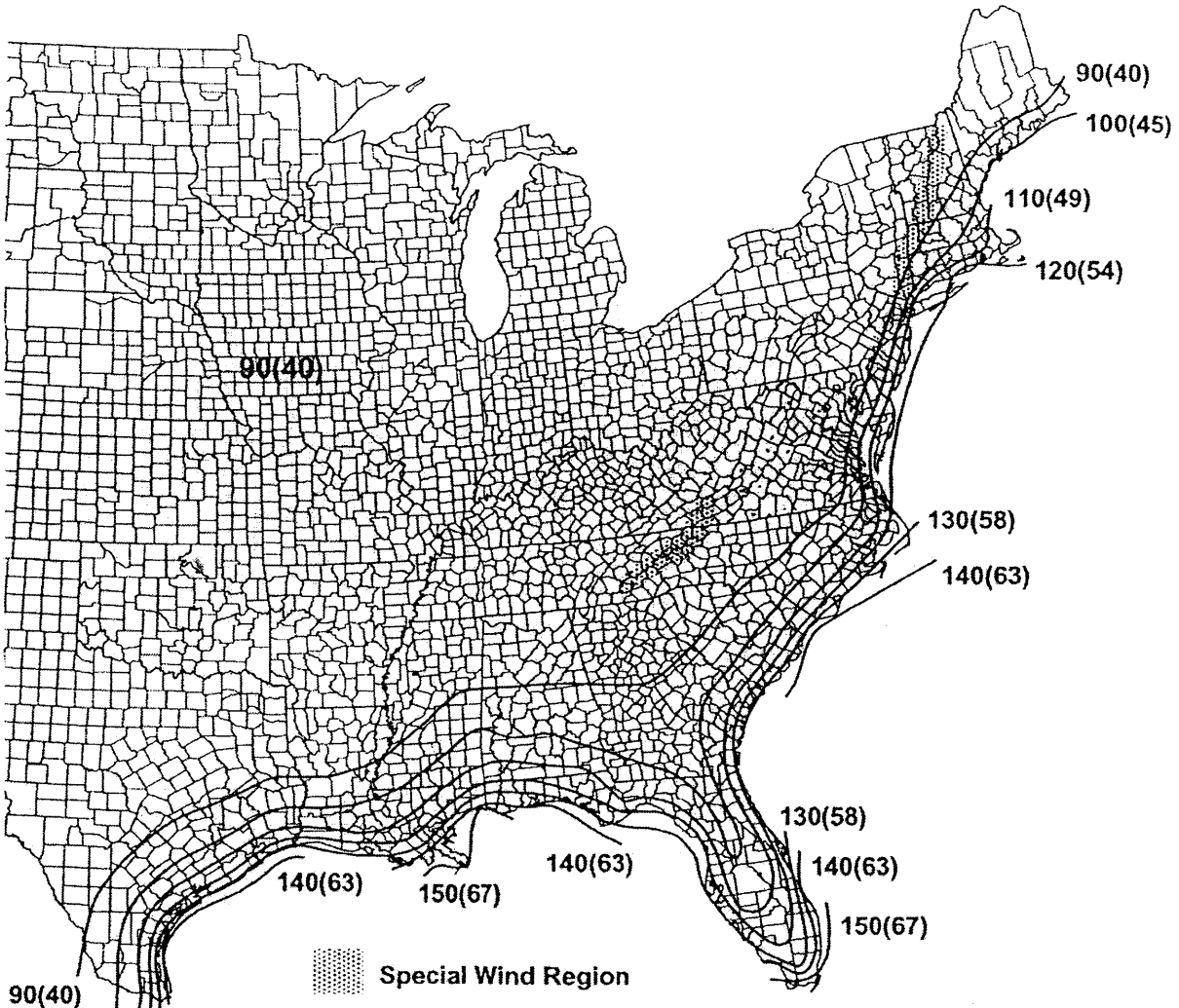

Location	V mph	(m/s)
Hawaii	105	(47)
Puerto Rico	145	(65)
Guam	170	(76)
Virgin Islands	145	(65)
American Samoa	125	(56)

Notes:

1. Values are nominal design 3-second gust wind speeds in miles per hour (m/s) at 33 ft (10 m) above ground for Exposure C category.
2. Linear interpolation between wind contours is permitted.
3. Islands and coastal areas outside the last contour shall use the last wind speed contour of the coastal area.
4. Mountainous terrain, gorges, ocean promontories, and special wind regions shall be examined for unusual wind conditions.

Figure 3.9 Basic Wind Speed (From ASCE 7-98)

where

$$K_1 = 0.95; \gamma = 4; \mu = 1.5$$

$$K_2 = 1 - \frac{|x|}{\mu L_h}$$

$$K_3 = e^{\frac{-\gamma z}{L_h}} \tag{3-18}$$

Definition of L_h, x and z is shown in Figure 3.10.

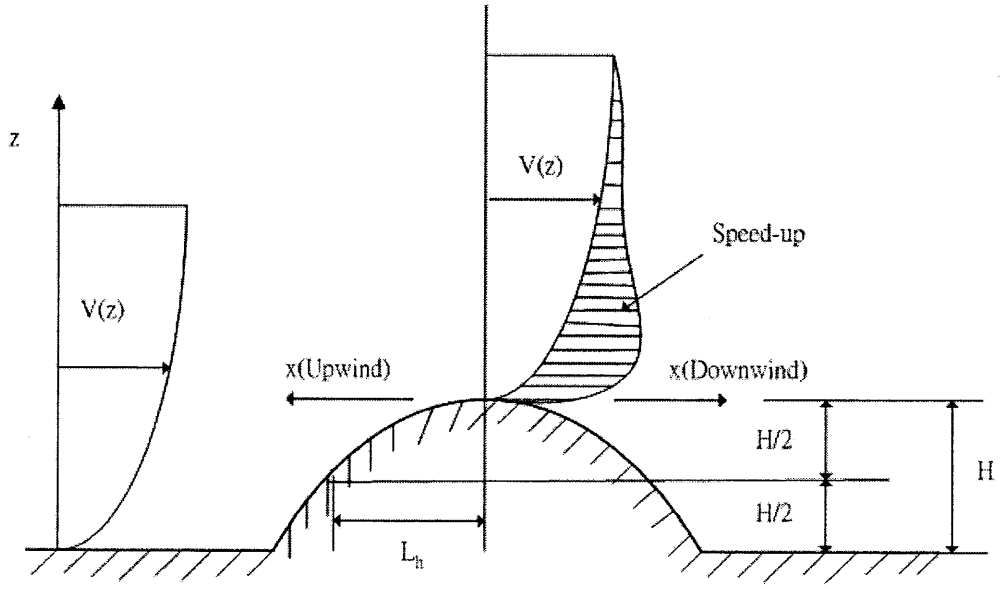

Figure 3.10 Definition of Variables used for Topographic Factor, K_{zt}

Assume $H/L_h = 0.5$, $x/L_h = 0.0$ and $z/L_h = 1.165$, such that K_1 multiplier = 0.53, K_2 multiplier = 1.00, K_3 multiplier = (1.165-1)/(1.5-1)*0.02 = 0.0066. Then,

$$K_1 = 0.95; \gamma = 4; \mu = 1.5$$

$$K_2 = 1 - \frac{0}{1.5 \times 200} = 1$$

$$K_3 = e^{\frac{-4 \times 233}{200}} = 0.0095$$

$$\Rightarrow K_{zt} = \left[1 + (0.53 \times 0.95)(1 \times 1)(0.0066 \times 0.0095)\right]^2 = 1.000063 \tag{3-19}$$

For wind directionality factor, $K_d = 0.85$. From Figure 3.9, basic wind speed is 110 miles per hour (use the last wind speed contour of the coastal area). Importance factor, I, is taken as 1.0 while the system belongs to category II.

Recall Eq.(3-14), to compute q_z

$$q_z = 0.00256 K_z K_{zt} K_d V^2 I$$
$$\Rightarrow q_z = 0.00256 \times 1.258 \times 1.000063 \times 0.85 \times 110^2 \times 1.0$$
$$\Rightarrow q_z = 33.1247 \left(lb / ft^2 \right) \tag{3-20}$$

For gust effect factor, G, use the following formula:

$$G_f = 0.925 \left(\frac{1 + 1.7 I_{\bar{z}} \sqrt{g_Q{}^2 Q^2 + g_R{}^2 R^2}}{1 + 1.7 g_v I_{\bar{z}}} \right) \tag{3-21}$$

in which I_z = intensity of turbulence; g_Q = peak factor for background response; g_R = peak factor for resonant response; g_v = peak factor for wind response. g_Q and g_v shall be taken as 3.4. The background response Q is given by

$$Q = \sqrt{\frac{1}{1 + 0.63 \left(\frac{B + h}{L_{\bar{z}}} \right)^{0.63}}} \tag{3-22}$$

in which B = horizontal dimension of structure measured normal to wind direction (ft); h = height of a structure. L_z = integral length scale of turbulence. The choice of the magnitude of B of the arch system is not easy to determine because the arch system is not a solid building with regular shape. The diameter of arch member is 5 ft, which means 10-ft width to be the width of obstacle for wind. Therefore, B is taken to be 10 ft.

$$L_{\bar{z}} = l \left(\frac{\bar{z}}{33} \right)^{\bar{\varepsilon}} \tag{3-23}$$

Substituting given constants, L_z becomes

$$L_{\bar{z}} = 320 \left(\frac{133}{33} \right)^{1/3.0} = 509.247 (ft) \tag{3-24}$$

And

$$Q = \sqrt{\frac{1}{1 + 0.63 \left(\frac{10 + 133}{509.247} \right)^{0.63}}} = 0.8828 \tag{3-25}$$

The resonant response factor, R, is calculated by

$$R=\sqrt{\frac{1}{\beta}R_nR_hR_B\left(0.53+0.47R_L\right)} \tag{3-26}$$

where

$$R_n=\frac{7.47N_1}{\left(1+10.3N_1\right)^{5/3}}$$

$$N_1=\frac{n_1L_{\bar{z}}}{\bar{V}_{\bar{z}}}$$

$$\bar{V}_{\bar{z}}=\bar{b}\left(\frac{z}{33}\right)^{\bar{\alpha}}V\left(\frac{88}{60}\right)$$

$$\eta>0\Rightarrow R_l=\frac{1}{\eta}-\frac{1}{2\eta^2}\left(1-e^{-2\eta}\right)$$

$$\eta=0\Rightarrow R_l=1 \tag{3-27}$$

where the subscript l in Eq.(3-27) shall be taken as h, B, and L respectively. That means

$$R_l=R_h\Rightarrow\eta=4.6\frac{n_1h}{\bar{V}_{\bar{z}}}\Rightarrow R_h=\frac{1}{\eta}-\frac{1}{2\eta^2}\left(1-e^{-2\eta}\right)$$

$$R_l=R_B\Rightarrow\eta=4.6\frac{n_1B}{\bar{V}_{\bar{z}}}\Rightarrow R_B=\frac{1}{\eta}-\frac{1}{2\eta^2}\left(1-e^{-2\eta}\right)$$

$$R_l=R_L\Rightarrow\eta=4.6\frac{n_1L}{\bar{V}_{\bar{z}}}\Rightarrow R_L=\frac{1}{\eta}-\frac{1}{2\eta^2}\left(1-e^{-2\eta}\right) \tag{3-28}$$

Substitute the given constants into Eq.(3-28), it yields to

$$\bar{V}_{\bar{z}}=0.45\times\left(\frac{133}{33}\right)^{0.25}\times110\times\frac{88}{60}=102.87$$

$$\eta=4.6\times\frac{0.3376\times133}{102.87}=2.0078\Rightarrow R_h=0.3763$$

$$\eta=4.6\times\frac{0.3376\times10}{102.87}=0.151\Rightarrow R_B=0.9065$$

$$\eta=4.6\times\frac{0.3376\times10}{102.87}=0.151\Rightarrow R_L=0.9065 \tag{3-29}$$

Here B = L =10 ft and N_1 = 1.6713 as calculated. Thus, R_n = 0.099. Assume damping ratio for each mode is 2% = 0.02, R equals to 0.3092.

Intensity of turbulence at height z is computed by

$$I_{\bar{z}} = c\left(\frac{33}{\bar{z}}\right)^{1/6} = 0.3\times\left(\frac{33}{133}\right)^{1/6} = 0.2378 \tag{3-30}$$

Peak factor for wind response is calculated by

$$g_R = \sqrt{2\ln(3600n_1)} + \frac{0.577}{\sqrt{2\ln(3600n_1)}}$$

$$\Rightarrow \sqrt{2\ln(3600\times 0.3376)} + \frac{0.577}{\sqrt{2\ln(3600\times 0.3376)}} = 3.922 \tag{3-31}$$

Recall Eq.(3-21), $G_f = 0.8994$.

For force coefficient factor, C_f, the formula is

$$C_f = 4.0\varepsilon^2 - 5.9\varepsilon + 4.0 \tag{3-32}$$

where ε = ratio of solid area to gross area of one structure face for segment under consideration. Take side projection of the arch system (Figure 3.12), compute the value of ε to be 2231.4 / 7354.94 = 0.3034. Because there is some overlap at upper bracing members and the round shape of arch, take ε to be 0.25 would still be conservative.

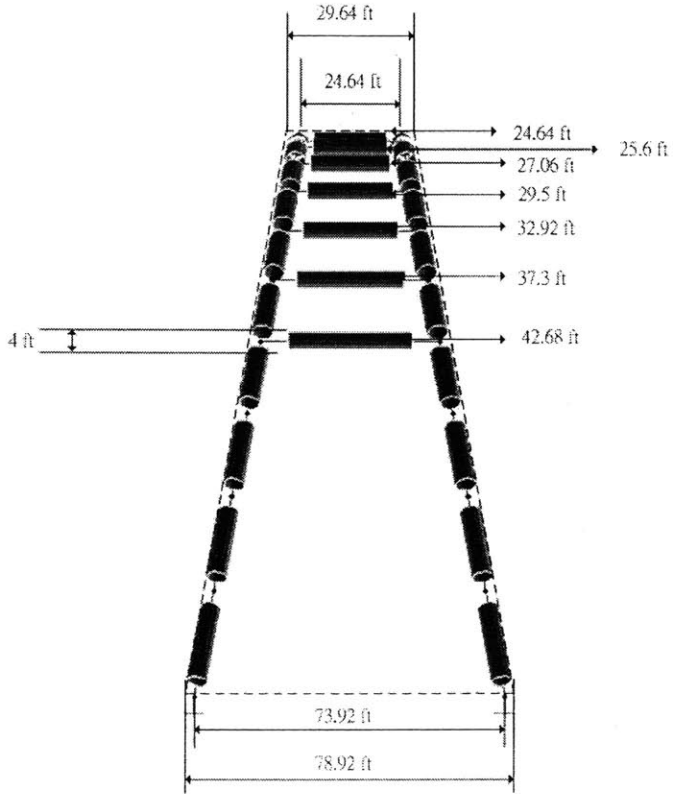

Figure 3.11 Side Projection of the System

Therefore, force coefficient factor C_f is computed to be 2.775. And finally, design wind load is to be 147582.63 lb = 147.583 kips.

The reduction of round shape from rectangle is because of the distribution of air current and the effect of vortex. The air current distribution is displayed in Figure 3.12.

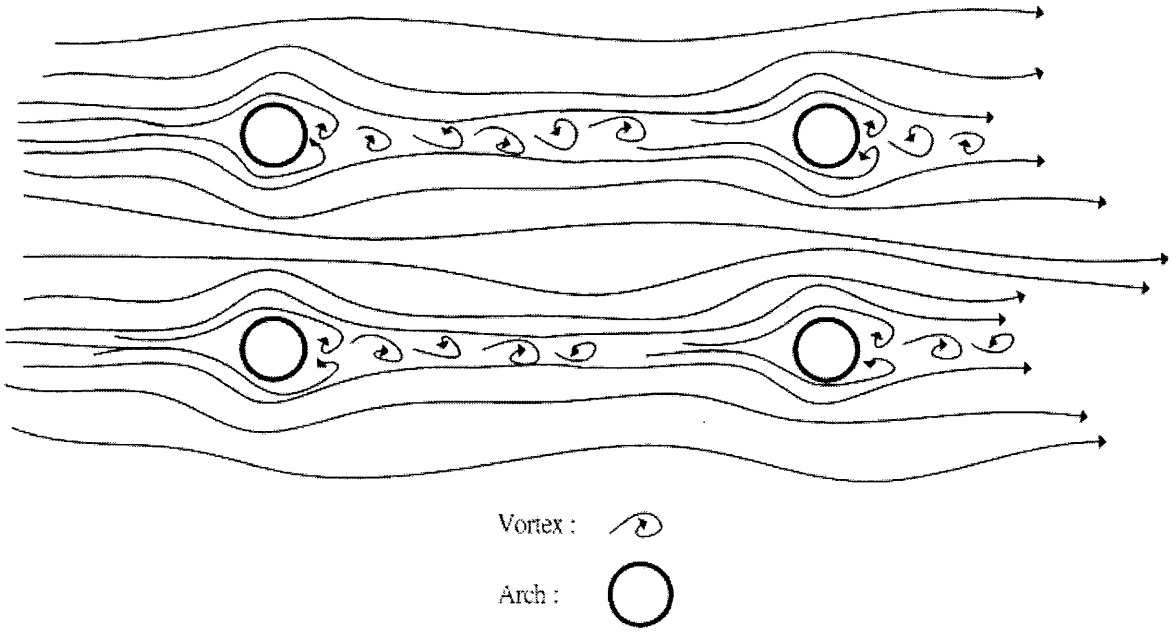

Figure 3.12 Distribution of Air Current (Top View)

If wind comes from the direction perpendicular to arch axis, different force coefficient factor ($C_f = 3.61$) is used and results in another wind load.

$$F = 33.1247 \times 0.894 \times 3.79 \times 899 = 101508.81(lb) \quad (3\text{-}33)$$

The application of horizontal distributed load will induce the problem of stability. This part is discussed in Chapter 4.

3.2.3 Concentrated Load

Concentrated loads are applied to the system when cables are hang below it or when pillars are supported above it. The application of hanging cables is usually for supporting a bridge slab (for through type arch bridge) or elevated structure. Pillars are used when arch is used in deck type arch bridge. Different types of bridge are shown in Figure 3.13. The magnitude of concentrated load is assumed to be constant and the result

of stiffness analysis will be normalized to obtain a dimensionless relationship between variables.

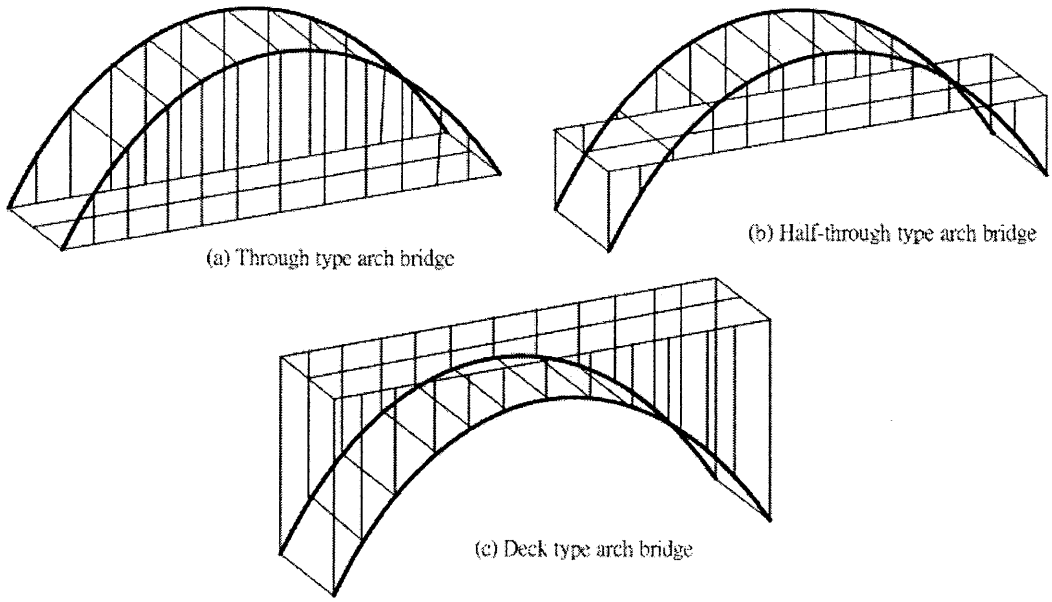

Figure 3.13 Different types of arch bridge

3.3 Numerical Approach

There are many available approaches to be used for research. They can be categorized into three main types: analytical, experimental and numerical. Their pros and cons are briefly discussed in the following section.

3.3.1 Analytical, Experimental and Numerical Approaches

The advantage of using analytical approach is its universality. Once governing equation is established and solved, an analytical answer is applicable to different cases of the same characteristics. Meanwhile, an analytical solution offers us the relationship between different variables. We can even derive some symbolic index for evaluating the response. The disadvantage of an analytical approach is establishing the model physically and solving the equation mathematically.

Another way is the experimental approach, which can be performed in model size (model test) or real size (full-scaled test). Nevertheless, experimental approach is

expensive because it requires hardware equipment, experimental material and a facility. It is not easy to exclude undesirable noise from the result. In addition, the correlation between experimental model and target structure must be carefully established.

A numerical approach might be the most cost-efficient scheme. If one can form the physical relationship between different variables, he can build numerical model simultaneously if the required physical constants are accessible. Numerical approaches earn their popularity because of their ability to solve problems that analytical approaches are incapable of solving, especially for structures of complicated shape.

The analysis is achieved by numerical approach.

3.3.2 Finite Element Method and Its Procedures

Finite element method (FEM) is a technique of solving differential equations of a boundary value problem. Because the governing equation of structures are differential equation in terms of displacement (or force), FEM can provide information about displacement (or force) which is essential for engineering analysis and design. Procedures of FEM (displacement method) are:

i) Divide a continuum into small regular (rectangle or triangle) element of finite number. They are connected with nodes.

ii) Assume nodal displacement as unknown variable, express the displacement between nodes by adequate displacement (shape) function. Continuity is required between elements.

iii) Solve for strain in the elements by displacement functions.

iv) Through physical relations, express stress in the elements in terms of nodal displacement.

v) Compute equivalent concentrated forces at nodes by stresses in elements. Then calculate nodal stiffness matrix.

vi) Compose nodal stiffness matrices into a structural stiffness matrix. The product of the structural stiffness matrix and an unknown displacement vector is the given nodal force vector.

vii) Solve the unknown displacement by matrix operation. Solve for stresses in the elements by nodal displacement.

Through rational dividing of the structure into elements and adopting adequate displacement function, the answer by FEM will be convergent and the same as analytical solution at nodes.

Structural Analysis Program (SAP) version 2000 is used for establishing numerical model and performing static and dynamic analyses. It is a commercial software package developed by Computers and Structures, Inc., California.

The results for several sample structures executed by SAP2000 are verified and compared with analytical solution in Appendix A.

3.4 Material

The default material in this thesis is steel. Steels are an iron based alloy with various outstanding characteristics such as resistance to abrasion and corrosion. A variety of steels exist with properties ranging from low to high strength, and from ductile to brittle. These properties are obtained by controlling the production, through the rolling process, the heat treatment, and through the combination and proportion of alloy elements such as Ni, Cr, and Mo, and so on.

The mechanical properties of steel are shown in Table 3.1.

Table 3.1 Mechanical Properties of Steel (E. Mizuno, 1997)

Unit Weight		7.70×10^{-2} N/cm^3	0.106×10^{-2} lb/in^3
Tensile Strength	Pure Iron	9.81×10^{1} MPa	14.22 ksi
	Mild Iron	$(1.96\sim3.92) \times 10^{2}$ MPa	28.42~56.84 ksi
	High Tensile Strength Steel	$(3.92\sim9.81) \times 10^{2}$ MPa	56.84~142.25 ksi
	High Strength Steel	$(8.83\sim13.7) \times 10^{2}$ MPa	128.04~198.65 ksi
	Super High Strength Steel	$(11.8\sim27.5) \times 10^{2}$ MPa	171.1~398.75 ksi
	Theoretical Strength	1370×10^{2} MPa	19865 ksi
Young's Modulus		2.06×10^{5} MPa	29.87×10^{3} ksi
Coefficient of Linear Expansion		1.23×10^{-5} / ° C	

Typical stress-strain curve for metal is also shown in Figure 3.14.

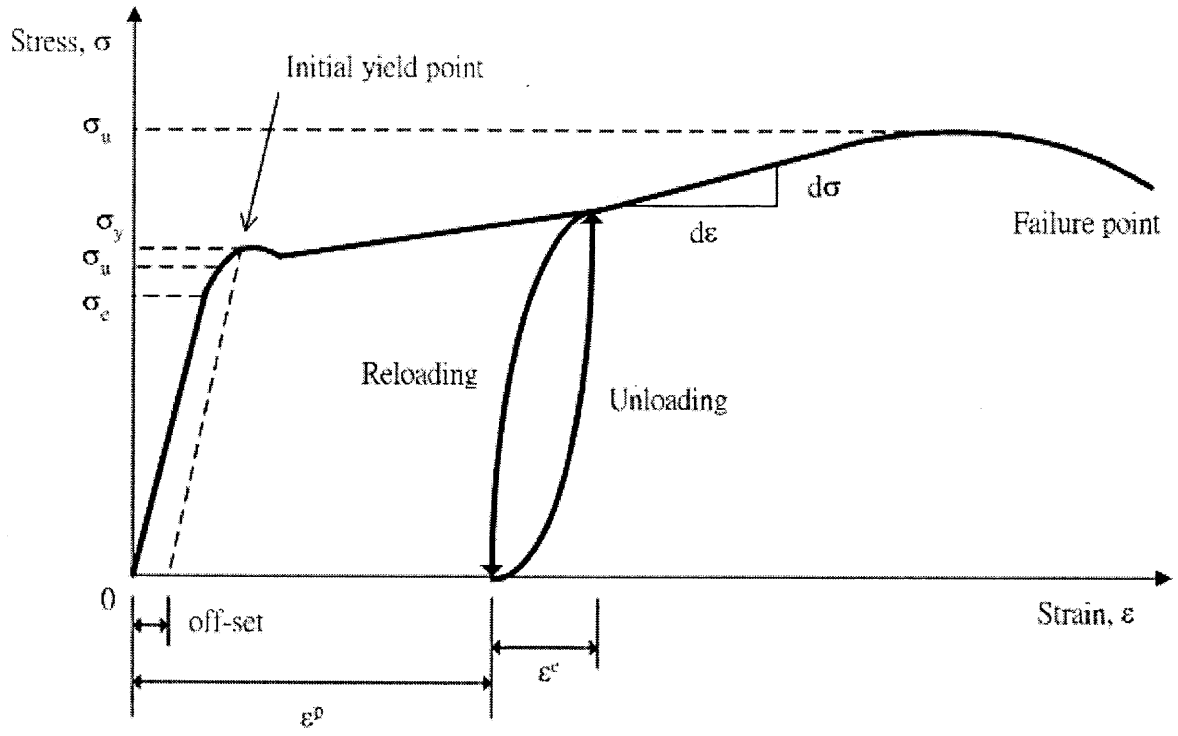

Figure 3.14 Typical Stress-Strain Curve for Metal

In Figure 3.14, σ_e is the maximum elastic stress, σ_y is the initial yield stress and σ_u is the ultimate stress. The stress-strain relationship in a certain range can be considered to be linear. The ultimate stress is also called proportional limit. The deformation within the proportional limit is linear. The limit at which the deformation always returns to its original state after unloading is called the elastic limit, σ_e. Once the stress is loaded beyond the elastic limit, a part of the deformation will remain even after the stress is fully decreased to zero. The irreversible strain is called inelastic strain and the reversible part is called elastic strain.

Steel (ASTM f_y = 36 ksi) is the default material in this thesis. Its weight per unit volume is 0.4908 kips/ft^3. Young's modulus is 4,176,000 kips/ft^2. Poisson's ratio is 0.3.

Chapter 4 Analysis of A Coupled Arch System

4.1 Overview

In this chapter, a coupled arch system is investigated through parametric analysis. First of all, the concept of arch-column analogy is introduced and an arch analogy coefficient is proposed. It is applied to the analogy between an arch and a column both subjected to vertical loading at top.

Parametric analysis is carried out by varying three characteristic parameters (rise-to-span ratio, leaning-to-depth ratio, and slenderness ratio) on vertical and horizontal stiffness. Two main types of boundary conditions are considered here.

A stability analysis is also performed. In-plane buckling loads and out-of-plane buckling loads are computed for different loads and brace members.

Finally, the structural efficiency of different arches is discussed using different perspectives.

4.2 Concept of Arch-Column Analogy

The similarity between arches and columns is due to the fact that their main internal actions are bending moment and axial force. Even though arches and beams support external loading perpendicular to their main axes, shear force is more important for beams than for arches. Thus, arches behave like columns more than beams.

Timoshenko (1936) has evaluated the buckling loads of fundamental types of columns with different boundary conditions. The buckling load of a prismatic column subjected to a vertical concentrated load at its top is computed with the following formula.

$$P_{cr} = \frac{\pi^2 EI}{L_r^{\ 2}} \tag{4-1}$$

in which P_{cr} = buckling load of a column; EI = bending rigidity of column; L_r = reduced length of column. When the column is hinge-supported at two ends, L_r is the total length. When the column is fixed-supported at two ends, L_r is half the total length.

It is known that arch structures are most efficient if they carry their load in such a way that the funicular curve coincides with the centroidal axis of the arch rib (Melan

1915; Spofford 1937; Leliavsky 1982). Such an arch experiences only small displacements before buckling. Typical examples of arches under pure axial compression are:

i) A circular arch subjected to uniform normal pressure

ii) A parabolic arch subjected to a uniform vertical load distributed along its horizontal projection

ii) A catenary arch subjected to a uniform vertical load distributed along its arch axis.

Timoshenko (1961) and Austin (1971) derived the formulas of critical load for the cases above. The critical axial force at a quarter-span point $N_{q,cr}$ and the critical horizontal reaction H_{cr} are given as follows:

$$N_{q,cr} = \frac{\pi^2 EI}{\left(k_N \frac{l}{2}\right)^2}$$

$$H_{cr} = \frac{\pi^2 EI}{\gamma \left(k_H L\right)^2}$$

$$\gamma = \sqrt{1+4\left(\frac{h}{L}\right)^2} \qquad (4\text{-}2)$$

where k_N, k_H = effective length factors; L, l = span length and total length of an arch, respectively, EI = in-plane bending rigidity.

It is naturally to analogize the stiffness of an arch to the stiffness of a column (Figure 4.1). Let's define an analogy coefficient, α_{arch}. For a column subjected to concentrated load at its top, the axial stiffness is expressed in terms of Eq.(4-3):

$$k_{col} = \frac{AE}{L_c} \qquad (4\text{-}3)$$

in which AE = axial rigidity; L_c = length of column.

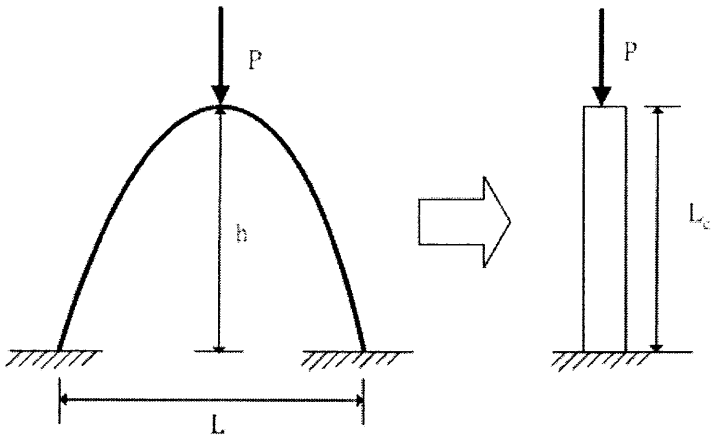

Figure 4.1 Arch-Column Analogy

The arch analogy coefficient, α_{arch} is defined as follows:

$$k_{arch} = \alpha_{arch} k_{col} = \alpha_{arch} \frac{AE}{L_c} \tag{4-4}$$

In Eq.(4-4), uniform cross section is applied on both the column and the arch. From Figure 4.1, in the case of a plane arch, one can find that α_{arch} is the function of the rise-to-span ratio, h/L. Through numerical analysis, the relationship between α_{arch} and h/L is obtained as shown in Figure 4.2.

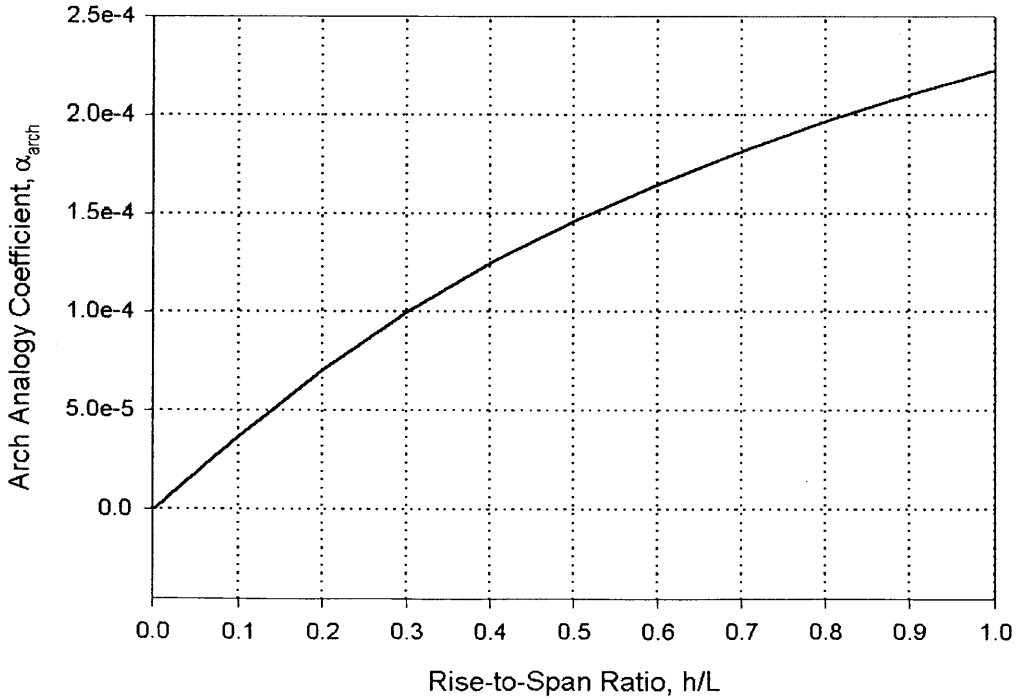

Figure 4.2 Arch Analogy Coefficients and Rise-to-Span Ratio (Two-Hinged Arch)

A numerical approach is applied and the expression of arch analogy coefficient is expressed in terms of the rise-to-span ratio. For a two-hinged arch, it has the following form

$$\alpha_{arch} = \frac{h}{L}\left[0.000367 - 0.000149\left(\frac{h}{L}\right)\right]$$

$$\Rightarrow k_{arch} = \frac{h}{L}\left[0.000367 - 0.000149\left(\frac{h}{L}\right)\right]k_{col}$$

$$\Rightarrow k_{arch} = \frac{h}{L}\left[0.000367 - 0.000149\left(\frac{h}{L}\right)\right]\frac{AE}{L_c}$$

$$\Rightarrow k_{arch} = \frac{AE}{L}\left[0.000367 - 0.000149\left(\frac{h}{L}\right)\right] \qquad (4\text{-}5)$$

in which h is the height of the arch, L is the span of the arch and L_c is the height of the column. Because $h = L_c$, the final form is obtained.

Similarly, the analogy coefficient for a fixed arch is also calculated and shown in Figure 4.3.

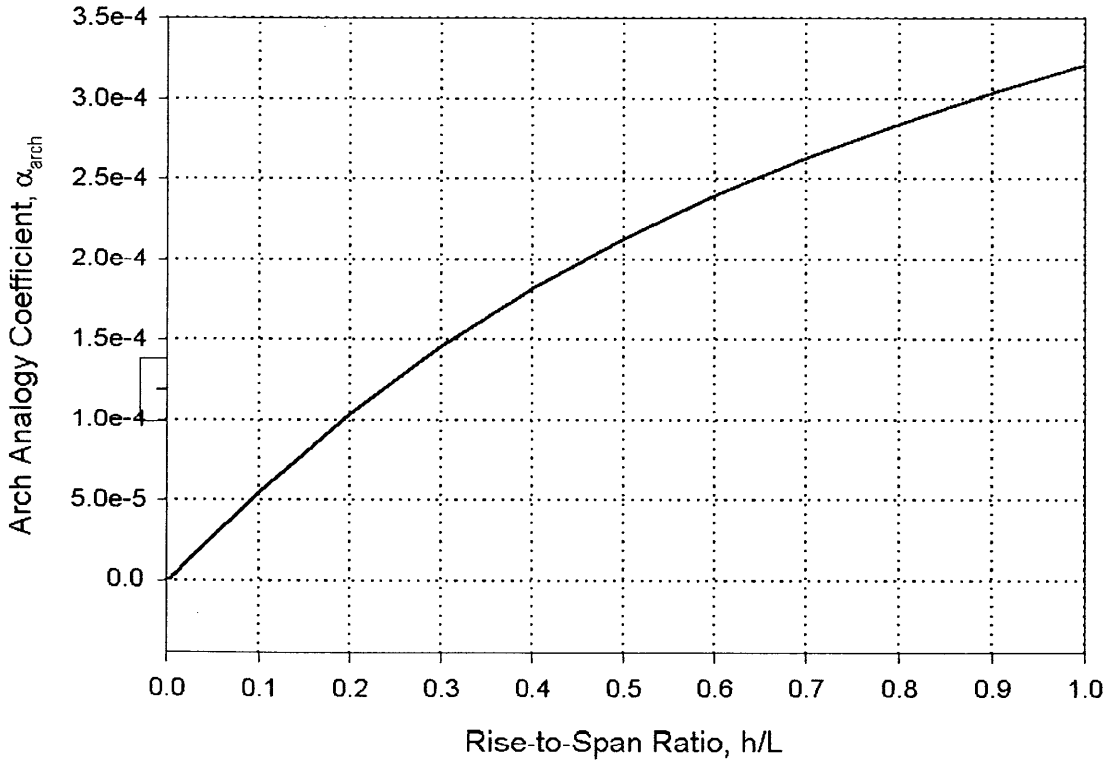

Figure 4.3 Arch Analogy Coefficient and Rise-to-Span Ratio (Fixed Arch)

The analogized arch stiffness expression for the fixed arch is

$$k_{arch} = \frac{h}{L}\left[0.000539 - 0.000224\left(\frac{h}{L}\right)\right]k_{col}$$

$$\Rightarrow k_{arch} = \frac{AE}{L}\left[0.000539 - 0.000224\left(\frac{h}{L}\right)\right] \quad (4\text{-}6)$$

Eqs.(4-5) and (4-6) are based on a circular tube section, with an outer diameter of 2 ft and thickness of 0.2 ft. The radius of gyration is 0.6403 ft. It should be noted that different areas can have the same moment of inertia, thus the corresponding radius of gyration is required to differentiate between cross sections. Transformation between different cross sections is given in Appendix B.

4.3 Rise-to-Span Ratio (RTS Ratio)

The rise-to-span ratio, h/L, plays an important role in the behavior of an arch. The difference between the load carrying capacity of high arches and low arches is of interest. Two types of boundary condition are considered here: hinged support and fixed support. Some material and geometrical properties are shown in Table 4.1.

Table 4.1 Material and Geometrical Properties of Numerical Model

Material Properties	
Material	AISC A36 Steel
Weight per volume	0.01 kips/ft^3 (0.005787 lb/in^3)
Modulus of elasticity	4,176,000 kips/ft^2 (29,000 kips/in^2)
Poisson's ratio	0.3
Yield stress	5,184 kips/ft^2 (36 kips/in^2)
Coefficient of thermal expansion	6.5 X 10^{-6} per degree (C)
Geometrical Properties	
Area of cross section	1.31 ft^2 (188.64 in^2)
Moment of inertia	0.4637 ft^4 (9615.28 in^4)
Radius of gyration	0.6403 ft (7.6836 in)
Shear area	0.656 ft^2 (94.46 in^2)
Plastic modulus	0.6507 kips/ft^2 (0.00452kips/in^2)
Span of arch	1400 ft (16800 in)

Since the investigation of the horizontal reactions of different arches subjected to different loads has been made by previous researchers (Melan(1915), Spofford(1937), Leontovich(1959), Leliavsky(1982) et al.), it is clear how stiffness varies with the rise-to-span ratio and the boundary conditions.

In these cases, stiffness is defined as

$$k = \frac{P}{\Delta} \tag{4-9}$$

in which k = stiffness; P = concentrated load; Δ = displacement (positive if with the same direction of loading.)

4.3.1 Vertical Stiffness

Numerical results will be given in 4.3.1 and 4.3.2 and a discussion will be presented in 4.3.3. The vertical axis is normalized stiffness with respect to maximum value, which is 1 in the plot. The effect of uniformly distributed loading on arch will be discussed in next section.

4.3.1.1 Two-Hinged Arch

Numerical results are illustrated in the following figures.

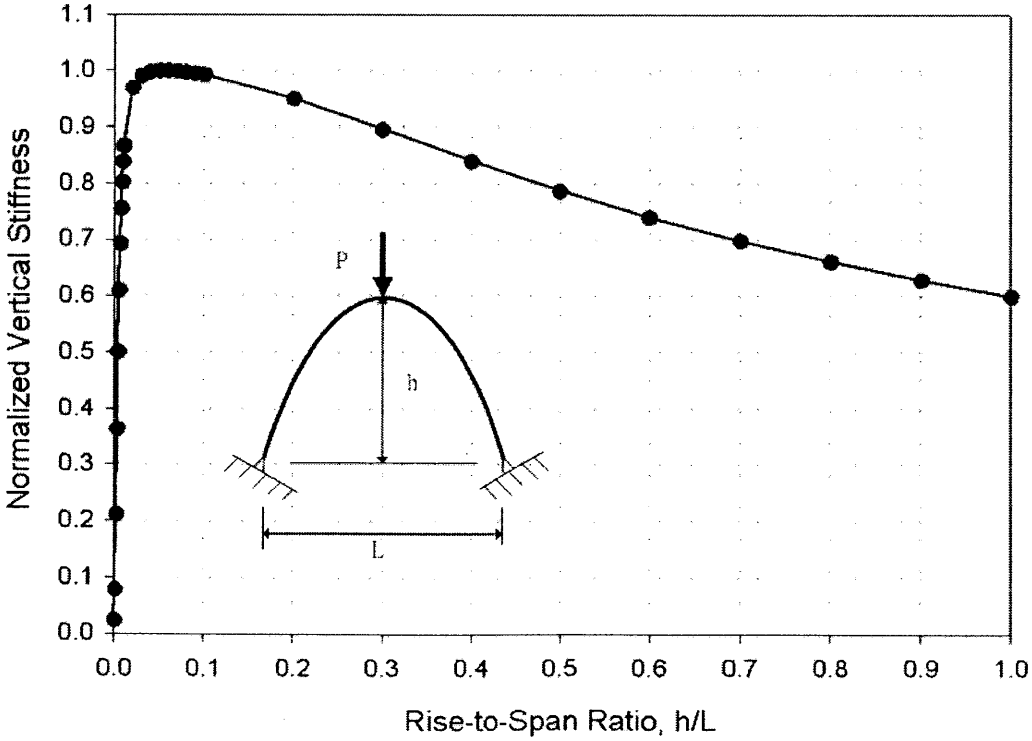

Figure 4.4 Rise-to-Span Ratio vs. Vertical Stiffness (Two-Hinged Arch)

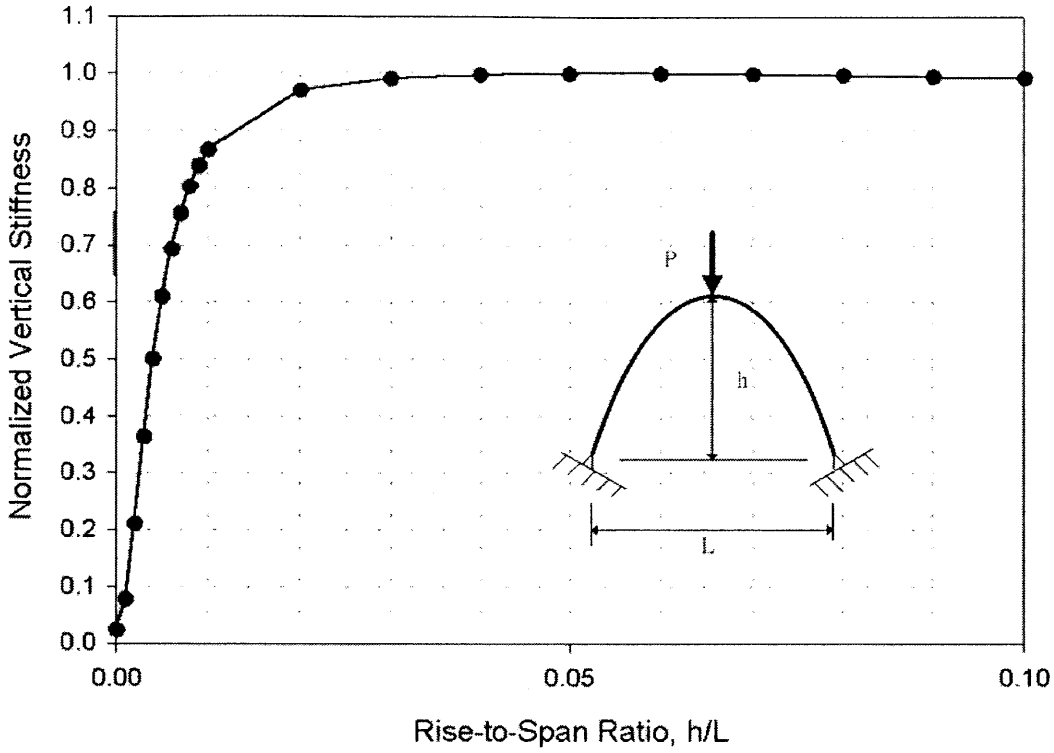

Figure 4.5 Rise-to-Span Ratio vs. Vertical Stiffness (Enlarged)

4.3.1.2 Fixed Arch

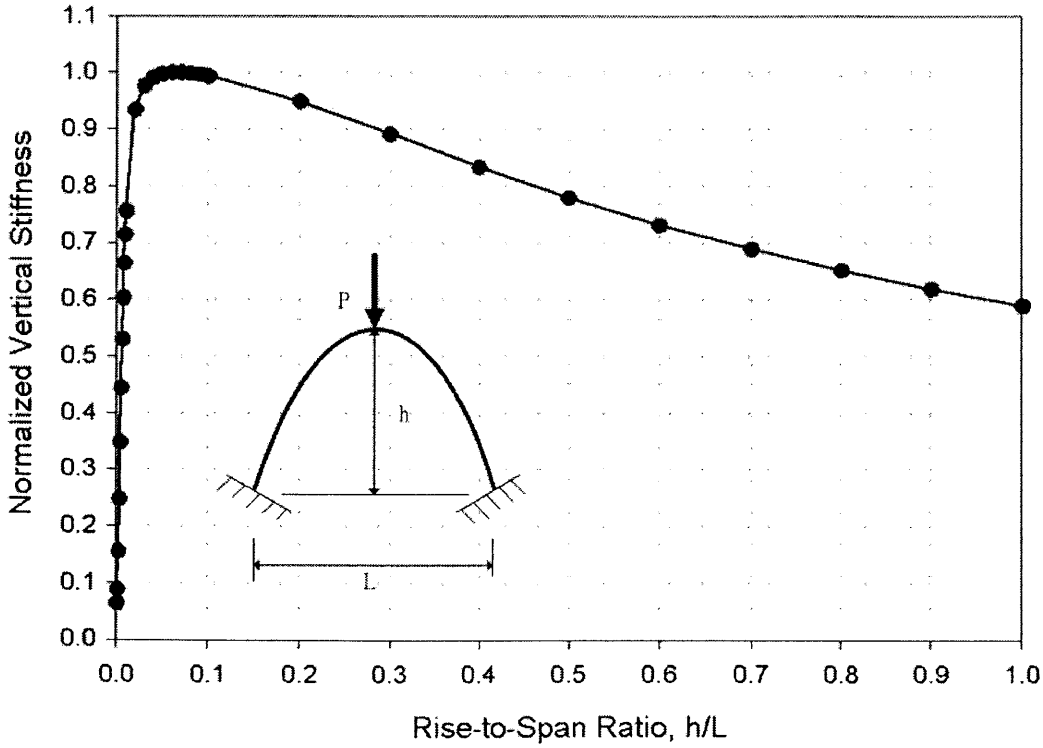

Figure 4.6 Rise-to-Span Ratio vs. Vertical Stiffness (Fixed Arch)

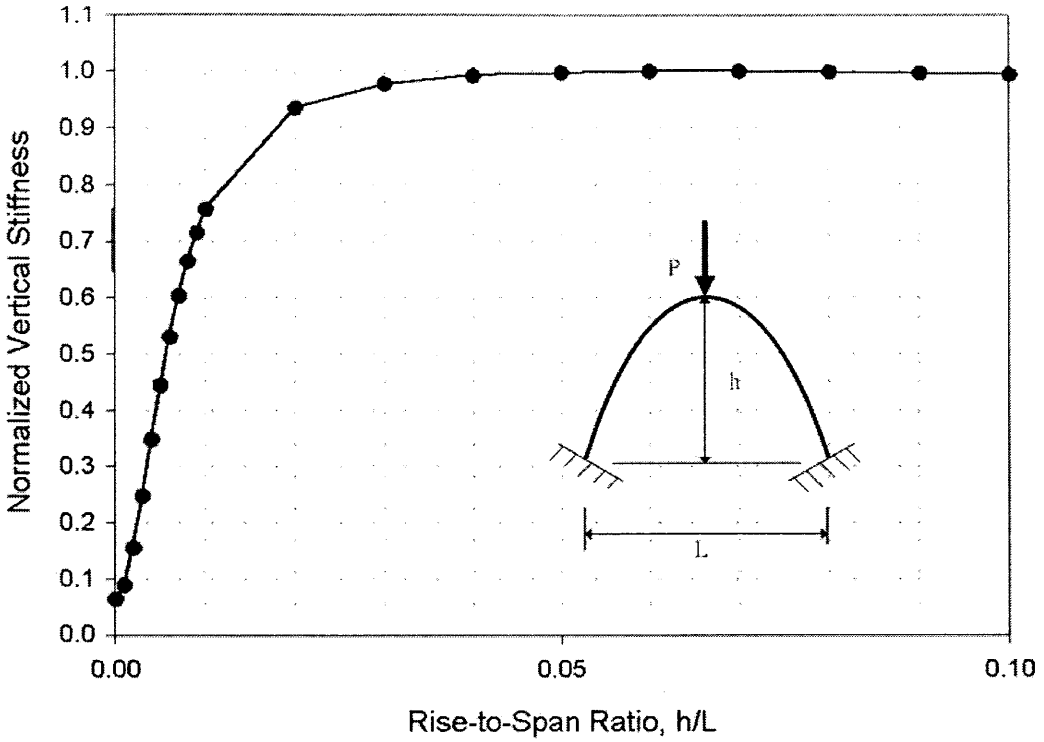

Figure 4.7 Rise-to-Span Ratio vs. Vertical Stiffness (Enlarged)

4.3.1.3 Discussion

With the information in Table 4.1, numerical results are obtained and arranged in Figures 4.4, 4.5, 4.6, and 4.7. Two facts are observed:

i) The maximum vertical stiffness of a two-hinged arch occurs when the rise-to-span ratio equals 0.06.

ii)The maximum vertical stiffness of a fixed arch occurs when the rise-to-span ratio equals 0.07.

From i) and ii), it is found that the strongest configuration of arch is with a small rise-to-span ratio (about 0.06). A stiffness ratio is defined as stiffness of two-hinged arch to stiffness of fixed arch. It is known that the arch with fixed ends will be stiffer than the hinged arch, thus, this ratio is always greater than unity. Figures 4.8 and 4.9 show the results.

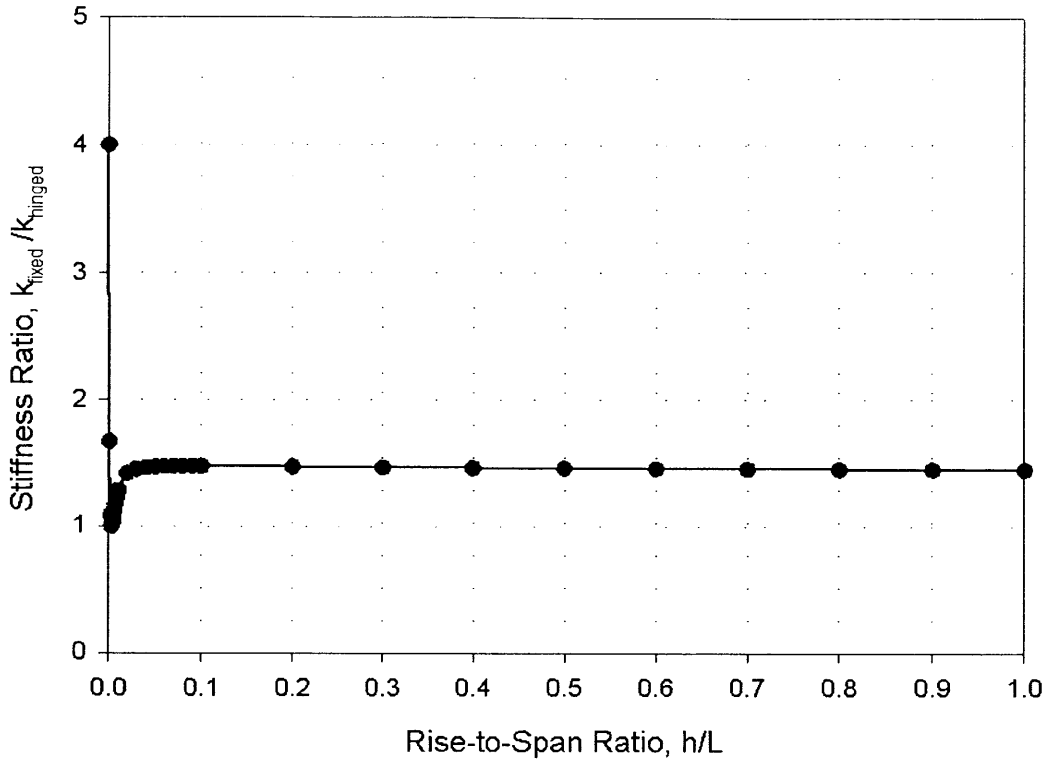

Figure 4.8 Vertical Stiffness Ratio, k_{fixed}/k_{hinged}

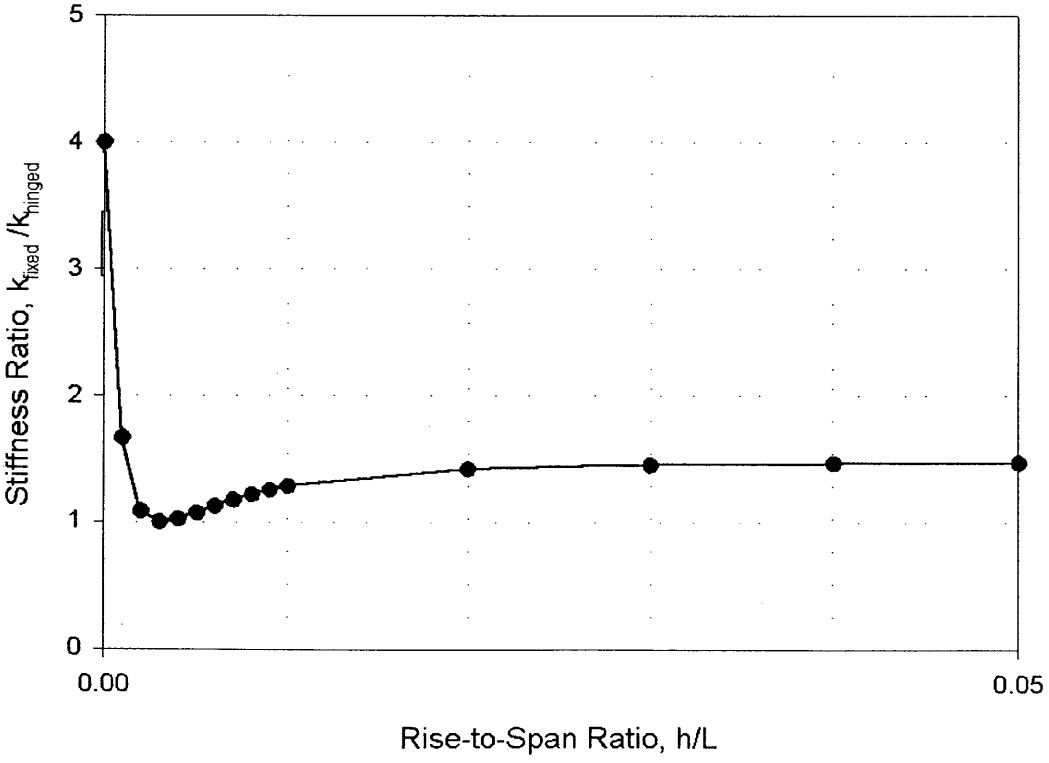

Figure 4.9 Vertical Stiffness Ratio (Enlarged)

Figure 4.8 shows the global trend of stiffness ratios with respect to the range of rise-to-span ratios between 0 and 1. Figure 4.9 shows enlarged parts of rise-to-span ratios ranging between 0 and 0.1.

For the vertical stiffness ratio, the contribution of boundary conditions decreases from 4 at first and reaches a minimum value of 1.0005 with respect to a rise-to-span ratio of 0.03. Then the curve increases to a level of 1.46 and remains stable in level. Several observed facts are arranged as follows:

i) The effect of boundary conditions is most pronounced when the rise-to-span ratio is zero (beam structure).

ii) When the rise-to-span ratio becomes 0.03, the contribution from fixed supports on stiffness will be almost the same as from simple support. That means, if one intends to design an arch subjected to concentrated loads at mid-span, in order to decrease the deflection by fixed supports, he must use a rise-to-span ratio greater than 0.01 or smaller than 0.001 to ensure his design purpose (if the rise-to-span ratio is not zero). That is to say, using fixed supports to decrease deflection will not be as efficient as one might expect during the range of rise-to-span ratio from 0.001 to 0.01.

iii) Notice that the value of the maximum ratio equals to an exact solution because

$$SimpleSupportedBeam \Rightarrow k_{simple} = \frac{48EI}{L^3}$$

$$FixedSupportedBeam \Rightarrow k_{fixed} = \frac{192EI}{L^3}$$

$$\Rightarrow \frac{k_{fixed}}{k_{simple}} = 4 \qquad (4\text{-}10)$$

when subjected to a concentrated load at mid-span.

iv) The contribution of a fixed support will be at most about 1.46 times than of simple support on vertical stiffness statically. However, when the stability problem is considered, this value will change.

v) When the rise-to-span ratio is over 0.02, the vertical stiffness ratio generally remains constant. This implies that when the rise-to-span ratio reaches a certain level, the contribution of a stronger support on stiffness becomes constant. Comparing to the very beginning value, one can say that the stiffness ratio decreases from the beginning and then maintains at a level.

vi) The change of curve between 0.001 and 0.01 of the rise-to-span ratio is interesting. Because the internal action of arch involves bending moment, shear force, and axial force, the interaction between them contributes the total stiffness.

The first decreasing segment means the bending rigidity at the two supports becomes less efficient than its original state. When the rise-to-span ratio reaches a specific value, their interaction improves the contribution and the stiffness ratio remains at a level.

The two types of boundary condition versus vertical and horizontal loads with respect to the rise-to-span ratio of zero are illustrated in Figure 4.10.

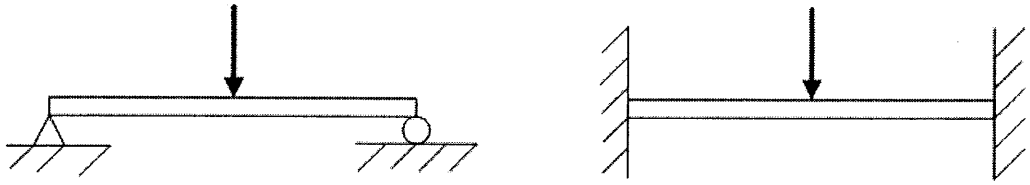

(a) Vertical Concentrated Load

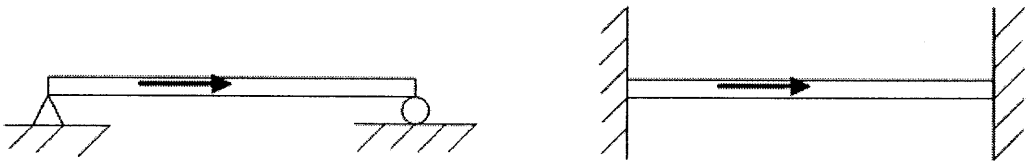

(b) Horizontal Concentrated Load

Figure 4.10 Different Loads and Different Boundary Conditions (RTS Ratio = 0)

4.3.2 Horizontal Stiffness

4.3.2.1 Two-Hinged Arch

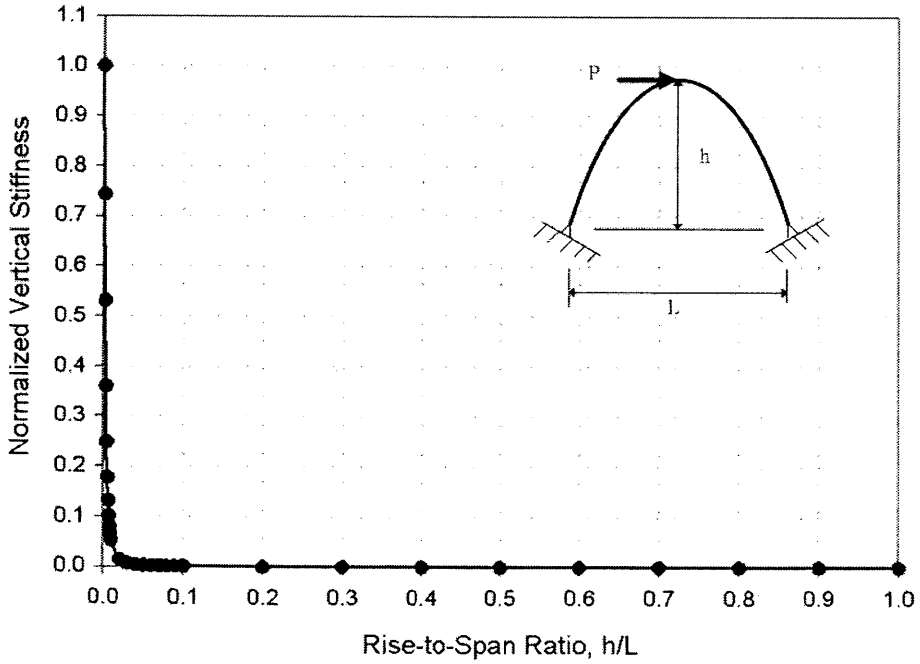

Figure 4.11 Rise-to-Span Ratio vs. Horizontal Stiffness (Two-Hinged Arch)

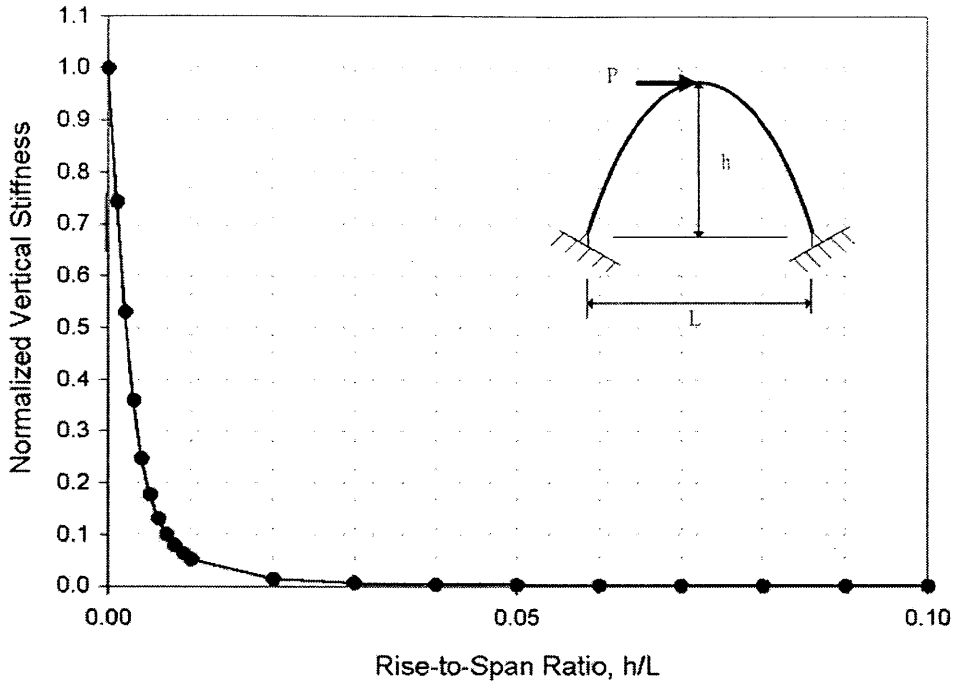

Figure 4.12 Rise-to-Span Ratio vs. Horizontal Stiffness (Enlarged between 0 and 0.1)

4.3.2.2 Fixed Arch

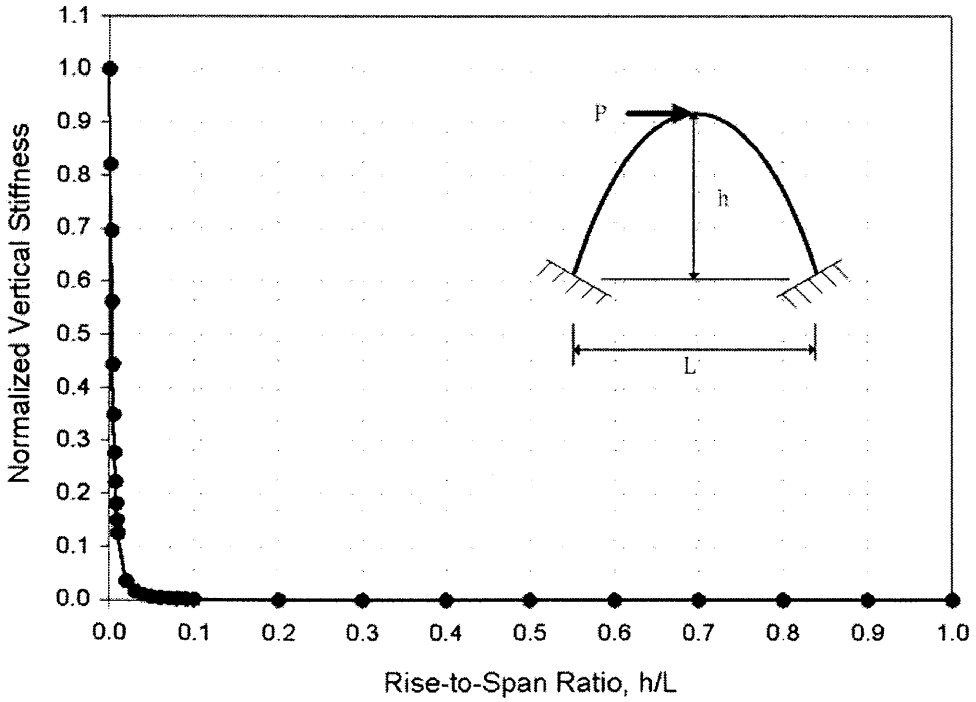

Figure 4.13 Rise-to-Span Ratio vs. Horizontal Stiffness (Fixed Arch)

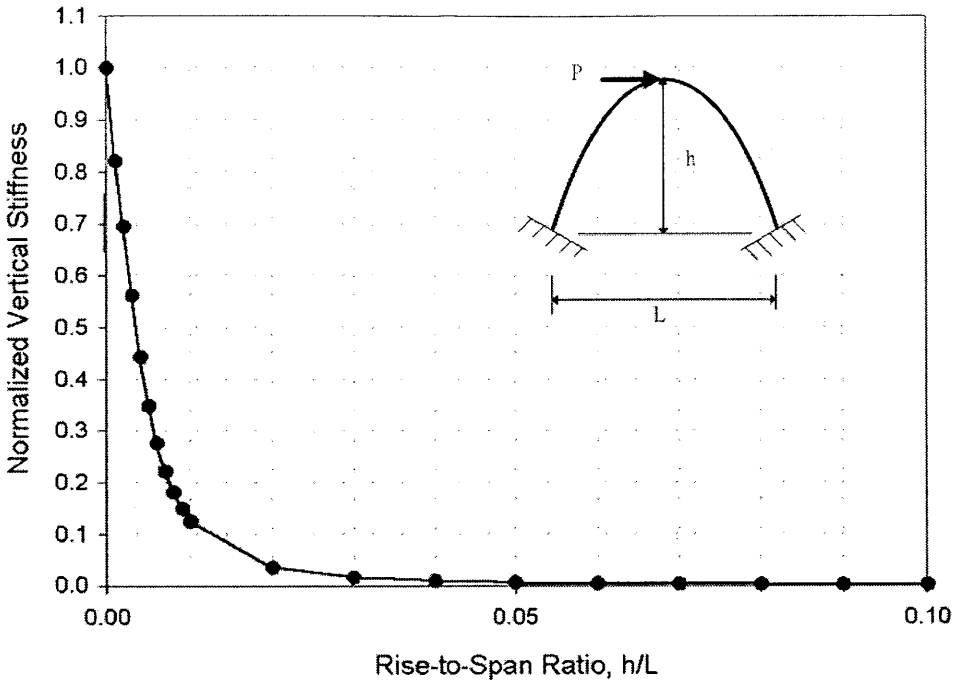

Figure 4.14 Rise-to-Span Ratio vs. Horizontal Stiffness (Enlarged)

4.3.2.3 Discussion

With the configuration in Table 4.1, numerical results are obtained and arranged in Figures 4.11, 4.12, 4.13, and 4.14. It is found that the maximum horizontal stiffness of two-hinged and fixed arches both occurs when the rise-to-span ratio equals 0. It is worth to point out that the values of horizontal stiffness with respect to the rise-to-span ratio greater than 0.05 are not zero! The normalized values of horizontal stiffness are in the order of magnitude of 10^{-4} ~ 10^{-6}. Their values are relatively smaller than the maximum but not zero.

In general, when the rise-to-span ratio increases, horizontal stiffness decreases sharply no matter what type of support is provided. However, the stiffness with fixed supports decreases more slowly than the stiffness with hinged supports.

From Figures 4.11~4.14, we cannot distinguish the effect of boundary conditions on horizontal stiffness because they are normalized to their individual maximum values. Hence, the plot of stiffness ratio is necessary for evaluating the effects of different supports. Figures 4.15 and 4.16 are given to show the effect.

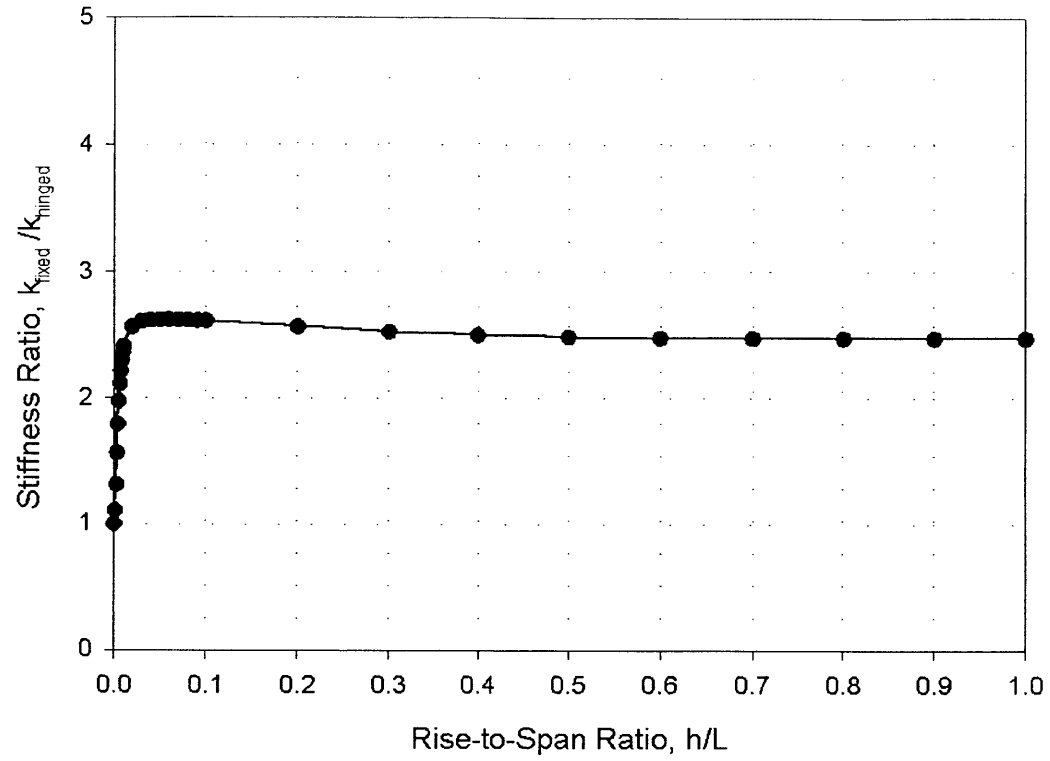

Figure 4.15 Horizontal Stiffness Ratio, k_{fixed}/k_{hinged}

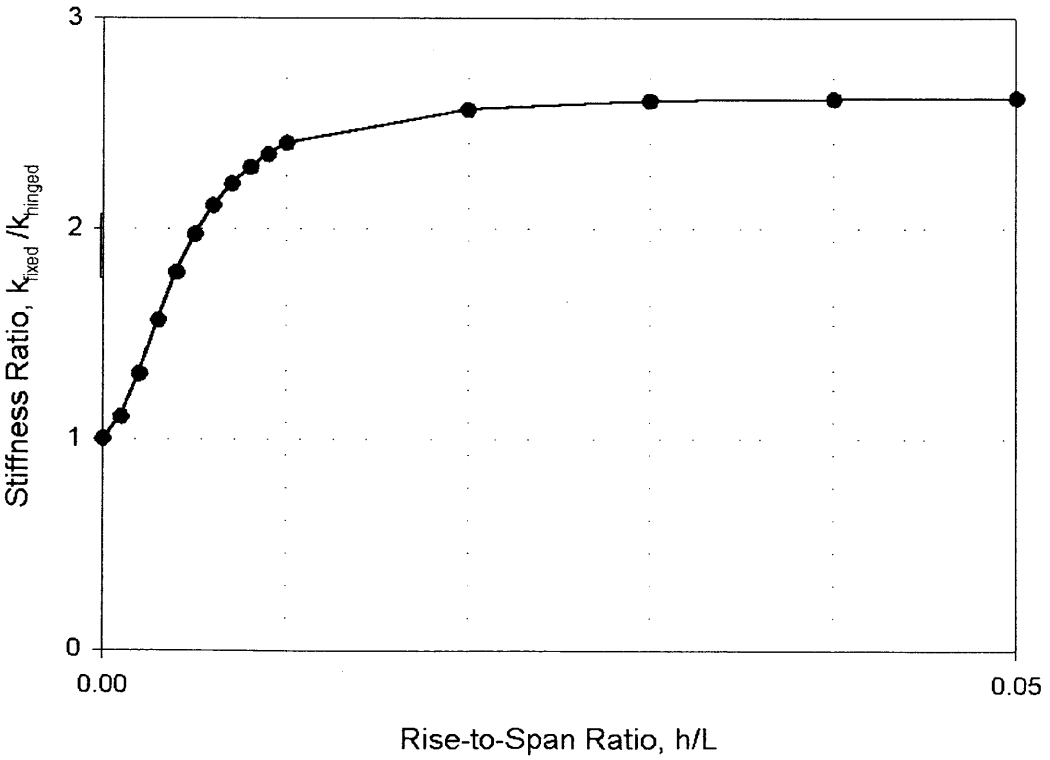

Figure 4.16 Horizontal Stiffness Ratio (Enlarged between 0 and 0.05)

The stiffness ratio increases from unity, reaches to a level of 2.5 then remains stable. It implies the maximum contribution from stronger support on horizontal stiffness in this case is limited to 2.5 times.

4.4 Leaning-to-Depth Ratio (LTD Ratio)

The leaning-to-depth ratio, L_d/D, not only determines the tilt angle of an arch but also indicates the contribution of brace members. The larger the ratio is, the smaller the tilt angle but the longer the brace member. Some researchers use tilt angle (Figure 4.17) to represent the configuration of an arch. The relationship between the tilt angle and the leaning-to-depth ratio is

$$\theta = \tan^{-1}\left[\frac{D}{2h}\left(1-\frac{L_d}{D}\right)\right] \tag{4-11}$$

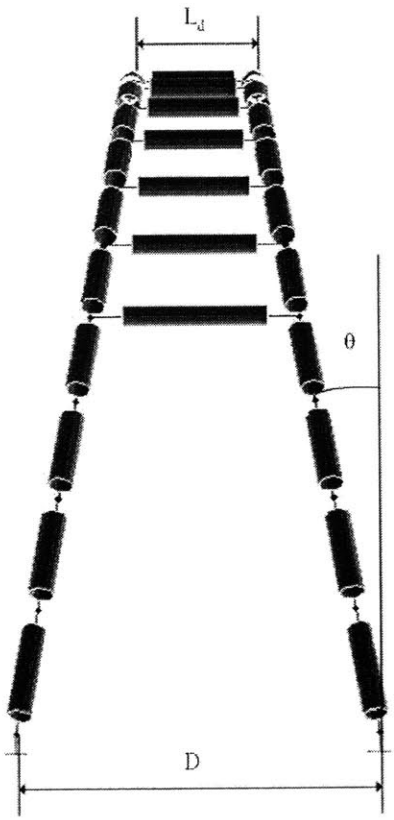

Figure 4.17 Leaning-to-Depth Ratio and Tilt Angle

When the leaning-to-depth ratio becomes zero, the two arches are connected at the

crown. There are brace members between two arches except the crown point. The braced range is fixed as an assumption, which means β is 0.6 as a constant in this thesis (Refer to Figure 4.18).

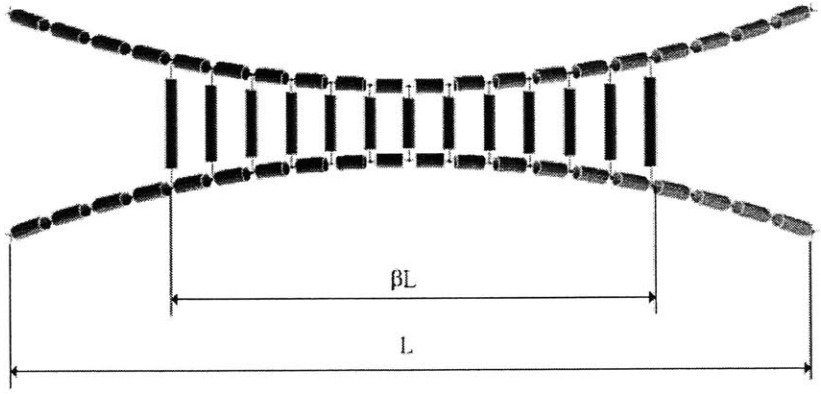

Figure 4.18 Braced Range

Numerical results of the leaning-to-depth ratio versus stiffness (vertical and horizontal) are displayed in the following sections.

4.4.1 Vertical Stiffness

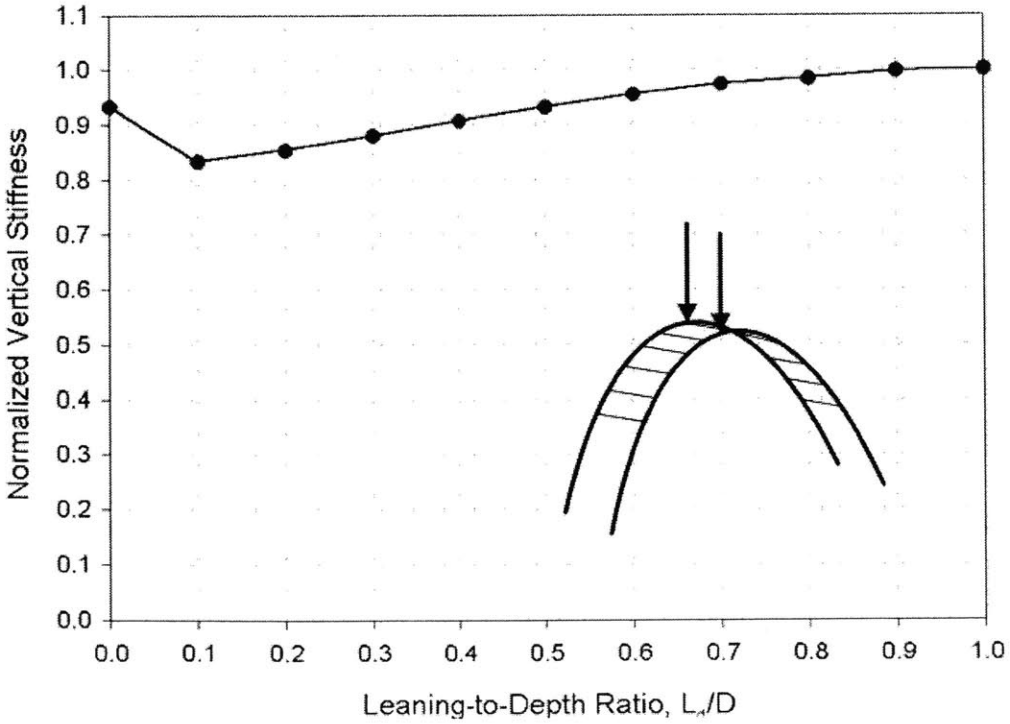

Figure 4.19 Leaning-to-Depth Ratio vs. Vertical Stiffness

4.4.2 Horizontal Stiffness

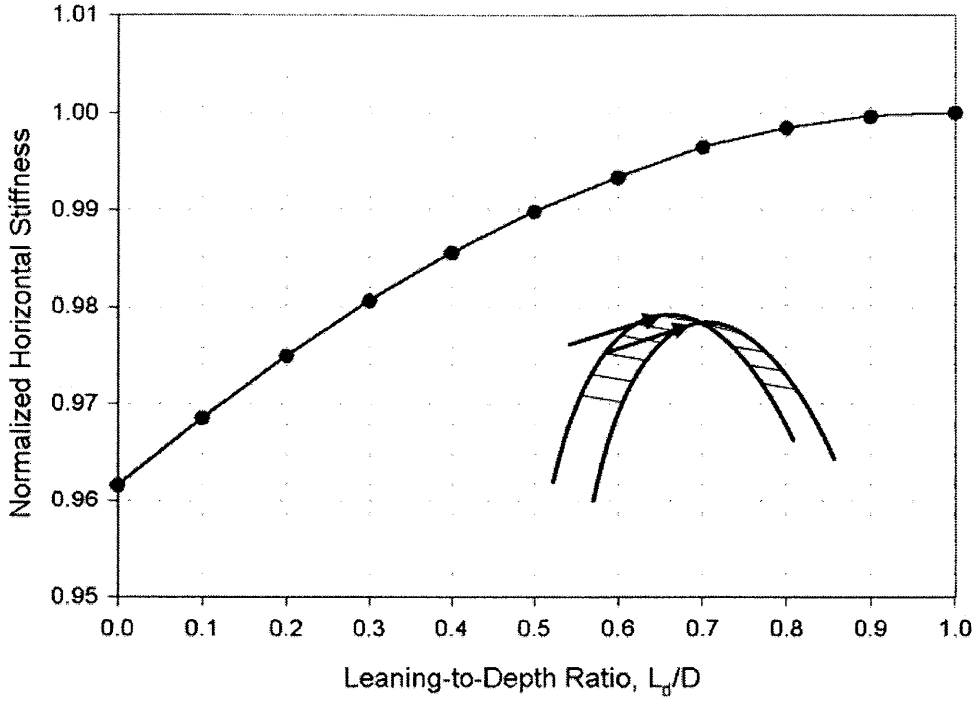

Figure 4.20 Leaning-to-Depth Ratio vs. In-Plane Horizontal Stiffness

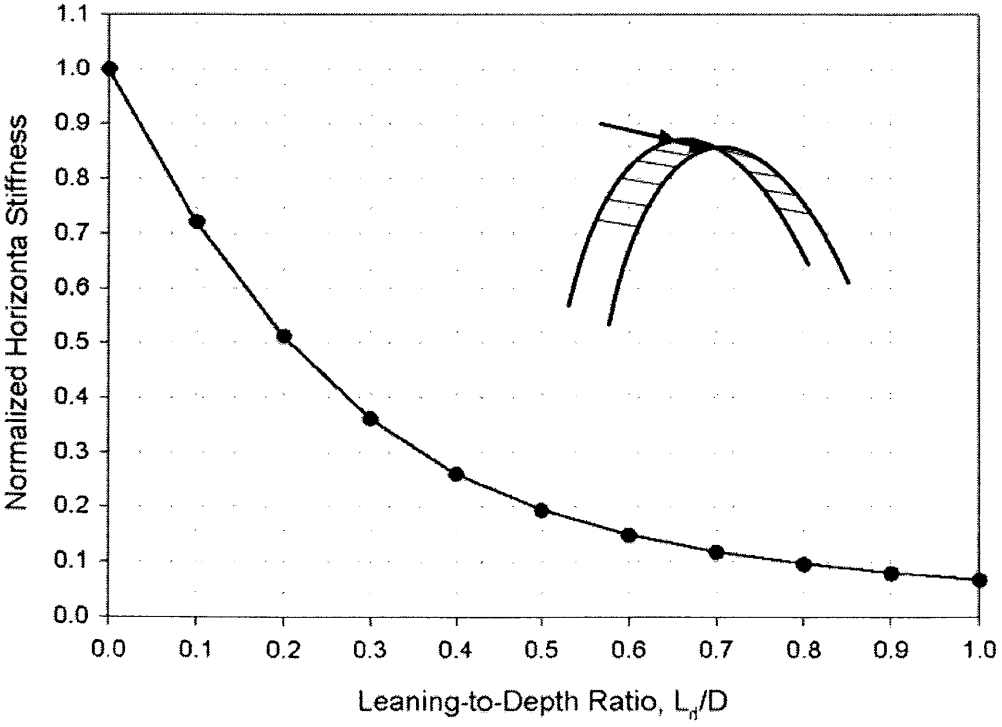

Figure 4.21 Leaning-to-Depth Ratio vs. Out-of-Plane Horizontal Stiffness

4.4.3 Discussion

From Figure 4.19, it is found that LTD ratio does not affect the vertical stiffness of the arch system to a large degree. The minimum stiffness occurs when two arches are slightly separated. When LTD ratio increases to unity, vertical stiffness approaches to maximum (LTD ratio = 1 is assumed to be the limit). This result is reasonable because when two arches tend to become vertical, the effect of torsion induced by vertical load in x-axis tends to diminish. Vertical stiffness increases from LTD ratio = 0.1 to LTD ratio = 0. The reason might be, when LTD ratio equals zero, that there is no brace member at the crown that happens to be the location where the vertical load is applied. We can check the variation of axial force in the brace members to see if the load-carrying mechanism changes or not. The numbering of brace members is shown in Figure 4.22. Since the structure and the loading are symmetrical, the distribution of axial force will also be symmetrical.

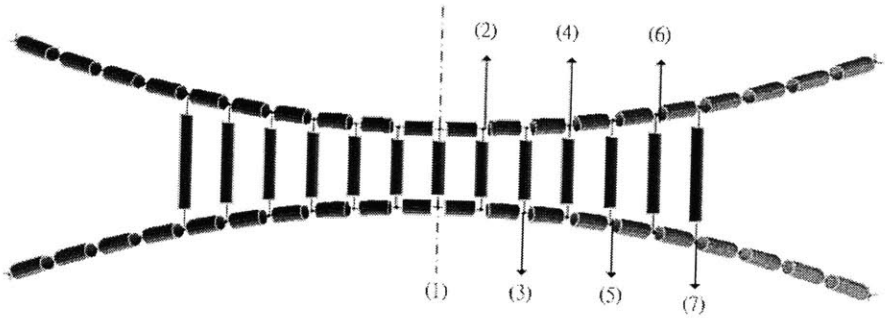

Figure 4.22 Numbering of Brace Members

From the distribution of axial forces in brace members (Figure 4.23), it is found that most of the brace members do not experience huge change in axial force when LTD ratio varies from zero to unity. There is only member 1, the one at crown, changes its axial force dramatically. One can also find that the change of axial force in member 1 corresponds to the change of vertical stiffness of structure. The results of statistical analysis of the similarity between these two curves are listed in Table 4.2.

Table 4.2 Results of Similarity Analysis by Statistics

Normalized Vertical Stiffness (NVS)		**Normalized Axial Force in Member 1** (NAV1)	
Mean value	0.851667	Mean value	0.871667

Variance	0.068631	Variance	0.070531
Covariance of NVS and NAV1		0.069306	
Correlation coefficient of NVS and NAV1		0.996142	

The correlation coefficient is 0.996142, which represents the high linear dependency between these two curves. The main reason may be because the position of member 1 happens to be the location of applied load, the load-carrying mechanism will be affected by the existence of member 1, especially when two arches are leaning against each other (LTD ratio = 0).

This phenomenon creates an interest to look at a representative member in the system that indicates the global behavior of system, corresponding to specific loading pattern. In this case, member 1 would be the representative member for vertical load acting over it.

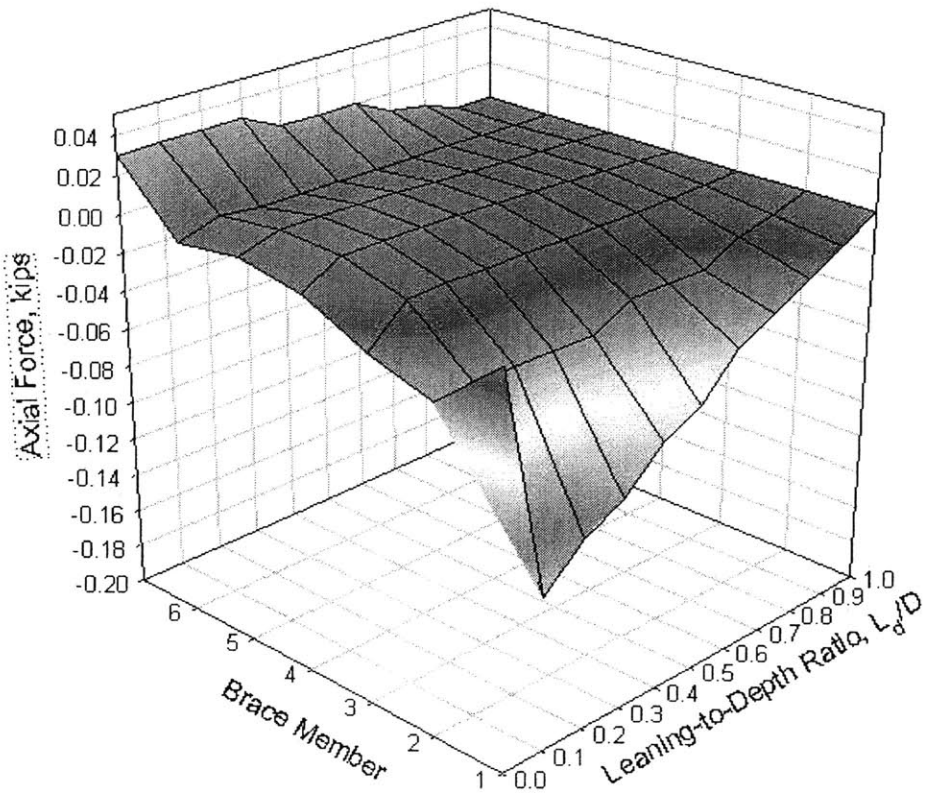

Figure 4.23 Variation of Axial Forces in Brace Members (Vertical Load)

From Figure 4.20, it is noted that decreasing LTD ratio results in a decrease of the in-plane horizontal stiffness. However, the change is not significant, less than 5% at most.

This is because the main contributor to in-plane horizontal stiffness, the two-arch system, does not change much with respect to the change of the LTD ratio. The contribution of the brace member to the in-plane horizontal stiffness is not essential.

Figure 4.21 shows that the out-of-plane horizontal stiffness decreases as the LTD ratio increases. It is because when the LTD ratio increases, two arches lose their horizontal component for resisting horizontal load. Thus, the stiffness decreases with respect to the increasing of the LTD ratio. One can also find that, increasing the LTD ratio will increase vertical stiffness in general, and increase in-plane horizontal stiffness. However, the out-of-plane horizontal stiffness decreases to a large degree (90% at most). Therefore, even a large LTD ratio can aid vertical and in-plane horizontal stiffness, when out-of-plane horizontal stiffness becomes an issue, a small LTD ratio is recommended.

The axial force distribution of in-plane horizontal stiffness is also provided in Figure 4.24. When taking an out-of-plane horizontal load, no axial force is generated in brace members.

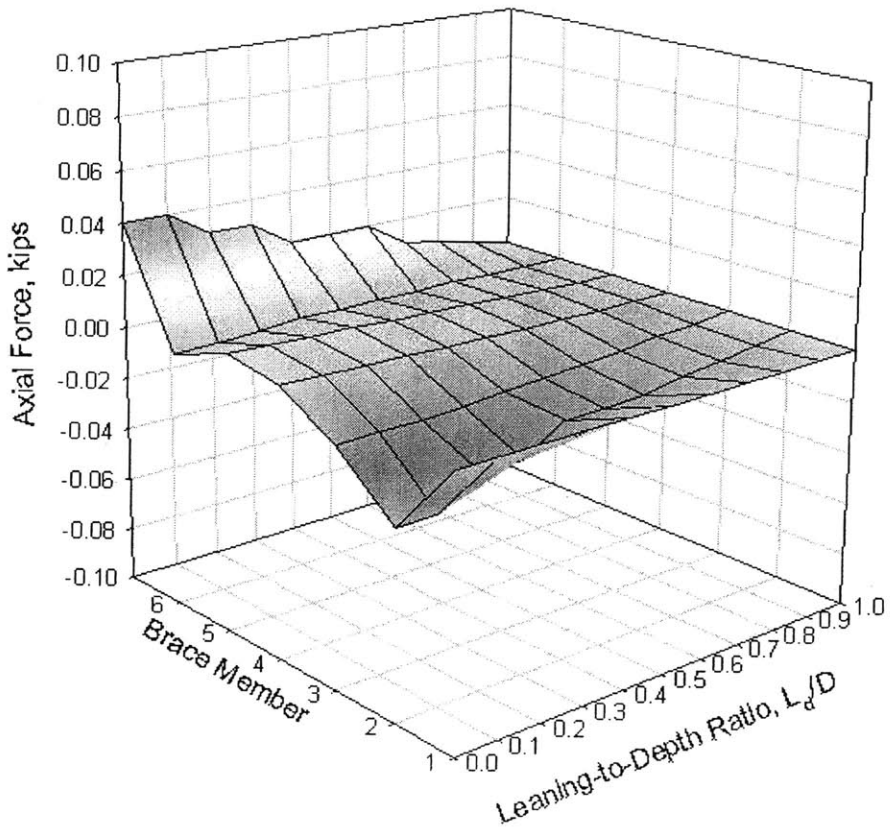

Figure 4.24 Variation of Axial Forces in Brace Members (In-Plane Horizontal Load)

4.5 Slenderness Ratio

Slenderness ratio is defined as

$$\frac{L}{r} = \frac{Length\ \ of\ \ Column}{Radius\ \ of\ \ Gyration} \tag{4-12}$$

Because of the geometry and symmetry, the slenderness ratio for an arch is defined as

$$\lambda = \frac{\frac{L_{arch}}{2}}{r} = \frac{L_{arch}}{2r} = \frac{Half\ \ Length\ \ of\ \ Arch}{Radius\ \ of\ \ Gyration} \tag{4-13}$$

in which the radius of gyration is computed at cross sections of the arch member. The following numerical results are based on a two-hinged arch model.

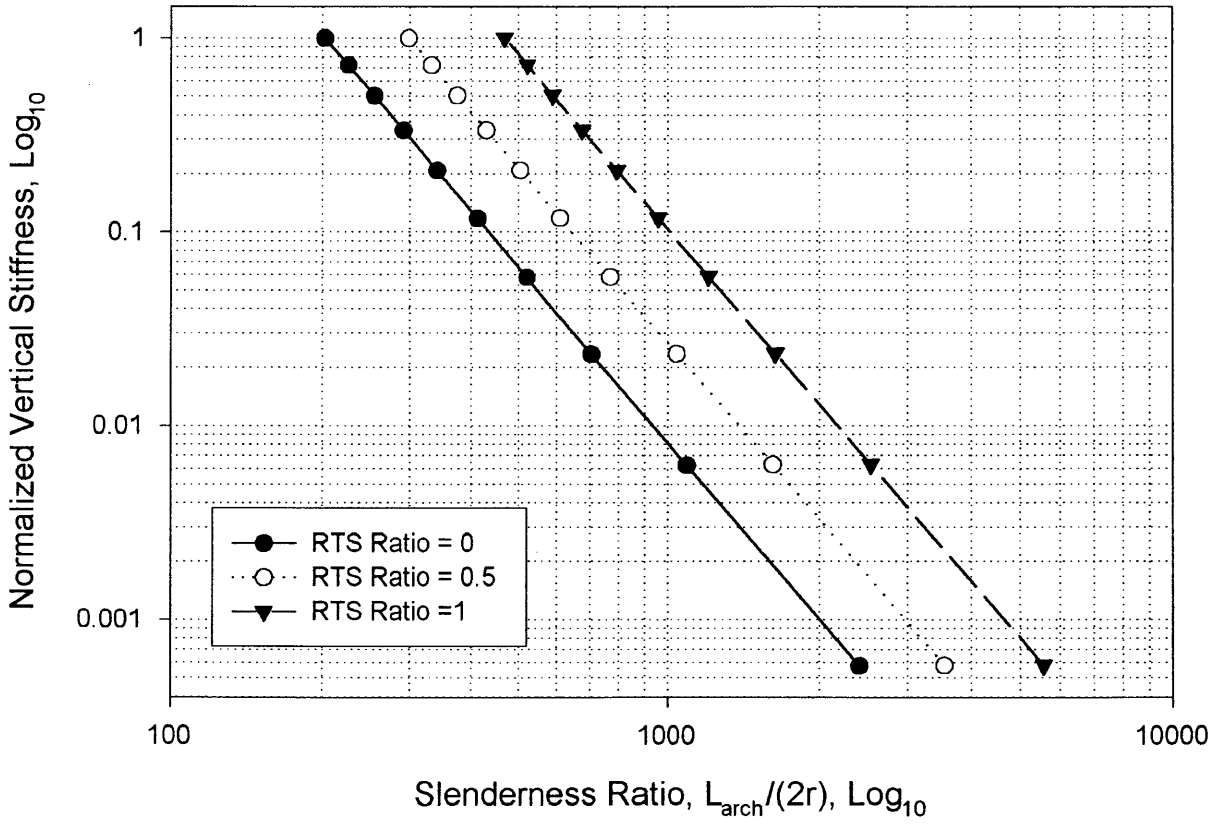

Figure 4.25 Slenderness Ratio and Vertical Stiffness

It is found that the relationship between the slenderness ratio of an arch and the

normalized vertical stiffness is log-log linear. The higher the ratio is, the weaker the arch is in the vertical direction.

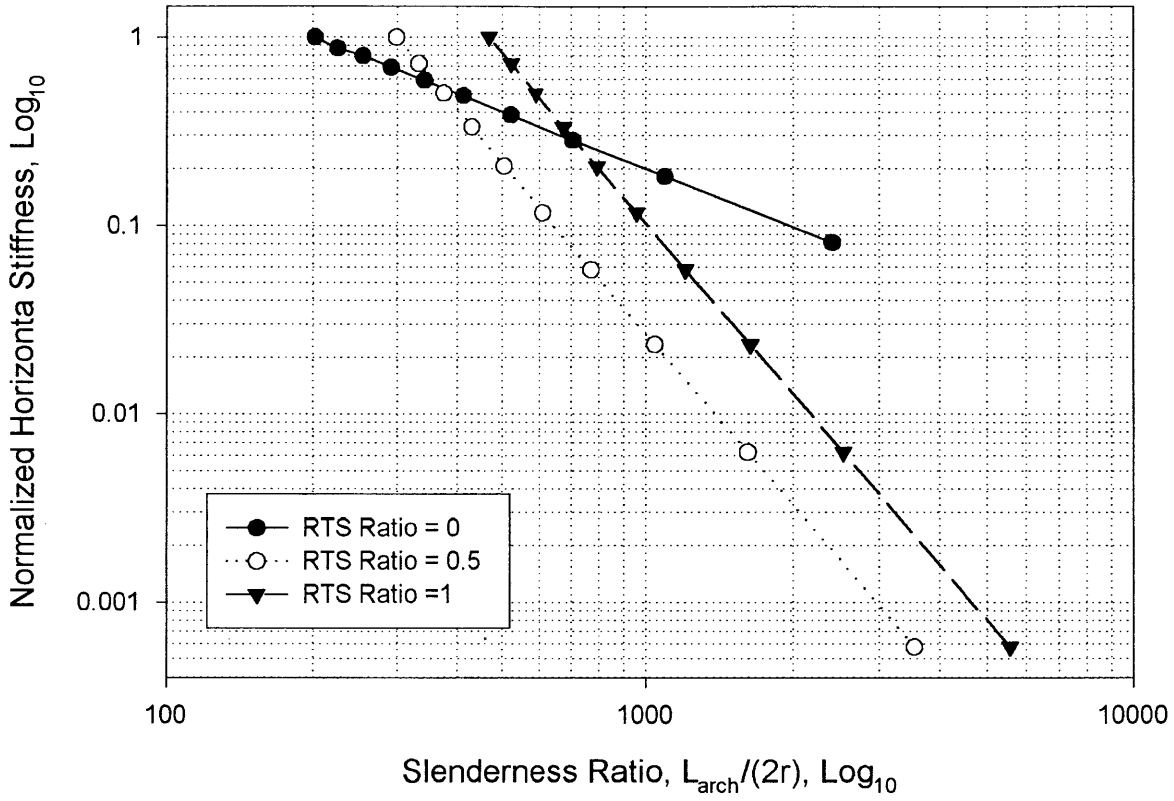

Figure 4.26 Slenderness Ratio and In-Plane Horizontal Stiffness

A similar situation occurs when considering in-plane horizontal stiffness. When the RTS ratio becomes zero, the arch degrades to beam. It takes horizontal load all by internal axial action, not like the other two types (RTS ratio = 0.5 and 1), its horizontal stiffness is stronger than any other RTS ratios.

Figures 4.25 and 4.26 are helpful for estimating the degree of stiffness by comparing it with the maximum and the minimum. Since these log-log lines are linear, one can easily determine the approximate value corresponding to specific slenderness ratio from the figure. Meanwhile, stiffness can be related to displacement by normalization and log-log illustration. Once two points are obtained (maximum and minimum), the line is generated.

Further discussion will be foundd in the section of deformation analysis.

4.6 Stability Analysis

The simplest prototype of a structural stability problem is a column under an axial compressive load. The column that is sufficiently slender will fail due to deflection to the side rather than crushing of the material. When the column fails, it loses its stability. The loss of stability is caused by the change of geometry of structures or structural components. This problem was noticed and solved almost half century ago (Timoshenko, 1953).

The onset of buckling failure primarily depends on the elastic modulus and the cross-section stiffness. It is also found that buckling failure is almost independent of the material strength or yield limit. The existence of a possible buckling failure implies the possibility of undesirable failure mode. The investigation of identifying these buckling modes and loads is usually called stability analysis.

For space arches two types of buckling failure exist; in-plane buckling and out-of-plane buckling. Their definition is given in section 2.6. The goal of stability analysis in this thesis is looking for the relationship between buckling load and characteristic parameters. Two failure modes are investigated here: symmetric and antisymmetric. Symmetric buckling is achieved by applying symmetric loads (concentrated and uniformly distributed) over the structure. The antisymmetric buckling is simulated by applying symmetric loads over the structure and extra horizontal load (wind load) from the side. The magnitude of wind load is calculated in Chapter 3. Wind load will be generated from two directions (x: in-plane; y: out-of-plane). The corresponding maximum wind loads are 0.301 kips/ft and 0.296 kips/ft in x and y directions, respectively.

Different magnitudes of wind load will be applied, and the change of buckling load will be observed. The contribution of the brace members in resisting different types of buckling is measured. In the following sections, numerical results are presented at first, and further discussion follows.

It should be pointed out that the in-plane buckling mode is achieved when a horizontal load comes from x-axis, which is the main plane the system is oriented on. The in-plane buckling mode to be defined here does not mean the system buckles in a real

plane. Nevertheless, when the system buckles in the in-plane buckling mode, there still will be out-of-plane deformation (except when the LTD ratio = 1) distributed along the two-arch system. The vocabulary "in-plane" is used because of main deformed direction is parallel with the arch plane (x-y plane). For out-of-plane buckling mode, the main deformed direction is perpendicular to the arch plane. Therefore, "out-of-plane" buckling mode is defined.

4.6.1 In-Plane Buckling

Many early papers on arch stability were devoted to linear stability problems. Austin (1971) and Timoshenko and Gere (1961) had summarized the work done by Gaber, Stussi, Kollbrunner, Hilman, Dischinger, and Dinnik. They considered the buckling of arches of constant cross section in which the arch is the funicular curve for the loading. In some cases (described in section 4.2), for geometrically perfect arches, the loading causes pure axial compression (no bending) at every cross section of the arch. The arches are free to buckle in their plane without restraint.

Austin and Ross (1976) extended the work done by Timoshenko and Gere (1961) and proposed critical load parameters and critical horizontal reaction parameters for uniform elastic arches in pure compression. Part of their work is illustrated in Figures 4.27 and 4.28.

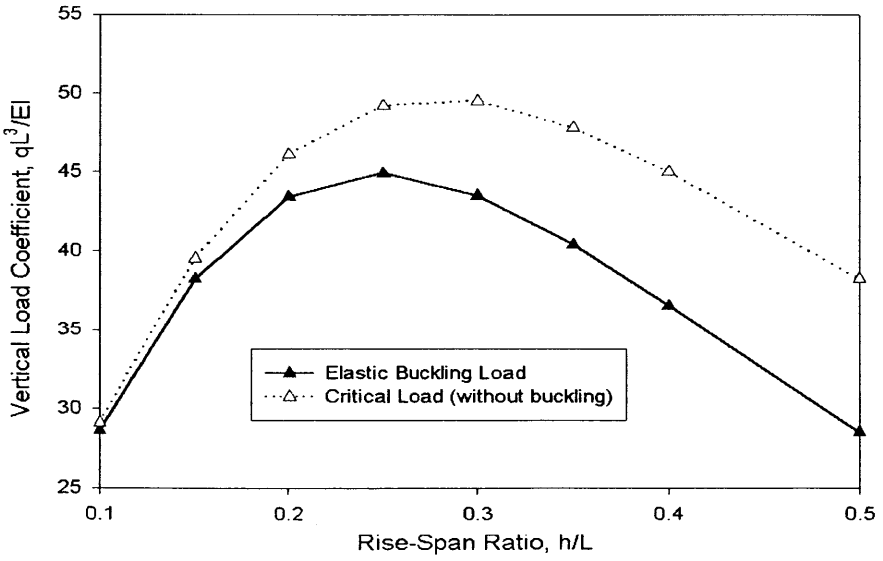

Figure 4.27 Elastic Buckling Load Parameter (By Austin and Ross, 1976)

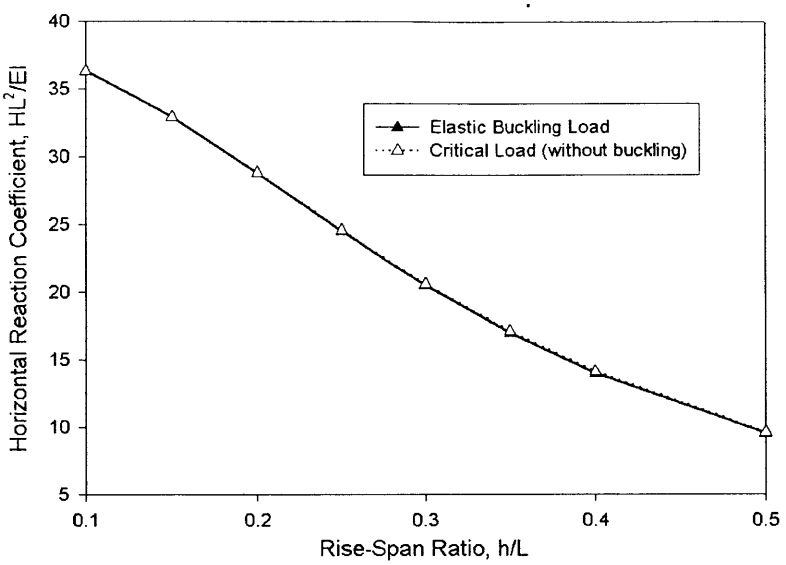

Figure 4.28 Elastic Buckling Horizontal Reaction Coefficient
(By Austin and Ross, 1976)

Expressing the relationship between buckling load and several parameters is performed by numerical investigation. A discussion is presented after these plots.

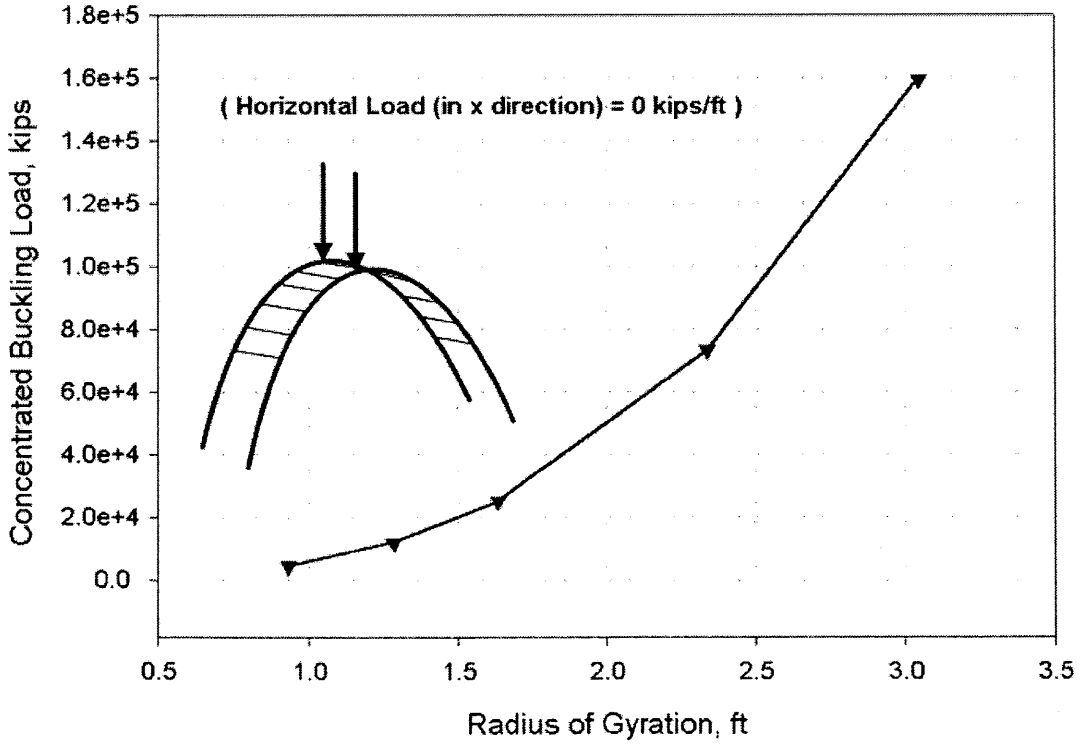

Figure 4.29 In-Plane Sym. Concentrated Buckling Load vs. Radius of Gyration

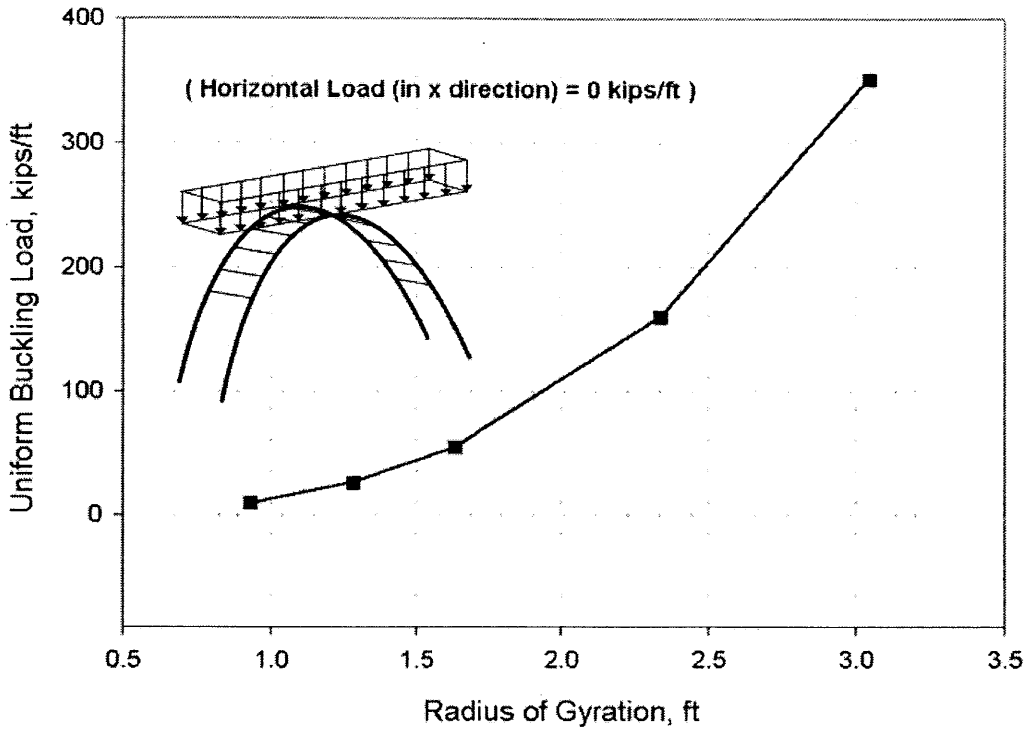

Figure 4.30 In-Plane Sym. Uniform Buckling Load vs. Radius of Gyration

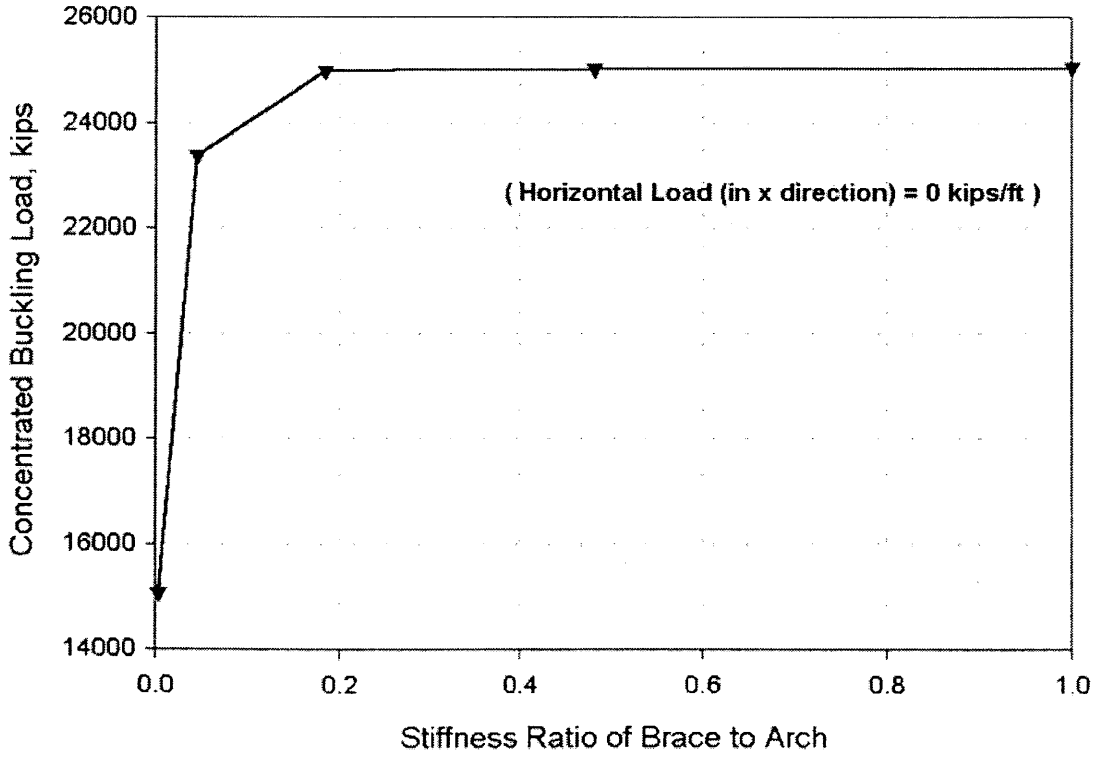

Figure 4.31 In-Plane Sym. Concentrated Buckling Load vs. Stiffness Ratio of Brace to Arch

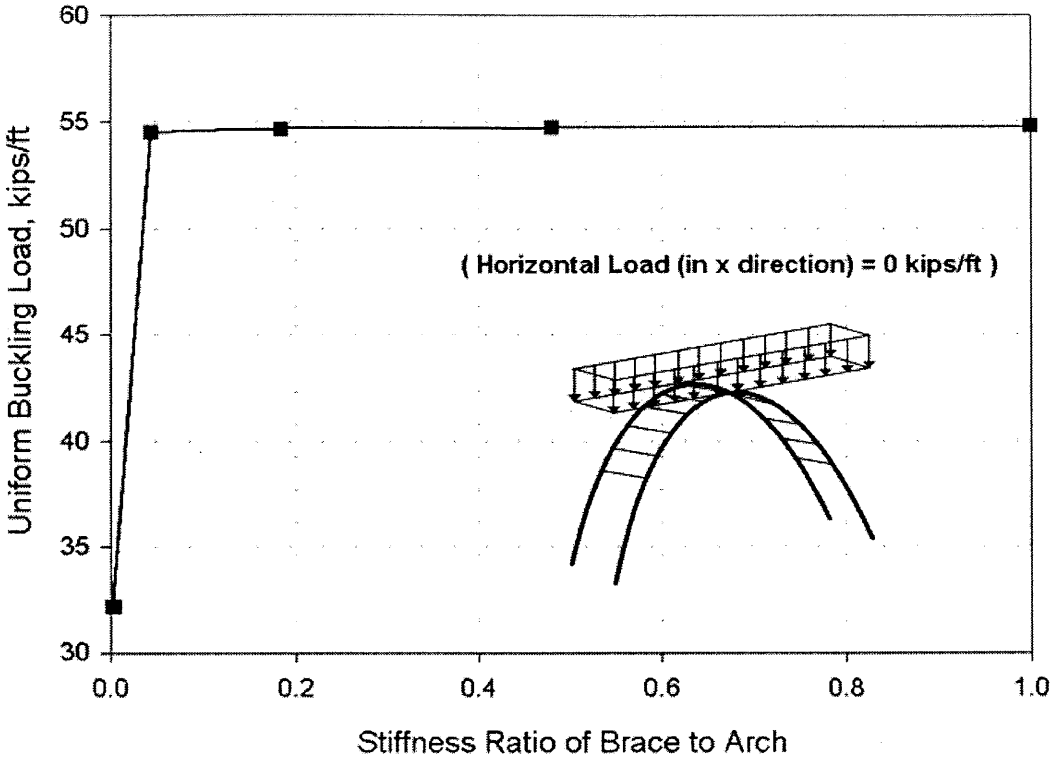

Figure 4.32 In-Plane Sym. Uniform Buckling Load vs. Stiffness Ratio of Brace to Arch

The radius of gyration used here is defined on the cross section of an arch. The cross sections of brace member remain constant in Figures 4.29 and 4.30. The stronger the arch member is, the larger the in-plane buckling load is, in the symmetric mode.

The stiffness ratio of the brace to the arch is defined as the ratio of the moments of inertia on the cross sections. The contribution of brace members to in-plane symmetric buckling mode is also investigated. In Figures 4.31 and 4.32, RTS ratio is 0.5 and LTD ratio is 0.33. It is found that the brace member should have at least 50% of the strength of the arch member; otherwise the entire system will buckle at much lower values in these cases.

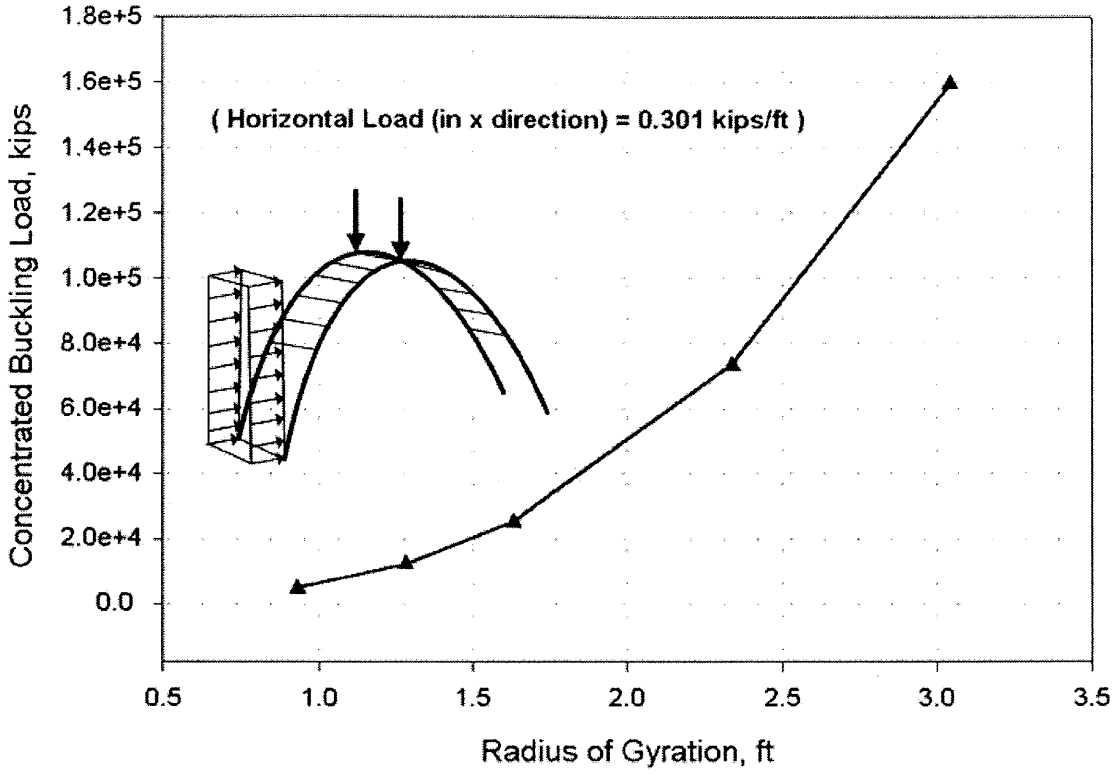

Figure 4.33 In-Plane AntiSym. Concentrated Buckling Load vs. Radius of Gyration

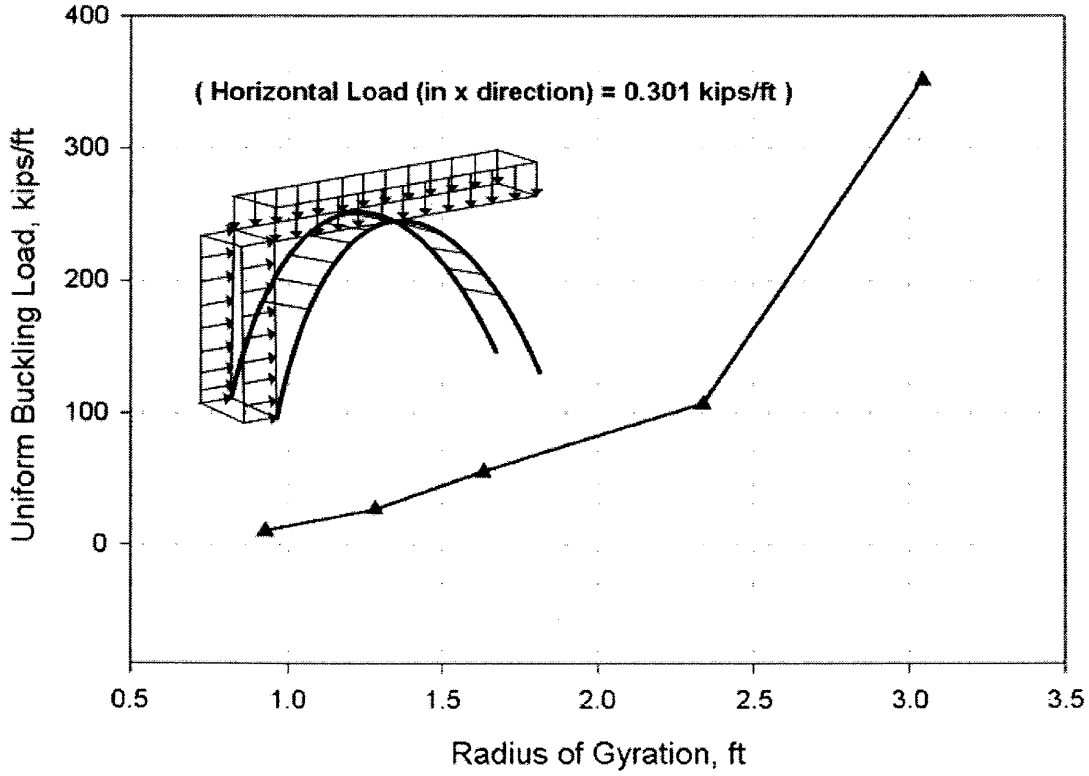

Figure 4.34 In-Plane AntiSym. Uniform Buckling Load vs. Radius of Gyration

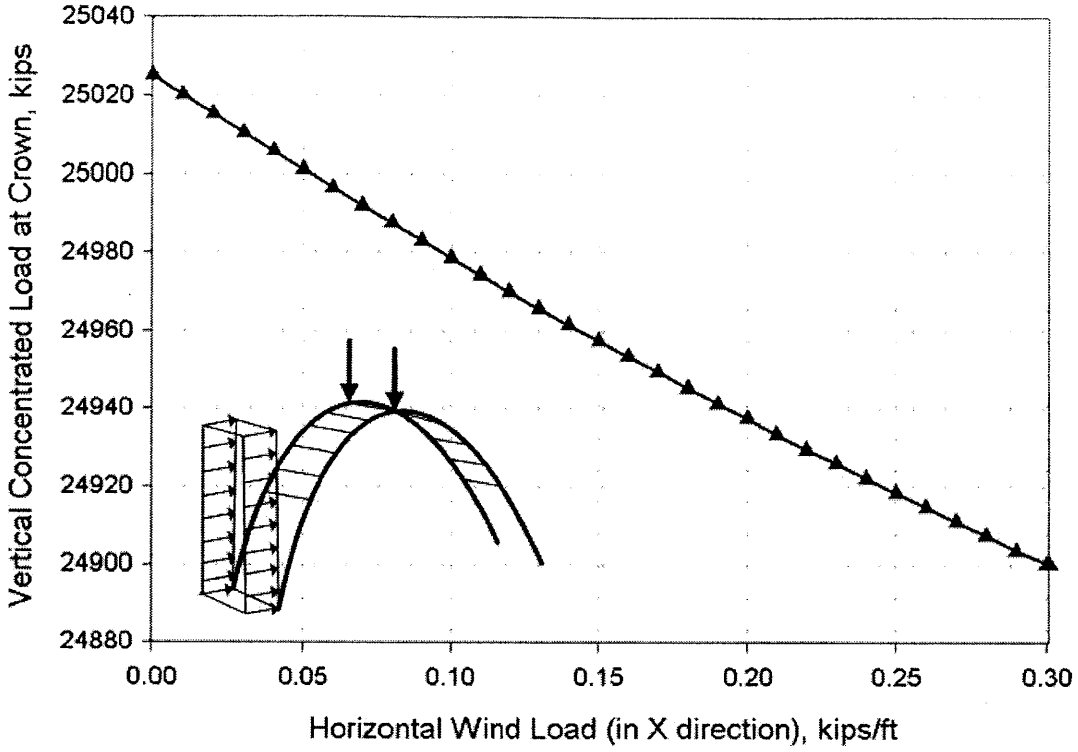

Figure 4.35 In-Plane AntiSym. Concentrated Buckling Load vs. Horizontal Wind Load

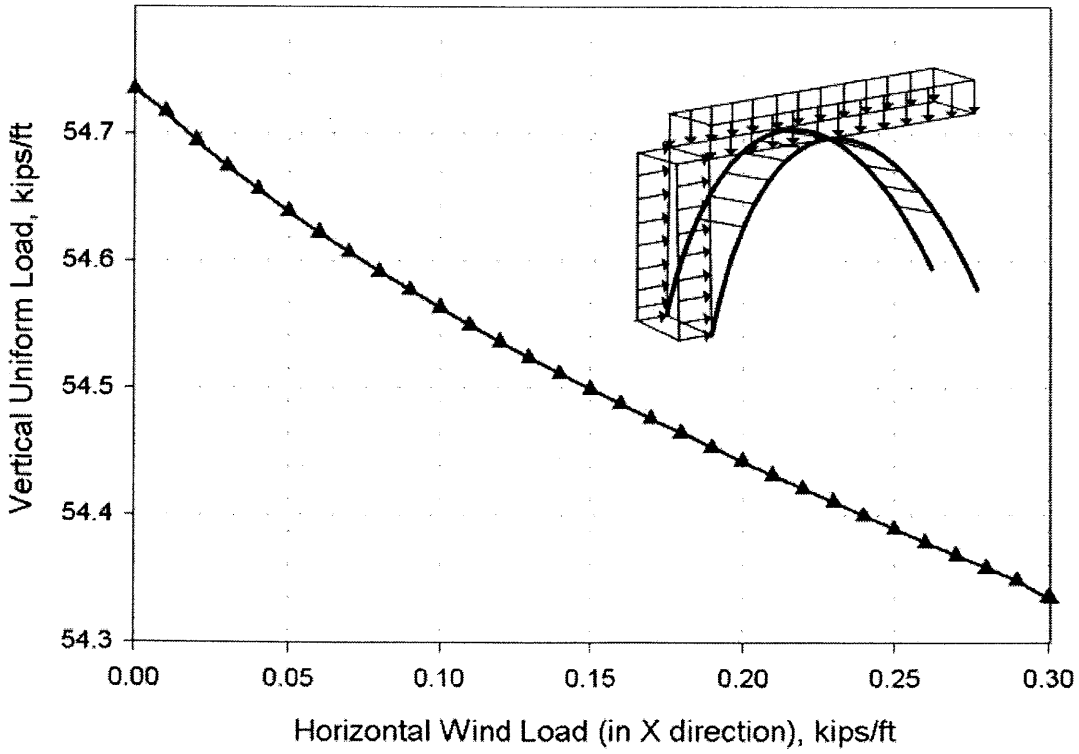

Figure 4.36 In-Plane AntiSym. Uniform Buckling Load vs. Horizontal Wind Load

Basically, from Figures 4.33 and 4.34, the trend of curves for the in-plane antisymmetric mode is similar to the one in the symmetric mode: the stronger the arch member is, the larger the in-plane buckling load is.

Since the horizontal wind load is relatively smaller than the vertical load (wind load is 0.301 kips/ft in x-axis, 0.296 kips/ft in y-axis; vertical concentrated load is 1 kips and uniform load is 1kips/ft), the decrease of the buckling load due to the introduction of lateral wind load is not significant in this case. However, the buckling load for the antisymmetric mode is smaller than the symmetric mode numerically. It is expected the larger the lateral load is, the larger the difference is.

From Figures 4.35 and 4.36, one can also find that increasing of the horizontal wind load will cause a decrease in the vertical buckling load, no matter whether the load is concentrated or uniformly distributed.

4.6.2 Out-of-Plane Buckling

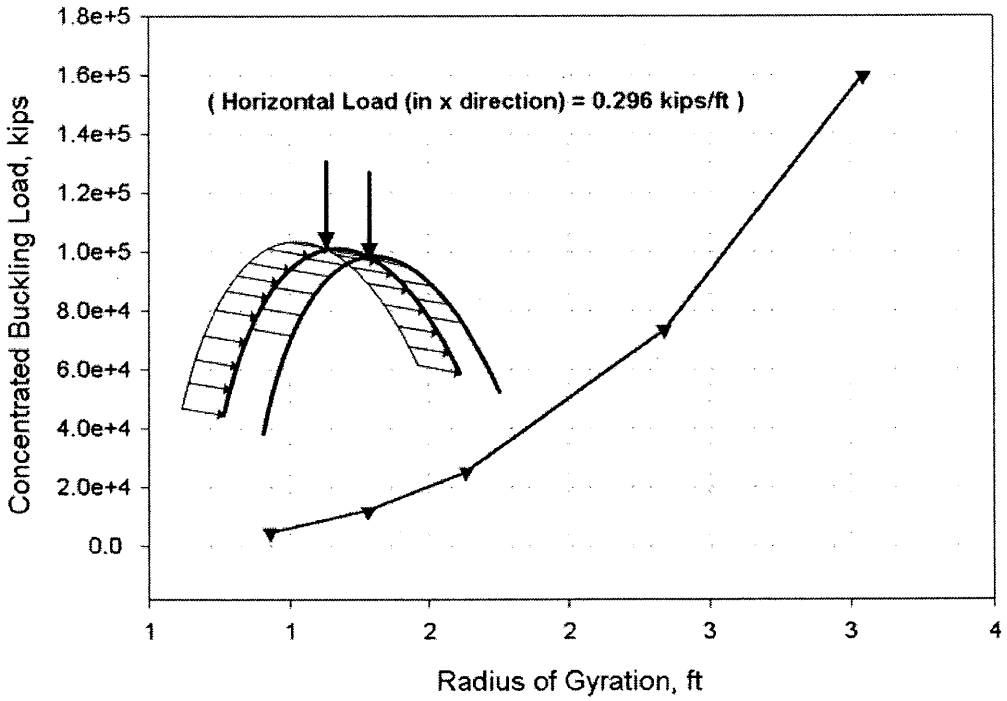

Figure 4.37 Out-of-Plane Sym. Concentrated Buckling Load vs. Radius of Gyration

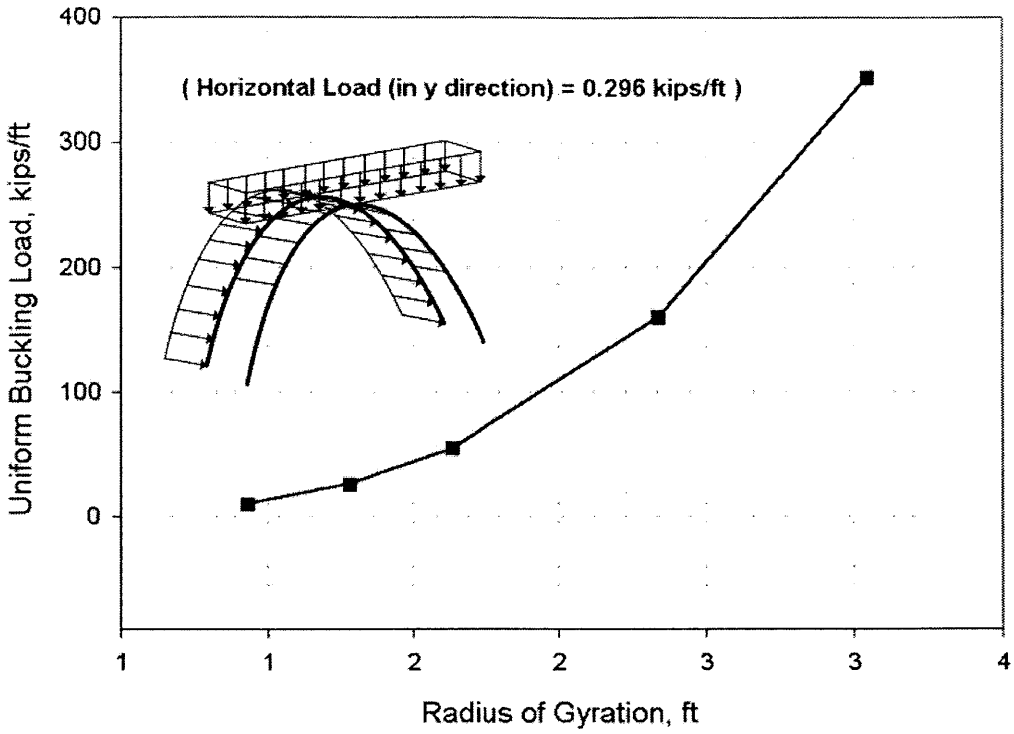

Figure 4.38 Out-of-Plane Sym. Uniform Buckling Load vs. Radius of Gyration

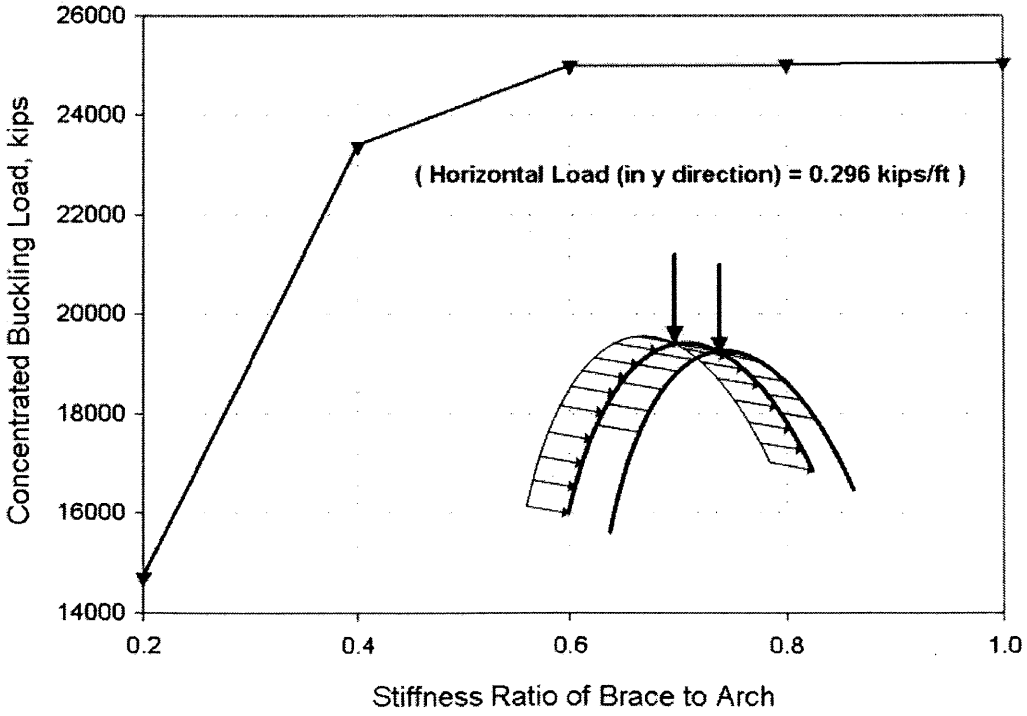

Figure 4.39 Out-of-Plane Sym. Concentrated Buckling Load vs. Stiffness Ratio of Brace to Arch

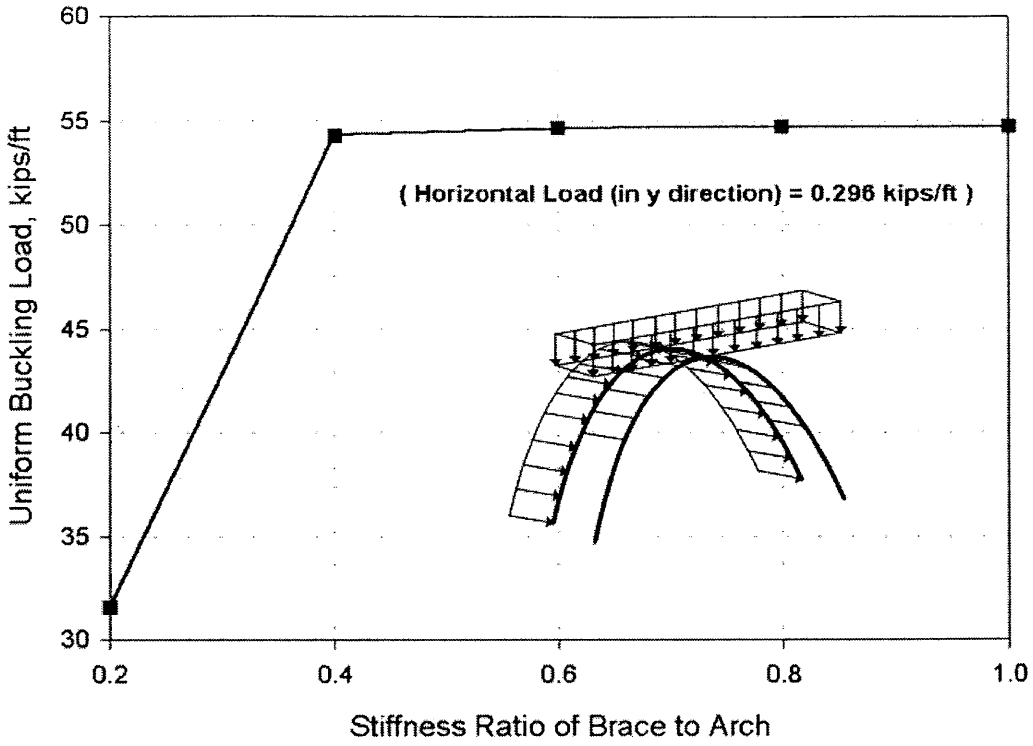

Figure 4.40 Out-of-Plane Sym. Uniform Buckling Load vs. Stiffness Ratio of Brace to Arch

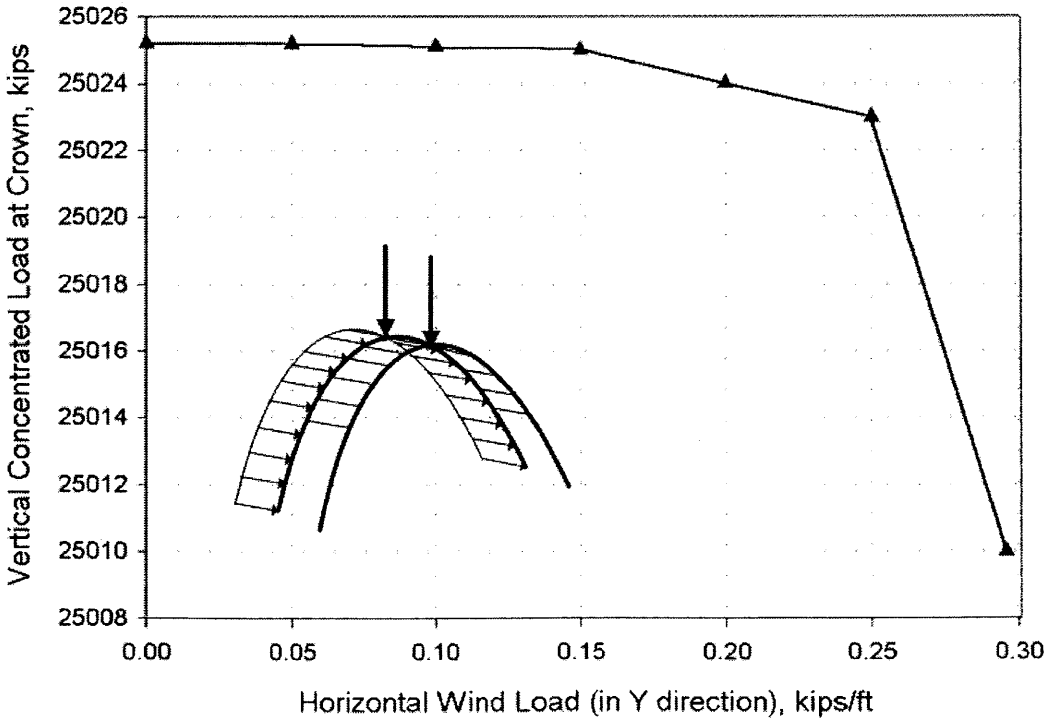

Figure 4.41 Out-of-Plane Sym. Concentrated Buckling Load vs. Horizontal Wind Load

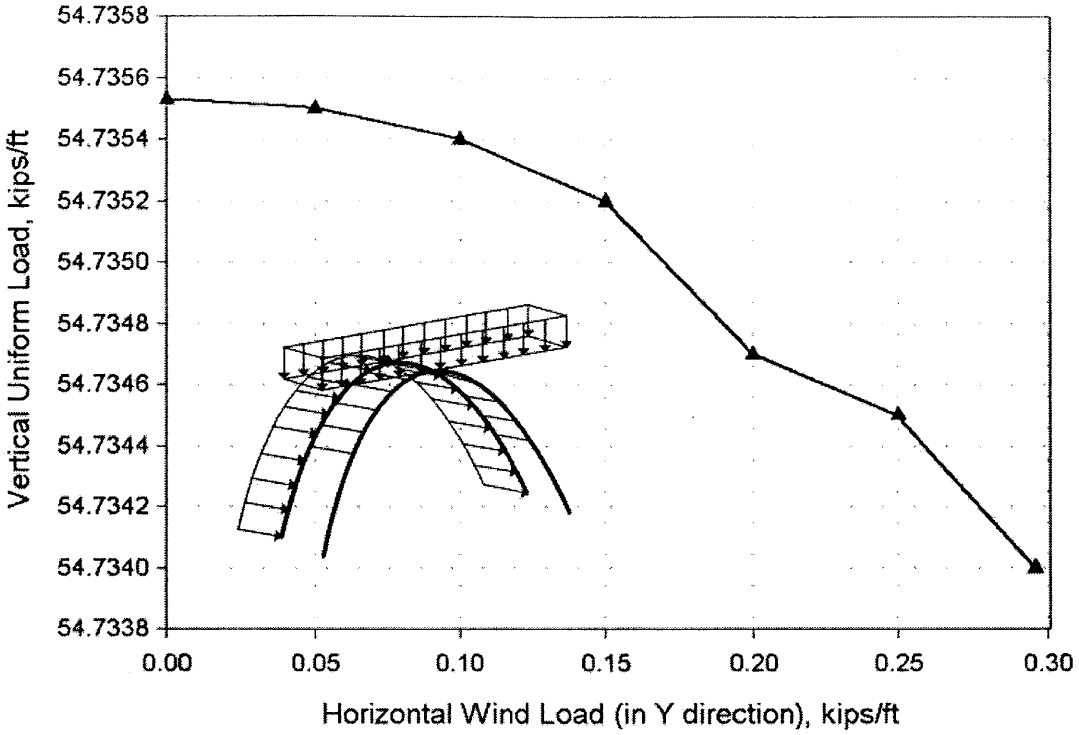

Figure 4.42 Out-of-Plane Sym. Uniform Buckling Load vs. Radius of Gyration

From Figures 4.37 and 4.38, the same fact is observed with in-plane symmetric and antisymmetric modes. Figures 4.39 and 4.40 reveal the suggestion drawn for in-plane symmetric mode: in order to prevent the system from failing due to low strength, it is suggested that the strength of the brace members should be greater than half the strength of arch member.

Comparing Figures 4.35, 4.36, 4.41, and 4.42, the decrease of buckling load in the in-plane antisymmetric mode is faster than in the out-of-plane antisymmetric mode, no matter whether the load is concentrated or uniformly distributed. Note the default RTS ratio is 0.5 and LTD ratio is 0.33 in these cases.

4.7 Displacement Analysis

Due to its geometry, the deformed shape of an arch is not linear or regular. The shape varies with the RTS ratio, the LTD ratio, the slenderness ratio, boundary conditions, loading types, and material types. In structural design, engineers usually are concerned about the maximum displacement. It can be global maximum displacement for entire building or local maximum relative displacement for each story (drift). For building-type structures, allowable story drift is usually regulated. By limiting story drift, maximum displacements of building can also be limited.

Unlike the building-type structure, an arch has no story drift to indicate the potential of excessive deformation. Two possible methods can be used to evaluate the deformation:

(1) Measure a single global maximum displacement to evaluate the condition of an arch.

(2) Measure the total local displacements between any two members and evaluate the condition of an arch by the sum of displacements.

For detail analysis, relative displacement between any two members is required to evaluate the condition of each member under multiaxial loading. However, method one is quicker for preliminary evaluations.

Because the global maximum displacement represents the accumulation of all local displacements (no matter positive or negative contribution), for specific loading, the variation of the global maximum displacement can indicate the change of condition of a structure. Besides, by generating an allowable global maximum displacement, it is presumed that the distribution of displacement is uniform, which means that the structure remains in elastic range.

A design chart considering the RTS ratio and slenderness ratio is offered for evaluating the stiffness of the arch system in vertical and in-plane horizontal stiffness. A two-hinged arch system is analyzed to generate the design chart. The default LTD ratio is 0.33, and the size of the brace member is assumed to be constant.

4.7.1 Vertical Displacement

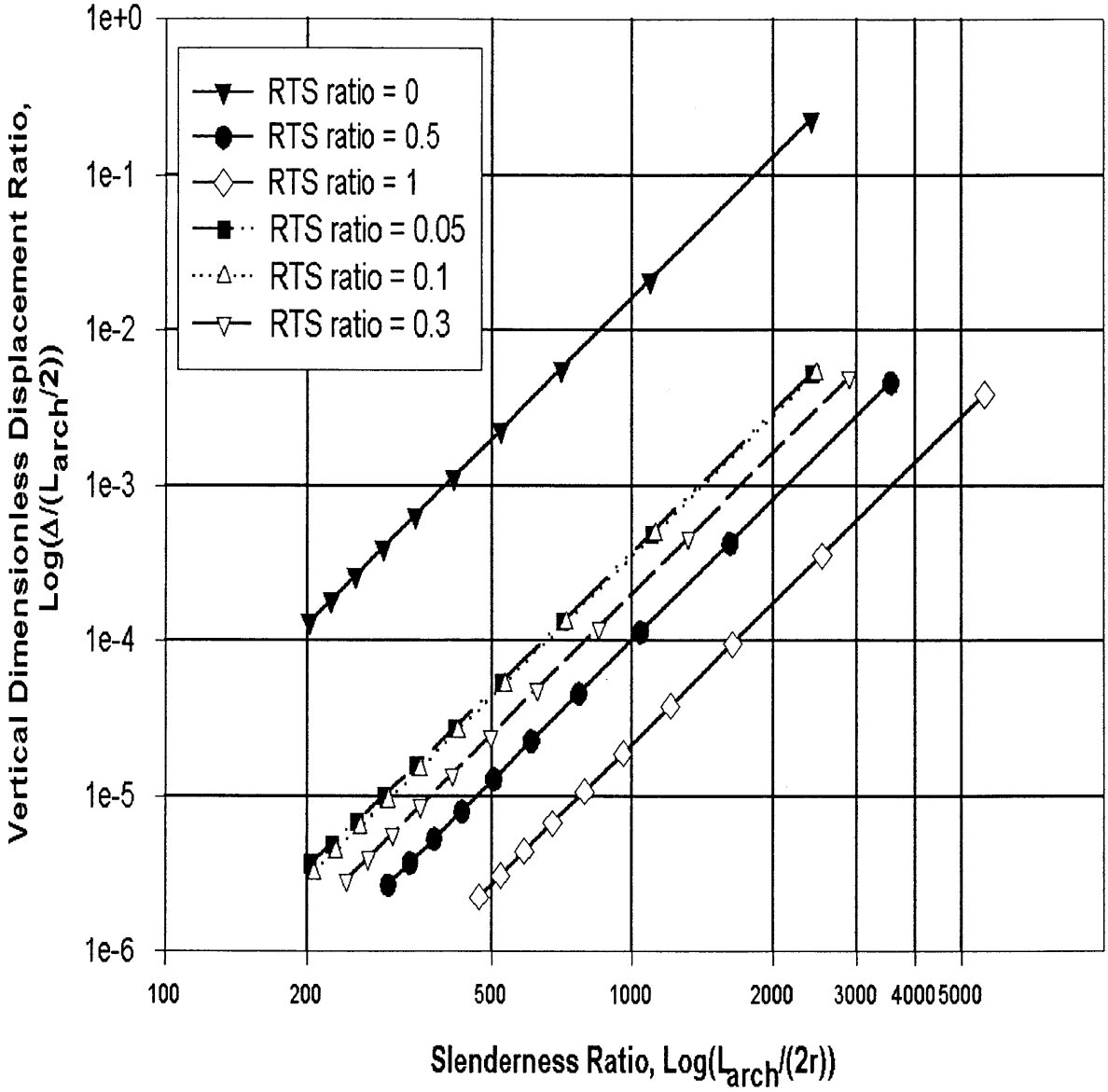

Figure 4.43 Design Chart for Vertical Dimensionless Displacement Ratio and Slenderness Ratio

4.7.2 Horizontal Displacement

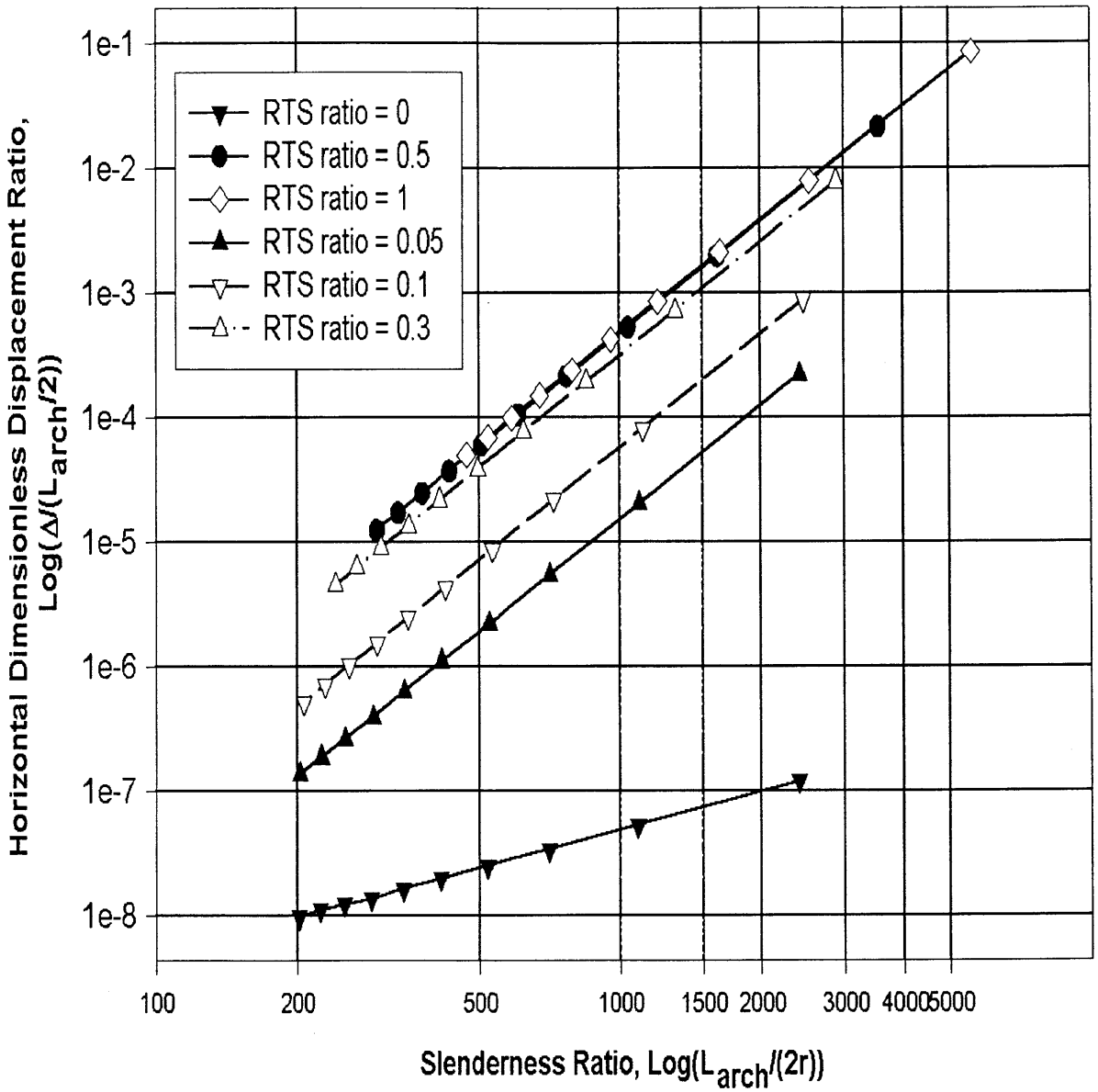

Figure 4.44 Design Chart for Horizontal Dimensionless Displacement Ratio and Slenderness Ratio

4.8 Other Issues

4.8.1 Structural Efficiency

The most efficient structure is the one that satisfies design requirements to the maximum degree and consumes the minimum resources (material). Looking for such a structure falls into the category of optimization. It is usual to establish a mathematical function including desired variables at first, then to solve the function under some constraints. Linear programming technique is often used to solve multi-variable optimization problems. In general, the strategy is to transform (map) a physical problem into a mathematical equation. If the mapping is correct, the mathematical solution should be the answer of physical problem. In this thesis, the "resource" is defined to be the material the structure consumes. The "capacity" is defined to be the stiffness of structure. It can be written as

$$e = \frac{\text{Capacity}}{\text{Resource}} \tag{4-14}$$

The larger e is, the more efficient the structure is. The goal of this section is to illustrate the relationship between consumed resources and obtained capacity with respect to different criteria.

Stiffness is usually considered as the capacity index of structure. The larger the stiffness is, the larger load the structure can take within in elastic range. Meanwhile, because deformation is inversely proportional to stiffness, large stiffness can bring small deformation. This is not to say that stiffness is the best solution for structure design, but explains the relationship between stiffness and deformation.

From Figures 4.4 and 4.5, the maximum vertical stiffness for a plane two-hinged arch occurs when the RTS ratio equals 0.06. From Figures 4.6 and 4.7, for a fixed arch, the RTS ratio is 0.07. Now the plots are redrawn with e and the RTS ratio in Figures 4.45 and 4.46.

In Figures 4.45 and 4.46, the efficiency index has been normalized such that it can be compared with normalized stiffness.

Comparison with horizontal stiffness is also provided in Figures 4.47 and 4.48 in the same manner. In order to display the difference between the curves, log-log coordinate is adopted.

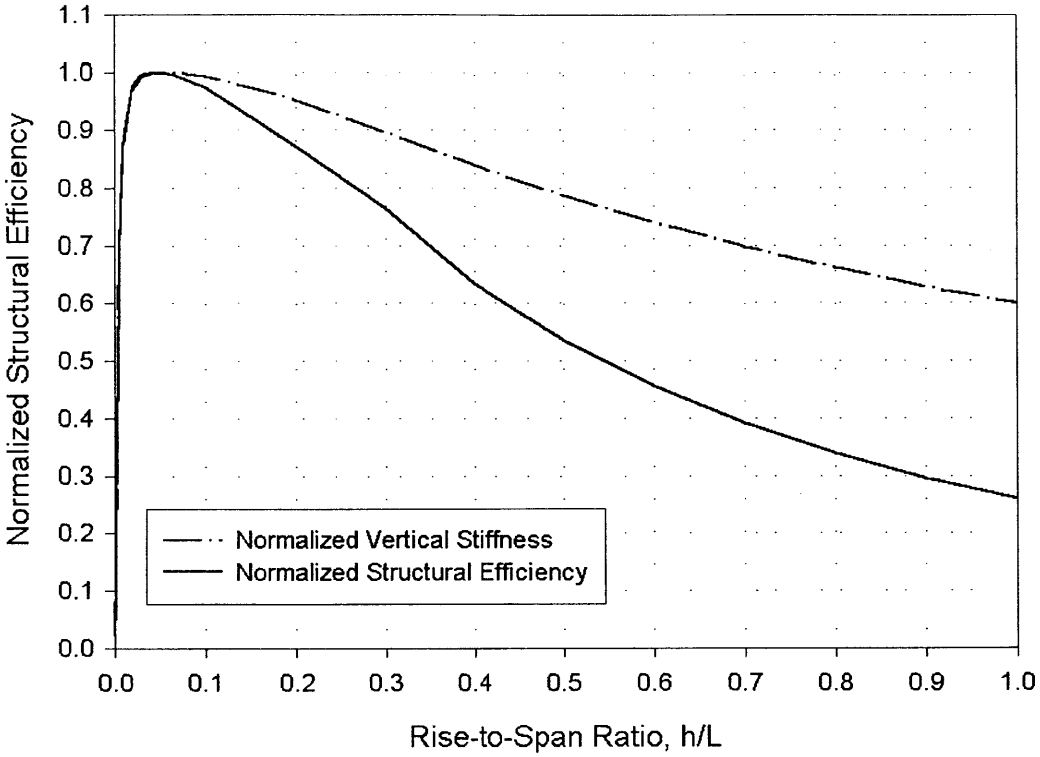

Figure 4.45 Structural Efficiency for Vertical Stiffness (Two-Hinged Arch)

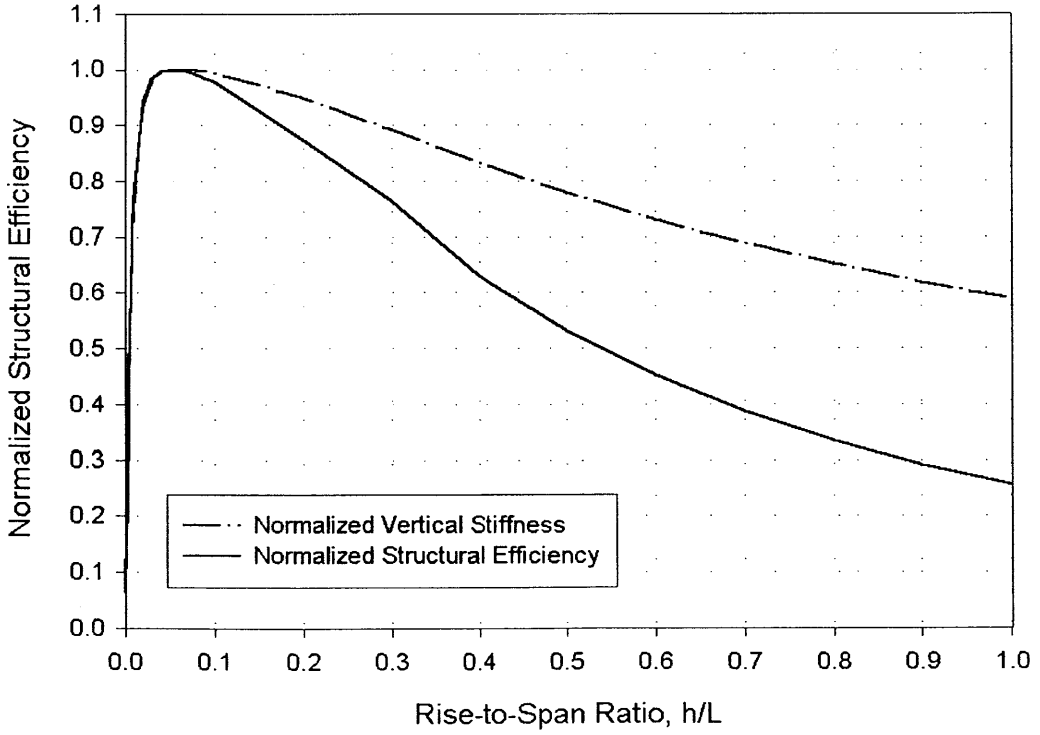

Figure 4.46 Structural Efficiency for Vertical Stiffness (Fixed Arch)

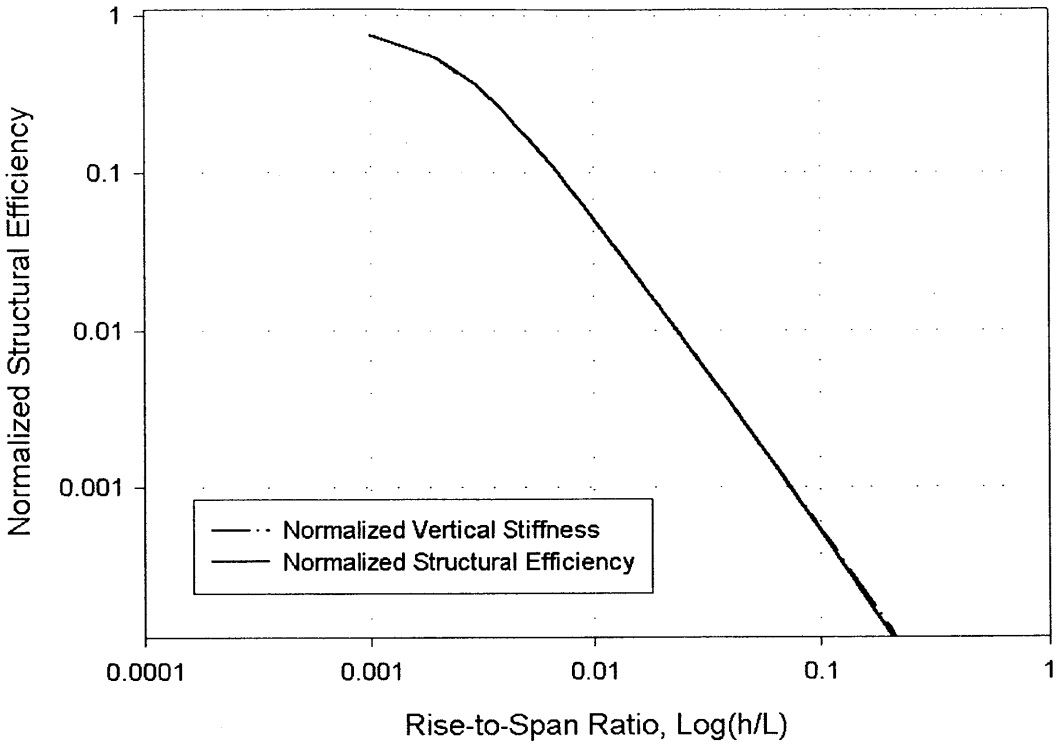

Figure 4.47 Structural Efficiency for Horizontal Stiffness (Two-Hinged Arch)

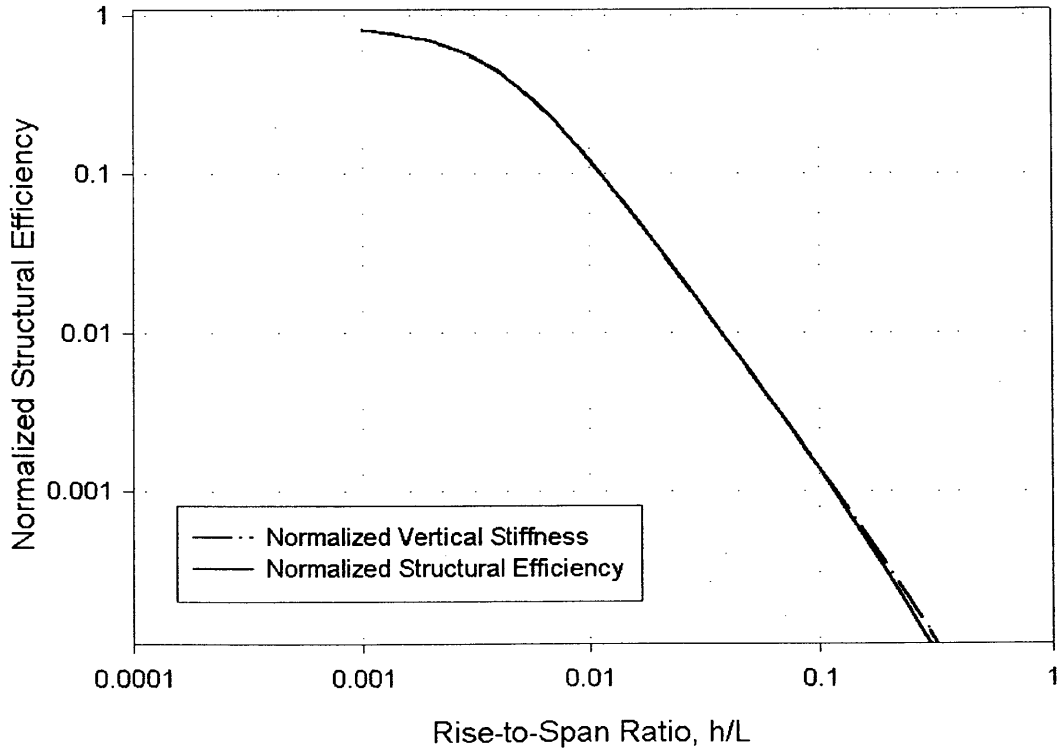

Figure 4.48 Structural Efficiency for Horizontal Stiffness (Fixed Arch)

From Figures 4.45 and 4.46, it is found that the higher the arch is, the less efficient it is for resisting vertical load. Different situations occur in Figures 4.47 and 4.48. The arch does not lose its efficiency when the RTS ratio increases.

The results drawn from Figures 4.45 and 4.46 only indicate the variation of efficiency with respect to the RTS ratio. Even when efficiency reaches its maximum, the corresponding configuration does not mean the arch is the "most efficient" structure. There is no comparison with other types of structures in the results.

4.8.2 Variation of Internal Actions

The variation of internal actions indicates the change of the load-carrying mechanism. It is of interest to know how these internal actions vary with the change of configuration. Take a plane arch with two hinged supports as example, internal actions to be considered here are axial force, bending moment, and shear force. Several arches of different heights are examined. The structure is subjected to a concentrated load at its crown. The total span of the arch is 700 ft. Results are illustrated in Figures 4.49, 4.50, and 4.51.

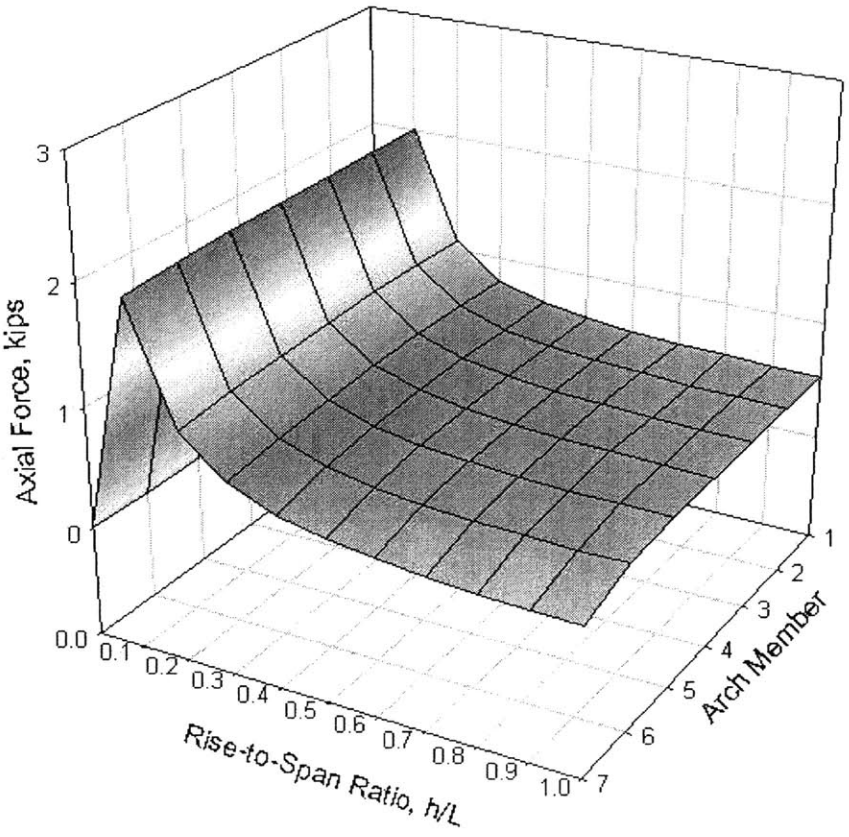

Figure 4.49 Variation of Axial Force and RTS Ratio

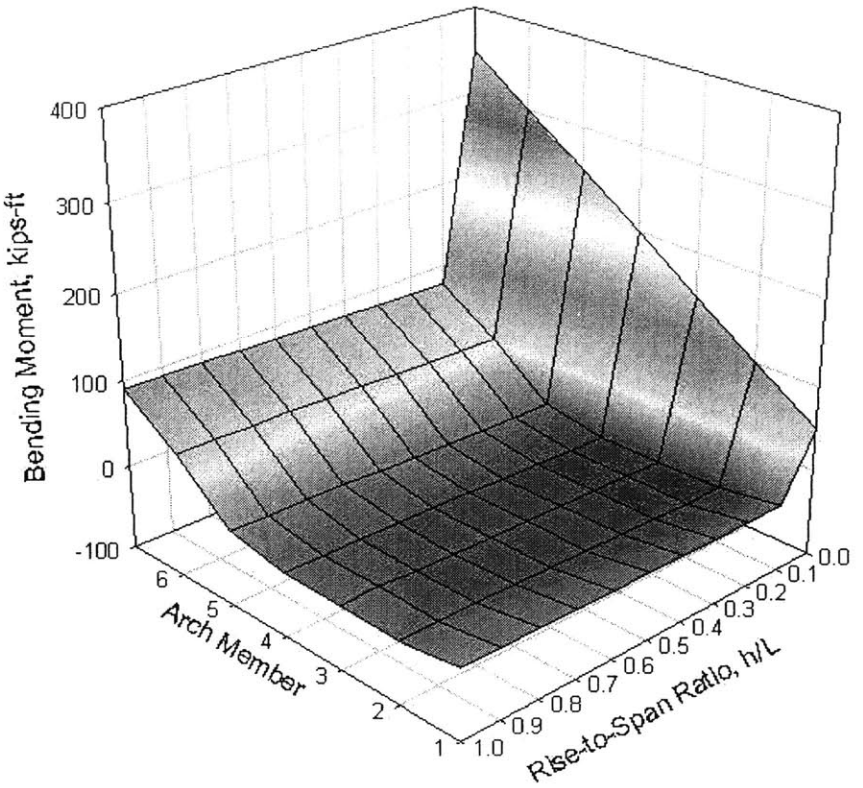

Figure 4.50 Variation of Bending Moment and RTS Ratio

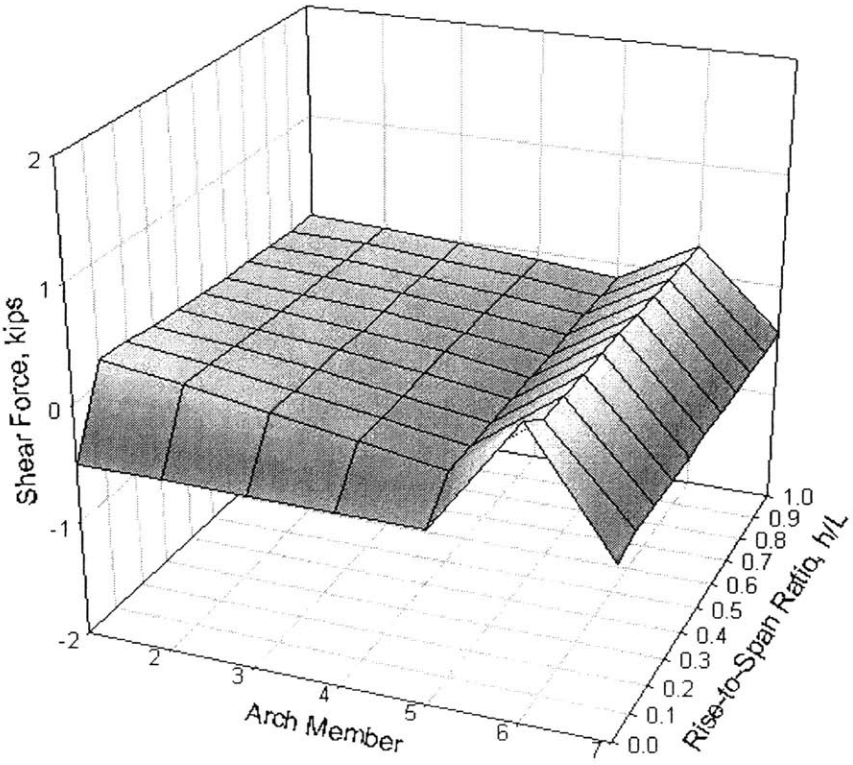

Figure 4.51 Variation of Shear Force and RTS Ratio

Arch members are numbered from the supports to the center. Because of symmetry, only half of total members are plotted.

Figure 4.49 exhibits the characteristic of an arch. The variation of axial force for each member follows the same pattern. They all reach a maximum when the RTS ratio is about 0.1. In Figures 4.50 and 4.51, the variation of bending moment and shear force for each member also follows similar pattern except when the RTS ratio becomes zero, at which the arch degrades to beam.

It should be pointed out that when the load pattern is fixed, some members would experience large internal action no matter how geometry changes. That means when an arch structure is applied, some member is always the focus under specific loading. In this case, member 6 is the critical one. Since no matter how the RTS ratio changes, it will experience relative large bending moment and maximum shear force.

Chapter 5 Conclusion

5.1 Results of Numerical Analysis

The influence of characteristic parameters on the behavior of a coupled arch system has been investigated using numerical analysis. The following conclusions are drawn:

(1) Arch-Column Analogy

An arch analogy coefficient is defined and related to the stiffness of a column. This approach allows us to compute the stiffness of a plane arch subjected to a concentrated load simply by multiplying the column stiffness (the height of column equals to the rise of arch) by the arch analogy coefficient. For a two-hinged parabolic arch, the result is

$$k_{arch} = \alpha_{arch} k_{col}$$

$$\Rightarrow k_{arch} = \frac{h}{L}\left[0.000367 - 0.000149\left(\frac{h}{L}\right)\right]\left(\frac{AE}{L_c}\right)$$

$$\Rightarrow k_{arch} = \frac{AE}{L}\left[0.000367 - 0.000149\left(\frac{h}{L}\right)\right] \qquad (4\text{-}5)$$

For a fixed parabolic arch, we find

$$k_{arch} = \frac{h}{L}\left[0.000539 - 0.000224\left(\frac{h}{L}\right)\right]k_{col}$$

$$\Rightarrow k_{arch} = \frac{AE}{L}\left[0.000539 - 0.000224\left(\frac{h}{L}\right)\right] \qquad (4\text{-}6)$$

In the above expressions, h is the rise of the arch, L is the span of the arch, A is the cross sectional area of column and arch, E is Young's modulus, L_c is the height of column. It is much faster to compute the stiffness of column than of arch. Thus, one can make use of Eq.(5-1) and (5-2) for the purpose of preliminary evaluation.

(2) Rise-to-Span Ratio (RTS Ratio)

For the vertical stiffness, there is a range of the RTS ratio for which the stiffness is high. Outside this range, arches lose over 20% of their maximum stiffness. In the case of a plane two-hinged parabolic arch, the range of RTS ratio is from 0.008 to 0.48. For a plane fixed parabolic arch, it is from 0.01 to 0.45. The influence of boundary condition turns out when comparing the

stiffness of two-hinge arch and of fixed arch. The vertical stiffness of fixed end arch is 1.46 times of two-hinged arch (RTS ratio = 0 is not considered).

The horizontal stiffness decreases sharply when the RTS ratio increases. It applies for both two-hinged and fixed arches. However, due to the intention of applying arch, the RTS ratio is usually much greater than 0.05. Numerical result can be interpreted as the stable development of the horizontal stiffness after the RTS ratio is greater than 0.05. By using fixed end supports, the horizontal stiffness can reach 2.5 times of using two-hinged support.

(3) Leaning-to-Depth Ratio (LTD Ratio)

Refer to Figure 5.1, when the LTD ratio increases from 0 to 1, the vertical stiffness varies in 20% and in-plane horizontal stiffness varies within 5%. For out-of-plane horizontal stiffness, it changes dramatically from 1 to less than 0.1. This fact indicates the importance of bracing member on resisting out-of-plane horizontal load.

From the viewpoint of out-of-plane horizontal stiffness, it is suggested that the LTD ratio should be as small as possible, such that out-of-plane horizontal stiffness will increase to a large amount. Nevertheless, from the viewpoint of in-plane horizontal stiffness, it is suggested that LTD ratio is as large as possible. From the viewpoint of vertical stiffness, it is suggested either LTD ratio is zero or as large as possible. Three curves of stiffness against LTD ratio are plotted in Figure 5.1.

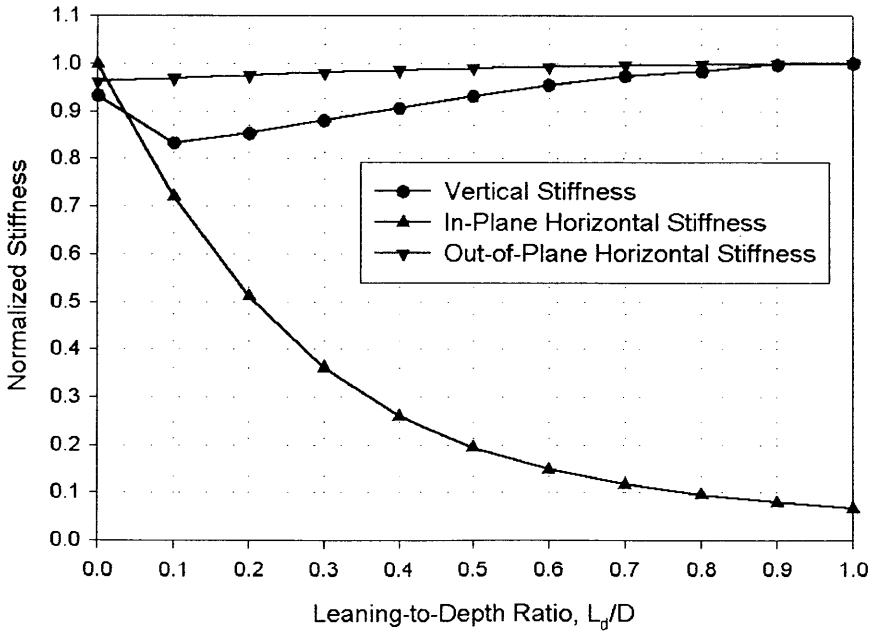

Figure 5.1 Stiffness versus LTD Ratio

The magnitude of LTD ratio depends on designer's intention and loading condition to determine the priority of stiffness direction.

(4) Slenderness Ratio

Figures 4.25 and 4.26 show that the relationship between the slenderness ratio and the normalized stiffness is log-log linear. One can create a design chart for many different RTS ratios with two points per single curve. It is suggested to compute the start and end points, then look for the desired value by interpolation.

(5) Stability Analysis

As expected, the buckling load increases with larger cross sections of the arch (evaluated by radius of gyration) and of the brace members (stiffness ratio of brace to arch). It decreases with increasing horizontal load. Details may be referred to section 4.6.

(6) Displacement Analysis

A design chart for evaluating the displacement of arch is proposed. It is plotted with dimensionless displacement ratio and slenderness ratio. The relationship between these two parameters is log-log linear. Different values of the RTD ratio are also considered.

(7) Structural Efficiency

Considering the concept of efficiency, when the RTS ratio is over about 1.6, efficiency is under 90% for the vertical stiffness in the case of two-hinged arch. For fixed arch, the bound of the RTS ratio is about 1.7.

5.2 Suggestions

(1) The concept of arch-column analogy may be applied on the correlation with other parameters. Some characteristic parameters may be needed to describe the correlation.

(2) Ultimate strength analysis could be applied on a coupled arch system.

(3) Using the concept of structural efficiency, one can evaluate the most efficient configuration with specific criteria. When multivariable analysis is performed, efficiency can be a useful concept. The influence of efficiency on other parameters may be discussed in the future.

(4) Dynamic effect is not considered in this thesis. Parametric analysis can be extended to the dynamic behavior of a coupled arch system.

(5) Local behavior is not in the consideration of this thesis. Some local behavior,

such as connection between brace and arch, might be an issue for global behavior.

(6) The assumption on material can be improved to be more realistic. In real cases, composite material is used frequently. The description of material in numerical model can be precise if experimental data is available.

(7) For real structures, cyclic behavior is much more important for static response. However, the difficulty might be the precise description of material behavior under cyclic loading, no matter high-cycle-low-amplitude loading or low-cycle-high-amplitude loading.

(8) Advanced numerical analysis software may be applied on further research, such as ABAQUS.

References

1. American Society of Civil Engineers, (2000). "Minimum Design Loads for Buildings and Other Structures", ASCE 7-98, Reston, Virginia.
2. Atwood, G., (1801)."A dissertation on the construction and properties of arches.", W. Bulmer and co. for Lunn, London.
3. Austin, W.J., (1971). "In-Plane Bending and Buckling of Arches", ASCE J.Struct. Div., Vol. 97, No. ST5, pp.1575-1592.
4. Austin, W.J., and T. J. Ross, (1976). "Elastic Buckling of Arches Under Symmetrical Loading", ASCE J. Struct. Div., Vol. 102, No. ST5, pp.1085-1095.
5. Bathe, K.-J., (1986). "Finite Element Procedures in Engineering Analysis", Springer-Verlag, New York.
6. Bensalem, A., A. Sibbald, and C.A. Fairfield, (1998). "The Use of Dynamic Characteristics for the Optimal Design of Arches", Computers & Structures, 68, pp.461-472.
7. Borlach, J.C., (1755). "Designs of Architecture for Arches or Gates: The Several Plans and Uprights Contained in Twenty Plates", J. Boydell, London.
8. Chini, S.A. and A.M. Wolde-Tinsae, (1988). "Critical Load and Postbuckling of Arch Framworks", ASCE J. Mech. Eng., Vol. 114, No. 9, pp.1435-1453.
9. Cross, H., (1963). "Arches, Continues Frames, Columns, and Conditions", Urbana, UIUC.
10. Elishakoff, I., Y. Li, and J.H. Starnes, Jr. (2001). "Non-Classical Problems in the Theory of Elastic Stability", Cambridge University Press, New York.
11. Fukumoto, Y.(editor) (1997). "Structural Stability Design -- Steel and Composite Structures", Pergamon, Oxford.
12. Galambos, T.V.(editor) (1998). "Guide to Stability Design Criteria for Metal Structures", John Wiley & Sons, New York.
13. Henrych, J. (1981). "The Dynamics of Arches and Frames", New York, Elsevier.
14. Lagarrigue, J.F. (1831). "Geometry of motion: Trisection of angles and arches (Trisection-compass, or, the compass of proportions, improved: in other words, construction of a mathematical instrument, whereby any angle and arch may be divided into three equal parts.)", New York.
15. Leliavsky, S. (1982). "Arches and Short Span Bridges", New York, Chapman and Hall.
16. Leontovich, V. (1959). "Frames and Arches: Condensed Solutions for Structural

Analysis", New York, McGraw-Hill.
17. Melan, J. (1915). "Plain and Reinforced Concrete Arches", New York, John Wiley&Sons.
18. Melbourne, C.(editor) (1995). "Arch Bridges", Thomas Telford, London.
19. Molly, S.J., R.H. Plaut, and J.-Y. Kim (1999). "Behavior of Pair of Leaning Arch-Shells Under Snow and Wind Loads", ASCE J. Eng. Mech., Vol. 125, No. 6, pp.663-667.
20. Nicholson, P. (1851). "Practical masonry, bricklaying, and plastering, both plain and ornamental; containing a new and complete system of lines for stone-cutting; for the use of workmen; with an ample detail of the theory and practice of constructing arches, domes, groins, niches, stairs, columns, &c. Bond, foundations, walls, bridges, tunnels, light-houses, &c. Ovens, furnaces, &c. The formation of mortars and cements; including, also, practical treatises on slating, plumbing, glazing, and a full description of the various materials employed in all these arts, /illustrated by numerous engravings, by artists of first-rate talent.", T. Kelly, London.
21. Nikolai A. Alfutov (Translated by E. Evseev & V.B. Balmont), (2000). "Stability of Elastic Structures", Springer-Verlag, New York.
22. Oden, J.T. (1991). "Finite Elements: An Introduction"
23. Papangelis, J.P. and N.S. Trahair (1987). "Flexural-Torsional Buckling Tests on Arches", ASCE J. Struct. Eng., Vol. 113, No. 7, pp.1433-1443.
24. Pi, Y.-L. and N.S. Trahair (1998). "Out-of-Plane Inelastic Buckling and Strength of Steel Arches", ASCE J. Struct. Eng., Vol. 124, No. 2, pp.174-183.
25. Pi, Y.-L. and N.S. Trahair (2000). "Inelastic Lateral Buckling Strength and Design of Steel Arches", Engineering Structures, 22, pp.993-1005.
26. Pi, Y.-L. and N.S. Trahair (1999). "In-Plane Buckling and Design of Steel Arches", ASCE J. Struct. Eng., Vol. 125, No.11, pp.1291-1298.
27. Plaut, R.H. and A. Hou (1998). "Deflection, Vibration, and Stability of A Pair of Leaning Arches", ASCE J. Struct. Eng., Vol. 124, No. 7, pp.748-753.
28. Timoshenko, S. (1934). "Theory of Elasticity", New York, McGraw-Hill.
29. Timoshenko, S. (1961). "Theory of Elastic Stability", McGraw-Hill, New York.
30. Sakimoto, T. and S. Komatsu (1983). "Ultimate Strength Formula for Steel Arches", ASCE J. Struct. Eng., Vol. 109, No. 3, pp.613-627.
31. Spofford, C.M. (1937). "The Theory of Continuous Structures and Arches", McGraw-Hill, New York.
32. Strang, G. and G.J. Fix (1973) "An Analysis of the Finite Element Method", Prentice-Hall, New Jersey.

33. Swain, G.F. (1896). "Notes on the theory of structures: comprising the stresses in beams, girders, and trusses, bridge designing graphical static, earth pressure and retaining walls, masonry dams, stone and iron arches, cantilevers, etc.".
34. Swan, A. (1794). "The British architect: The builder's treasury of staircases. (Containing, I. An easier, more intelligible, and expeditious method of drawing the five orders, than has hitherto been published ... II. Likewise stair cases ... III. Designs of arches, doors and windows. IV. A great variety of new and curious chimney-pieces ... V. Corbels, shields, and other beautiful decorations. VI. Several useful and necessary rules of carpentry. ... The whole being illustrated with upwards of one hundred designs and examples, curiously engraved on sixty folio copperplates.)", J. W. Folsom for J. Norman, Boston.
35. Washizu, K. (1968). "Variational Methods in Elasticity and Plasticity", Pergamon, London.
36. Wilson, E.L. (1976). "Numerical Methods in Finite Element Analysis", Prentice-Hall, New Jersey.
37. Zienkiewicz, O.C. (1971). "The Finite Element Method in Structural and Continuum Mechanics", McGraw-Hill, London.

Appendix

A. Verification of SAP

Because of the digital nature of the outcome of computer program, the verification of commercial program (SAP) is achieved by comparing them with existing analytical solutions. The goal of structural analysis is the evaluation of internal actions (axial, shear, bending, and torsion) and deformations (vertical, horizontal, and rotational). Once designers obtain this information, they can determine the dimensions of members using specified material and check for stability. If one inputs several candidate cross sections, the program can also select the cross section that satisfies the demand.

The verification of SAP2000 must cover two aspects: force and deformation. Several types of structures will be selected as examples in the following sections.

A. 1 Plane Simple-Supported Beam

From the knowledge of mechanics of materials, we know the end actions and the internal forces of a plane simple-supported beam. Also, the deformation can be evaluated from the analytical formulation.

Suppose a plane simple-supported beam supporting a concentrated point load in the middle of the span illustrated below,

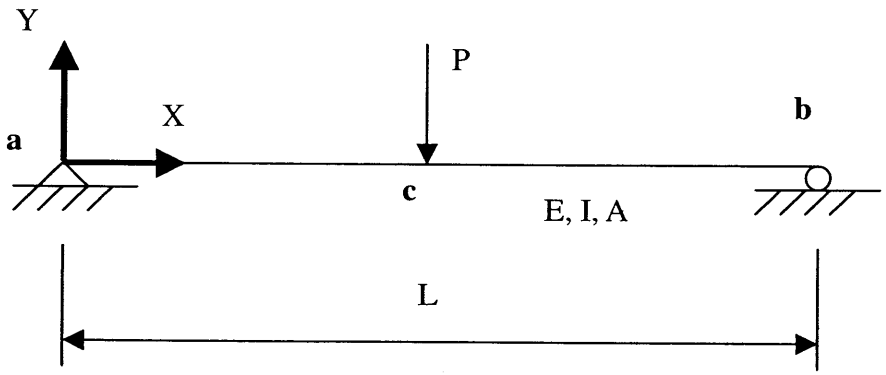

Figure A.1 A plane simple-supported beam—Point Load

It is known that the maximum shear force and bending moment are P/2 and PL/4, respectively. Because of the assumption of small deformation and elastic structure, there is no axial force through the whole beam. The maximum settlement (vertical deformation) occurs at point c and its form is:

$$\Delta_c = -\frac{PL^3}{48EI} \tag{A-1}$$

The maximum rotation occurs at point a and b and its form is:

$$\theta_a = -\theta_b = -\frac{PL^2}{16EI} \tag{A-2}$$

By establishing a numerical model of the parameters in SAP2000, we can obtain the maximum internal forces and deformations. The parameters are shown below:

Span (L) = 100 ft
Young's modulus (E) = 4176000 psf
Height of cross-section = 1 ft
Width of cross-section = 1.5 ft
Area (A) = 1.5 ft^2
Moment of inertia (I_z) = 0.2813 ft^3
Concentrated point load = 1000 Kips

The analytical solutions are:

Maximum axial force = 0 Kips
Maximum shear force = 100/2 =50 Kips (point a)
Maximum bending moment = 100*100/4 = 2500 Kips-ft (point c)
Maximum vertical deformation = -(100*100^3)/(48*4176000*0.2813)
= -1.7734 ft (point c)
Maximum rotation angle = -(100*100^2)/(16*4176000*0.2813)
= -0.05320 radius (point a)

The numerical solutions by SAP2000 are:

Maximum axial force = 0 Kips
Maximum shear force = 50 Kips (point a)
Maximum bending moment = 2500 Kips-ft (point c)
Maximum vertical deformation = -1.7749 ft (point c) ... $\varepsilon_\Delta = 0.083\%$
Maximum rotation angle = -0.05321 radius (point a) ... $\varepsilon_\theta = 0.019\%$

Since the error level is much lower than required precision, numerical solutions could be considered as identical as analytical solutions. In fact, the differences are resulted from numerical iteration and digital truncation during computation.

If considering uniform distributed loading only, such as gravity load, the case becomes:

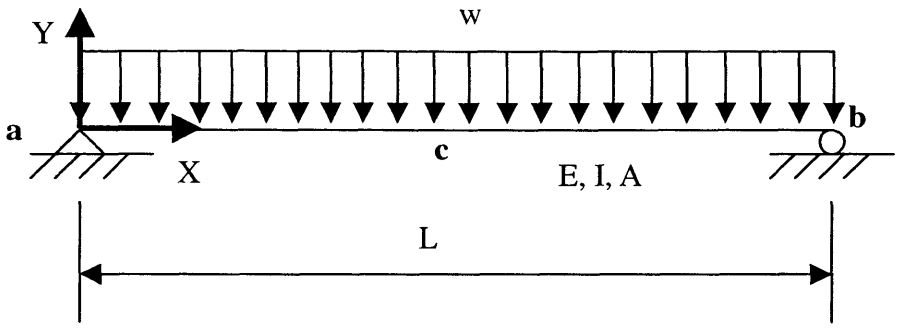

Figure A.2 A plane simple-supported beam—Uniform Load

Suppose the beam is made of steel, the weight per unit volume is 0.4908 Kips/ft^3 (0.284 lb/in^3) as the value of structural steel (ASTM-A36). In terms of the load per unit length, it is 0.4908*1.5*1 = 0.7362 Kips/ft = w. Again, maximum axial force is zero due to the previous assumption. The analytical solutions for deformations and internal forces are:

$$\Delta_c = -\frac{5wL^4}{384EI} \tag{A-3}$$

$$\theta_a = -\theta_b = -\frac{wL^3}{24EI} \tag{A-4}$$

$$V_{max} = V_a = -V_b = \frac{wL}{2} \tag{A-5}$$

$$M_{max} = M_c = \frac{wL^2}{8} \tag{A-6}$$

Substitute the material parameters into the expressions above, and give the results below:

Maximum axial force = 0 Kips

Maximum shear force = 100*0.7362/2 =36.81 Kips (point a)

Maximum bending moment = 0.7362*100^2/8 = 920.25 Kips-ft (point c)

Maximum vertical deformation = -(5*0.7362*100^4)/(384*4176000*0.2813)
= -0.8160 ft (point c)

Maximum rotation angle = -(0.7362*100^3)/(24*4176000*0.2813)
= -0.0261 radius (point a)

The numerical solutions by SAP2000 are:

Maximum axial force = 0 Kips

Maximum shear force = 36.81 Kips (point a)

Maximum bending moment = 920.16 Kips-ft (point c) ... $\varepsilon_M = -0.0098\%$

Maximum vertical deformation = -0.81655 ft (point c)... $\varepsilon_\Delta = 0.067\%$

Maximum rotation angle = -0.02611 radius (point a)... $\varepsilon_\theta = 0.038\%$

Similarly, exclude the computing errors (truncation and iteration), numerical solutions are identical to analytical solutions.

Now change the structure from a simple supported beam to a cantilever beam

A.2 Plane Cantilever Beam

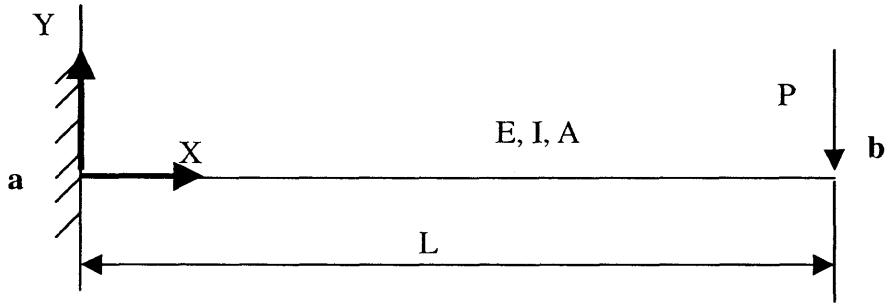

Figure A.3 A plane cantilever beam—Point Load

Suppose a cantilever beam illustrated above, the corresponding internal forces and deformations in terms of analytical formulation are shown below: (Axial force is zero.)

$$V_{max} = V_a = P \tag{A-7}$$

$$M_{max} = M_a = -PL \tag{A-8}$$

$$\Delta_{max} = \Delta_b = -\frac{PL^3}{3EI} \tag{A-9}$$

$$\theta_{max} = \theta_b = -\frac{PL^2}{2EI} \tag{A-10}$$

Material properties are the same as the case of simple supported beam. The analytical solutions are:

Maximum axial force = 0 Kips

Maximum shear force = 100 Kips (point a)

Maximum bending moment = -100*100 = -10000 Kips-ft (point a)

Maximum vertical deformation = $-(100*100^3)/(3*4176000*0.2813)$

= -28.376 ft (point b)

Maximum rotation angle = $-(100*100^2)/(2*4176000*0.2813)$

= -0.4256 radius (point b)

The numerical solutions by SAP2000 are:

Maximum axial force = 0 Kips

Maximum shear force = 100 Kips (point a)

Maximum bending moment = -9999.64 Kips-ft (point a) ... $\varepsilon_M = -0.0036\%$

Maximum vertical deformation = -28.3851 ft (point b) ... $\varepsilon_\Delta = 0.0321\%$

Maximum rotation angle = -0.4257 radius (point b) ... $\varepsilon_\theta = 0.0235\%$

The error level is so low that the difference can be neglected, which means the numerical solutions are identical to analytical solutions.

In the case of uniformly distributed loading,

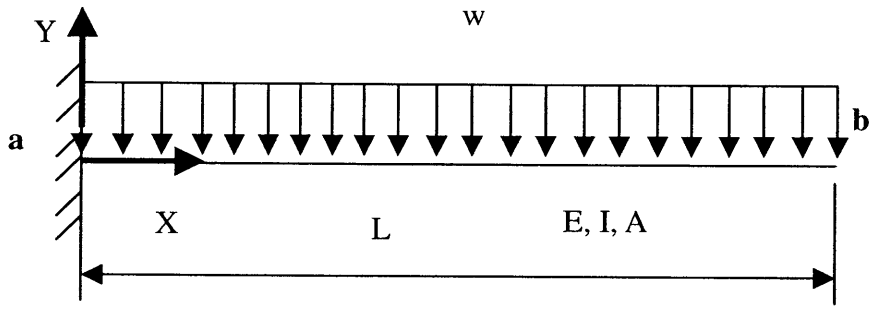

Figure A.4 A plane cantilever beam—Uniform Load

Analytical solutions are:

$$F_{max} = 0 \quad \text{(Axial force = 0)} \tag{A-11}$$

$$V_{max} = V_a = wL \tag{A-12}$$

$$M_{max} = M_a = -\frac{wL^2}{2} \tag{A-13}$$

$$\Delta_{max} = \Delta_b = -\frac{wL^4}{8EI} \tag{A-14}$$

$$\theta_{max} = \theta_b = -\frac{wL^3}{6EI} \tag{A-15}$$

Assume the material properties are the same as previous cases. Substitute the material parameters into the formulation above and obtain the digits below: (w = 0.7362 Kips/ft)

Maximum axial force = 0 Kips

Maximum shear force = 73.62 Kips (point a)

Maximum bending moment = $-0.7362*100^2/2$ = -3681 Kips-ft (point a)

Maximum vertical deformation = $-(0.7362*100^4)/(8*4176000*0.2813)$

= -7.833 ft (point b)

Maximum rotation angle = $-(0.7362*100^3)/(6*4176000*0.2813)$

= -0.1045 radius (point b)

The numerical solutions by SAP2000 are:

Maximum axial force = 0 Kips

Maximum shear force = 73.61 Kips (point a)

Maximum bending moment = -3680.64 Kips-ft (point a)... $\varepsilon_M = -0.0136\%$

Maximum vertical deformation = -7.83632 ft (point b) ... $\varepsilon_\Delta = 0.0424\%$

Maximum rotation angle = -0.10446 radius (point b) ... $\varepsilon_\theta = -0.0383\%$

Consider the error generated from computing process, the numerical solution computed by SAP2000 is correct.

B. Transformation between Different Cross Sections

The definition of moment of inertia (or second moment of area) with respect to different axes in plane Cartesian coordinate system is:

$$I_x = \int_A h_y^2 dA \tag{B-1}$$

$$I_y = \int_A h_x^2 dA \tag{B-2}$$

They can be illustrated on the following figure.

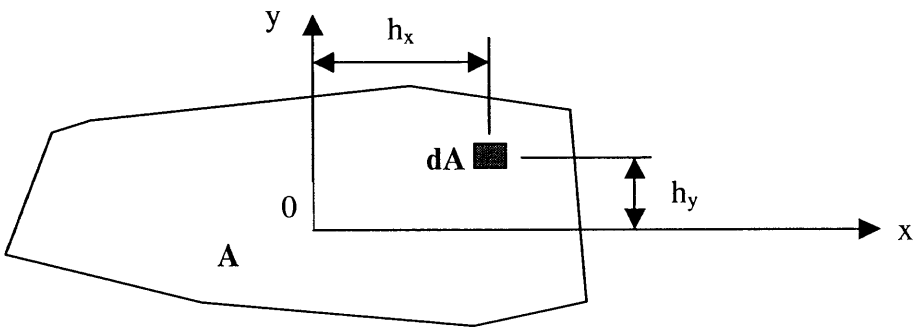

Figure B.1 Definition of moment of inertia

In polar coordinate system, it is called polar moment of inertia and has the form as:

$$J_0 = \int_A h^2 dA \tag{B-3}$$

where r is the distance from original point to dA. Because $h^2 = x^2 + y^2$, therefore,

$$J_0 = \int_A h^2 dA = \int_A (x^2 + y^2) dA = \int_A x^2 dA + \int_A y^2 dA = I_y + I_x \tag{B-4}$$

The radius of gyration with respect to x-axis, r_x, is defined as:

$$I_x = r_x^2 A \tag{B-5}$$

Thus,

$$r_x = \sqrt{\frac{I_x}{A}} \tag{B-6}$$

Similarly,

$$I_y = r_y^2 A \qquad r_y = \sqrt{\frac{I_y}{A}} \tag{B-7}$$

$$J_0 = r_0^2 A \qquad r_0 = \sqrt{\frac{I_0}{A}} \tag{B-8}$$

Moreover,

$$r_o^2 = r_x^2 + r_y^2 \tag{B-9}$$

Recall the theorem of parallel-axis, which expresses the translation of moment of inertia from neutral axis to any axis parallel to it, it says:

$$I_{x'} = I_0 + Ad^2 \tag{B-10}$$

where I_0 is the moment of inertia with respect to neutral axis,

I_x is the moment of inertia with respect to x' axis paralleling to neutral axis,

A is the area,

d is the shortest distance between x' axis and neutral axis.

By applying this theorem, the moment of inertia of any cross section with complex shape can be separated into several simple, regular shapes to calculate the individual moment of inertia with respect to their local neutral axes. After that, sum up these numbers and compute r_x, the location of neutral axis. Then the distance from neutral axis to local neutral axis and add the term Ad^2 to obtain the moment of inertia with respect to the neutral axis of the whole cross section.

The moment of inertia of a rectangular cross section is calculated as follows:

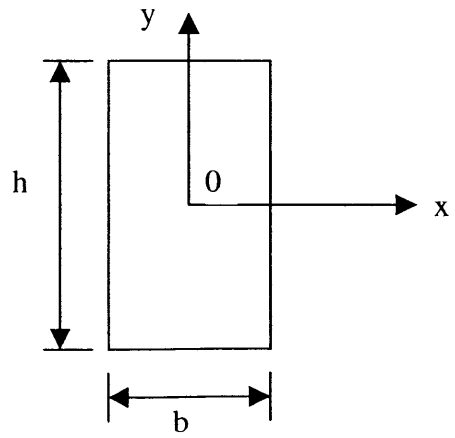

Figure B.2 Rectangular cross section

$$I_x = \int_A y^2 dA = \int_{-\frac{h}{2}}^{\frac{h}{2}} y^2 (b dy) = \frac{bh^3}{12} \tag{B-11}$$

The moment of inertia of a circle is calculated as follows:

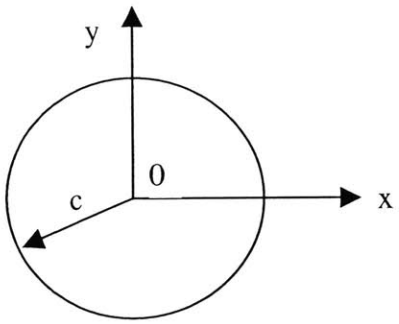

Figure B.3 Circular cross section

$$J_0 = I_x + I_y = 2I_x = \int_A h^2 dA = \int_0^c h^2 (2\pi h dh) = \frac{\pi c^4}{2} \tag{B-12}$$

Then,

$$I_x = \frac{J_0}{2} = \frac{\pi c^4}{4} \tag{B-13}$$

Suppose a cross section A illustrated below;

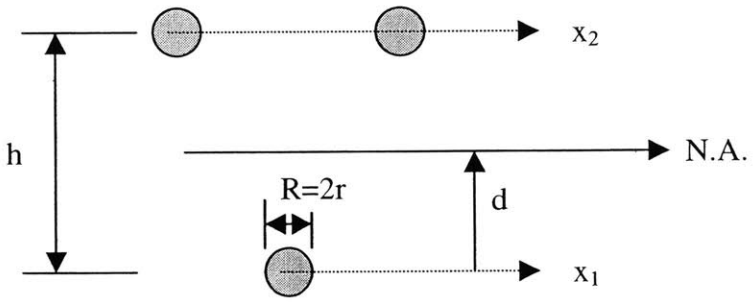

Figure B.4 Design cross section -- Section A

First of all, calculate the position of neutral axis:

$$2\left[\frac{\pi r^4}{4} + \pi r^2 h^2\right] + \frac{\pi r^4}{4} = 3\left[\frac{\pi r^4}{4}\right] + 3\pi r^2 d^2$$

$$\Rightarrow 2h^2 = 3d^2$$

$$\Rightarrow d = \frac{\sqrt{2}}{3} h \tag{B-14}$$

The moment of inertia of this cross section with respect to its neutral axis is:

$$I_0 = \frac{\pi r^4}{4} \times 3 + 2\pi r^2 \times \left(\frac{3-\sqrt{2}}{3}\right)^2 \times h^2 + \pi r^2 \times \left(\frac{\sqrt{2}}{3}\right)^2 d^2$$

$$\Rightarrow \pi r^4 \left[\frac{3}{4} + \left(\frac{h}{r}\right)^2 \times \frac{4}{3}\left(2-\sqrt{2}\right)\right] \qquad \text{(B-15)}$$

Suppose a cross section B illustrated below;

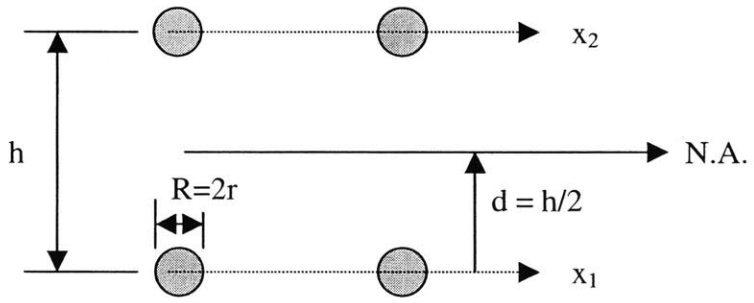

Figure B.5 Design cross section --Section B

Because of symmetry, the neutral axis of this cross section is located on the half of the depth. The moment of inertia of this cross section with respect to its neutral axis is:

$$I_0 = \frac{\pi r^4}{4} \times 4 + 4\pi r^2 \times \left(\frac{h}{2}\right)^2$$

$$\Rightarrow \pi r^4 \left[1 + \left(\frac{h}{r}\right)^2\right] \qquad \text{(B-16)}$$

Suppose a cross section C illustrated below;

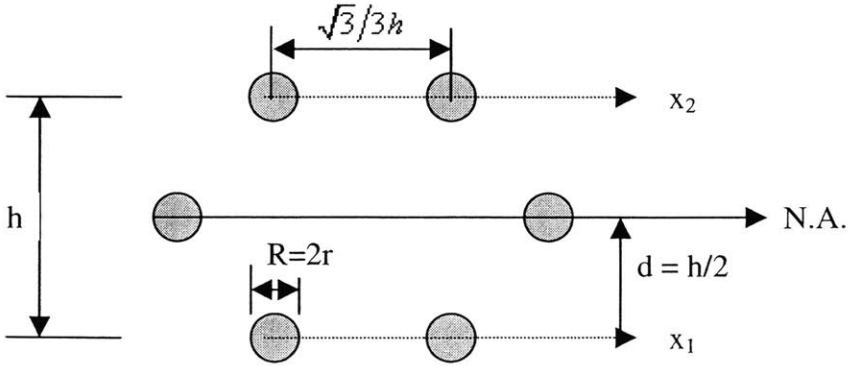

Figure B.6 Design cross section -- Section C

Since the orientation shown above is symmetrical, the neutral axis is also located on the half of the depth. The moment of inertia with respect to its neutral axis is:

$$I_0 = \frac{\pi r^4}{4} \times 6 + 4\pi r^2 \times \left(\frac{h}{2}\right)^2$$

$$\Rightarrow \pi r^4 \left[\frac{3}{2} + \left(\frac{h}{r}\right)^2\right] \tag{B-17}$$

We can express the required depth in terms of the given moment of inertia and radius of the member. For section A, the required depth is:

$$h_{req} = r\sqrt{\frac{3}{4(2-\sqrt{2})}\left[\frac{I_0}{\pi r^4} - \frac{3}{4}\right]} \tag{B-18}$$

For section B,

$$h_{req} = r\sqrt{\left[\frac{I_0}{\pi r^4} - 1\right]} \tag{B-19}$$

For section C,

$$h_{req} = r\sqrt{\left[\frac{I_0}{\pi r^4} - \frac{3}{2}\right]} \tag{B-20}$$

The design of such cross section can be accomplished by obtaining the design moment of inertia (I_0) from the analysis of the whole structure and assuming the size of the member (r). If there is any constraint from any other criterion about the required depth, one can easily determine the required radius of the member. However, since the cross section of the member we used here is not so popular in practical design (the solid section), the relationship between a solid section and a tube section is established in the following paragraph.

Suppose a tube section consisted of same area and same moment of inertia as a circular cross section (Figure 3),

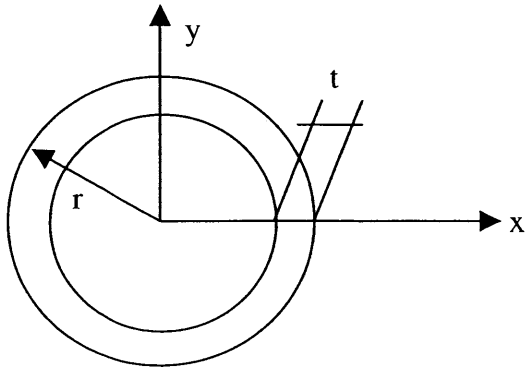

Figure B.7 Tube Cross Section

r is the outer radius of the tube, t is the thickness of the tube.

The area of the tube should be equal to the area of the circle. Meanwhile, the moment of inertia of the tube should be equal to the moment of inertia of the circle. These two conditions give us two constraints on establishing the relationship between a tube and a circle.

From the constraint of same area, we have

Area of a circle (Figure 3): $A = \pi c^2$ (B-21)

Area of a tube (Figure 7): $A = \pi\left[r^2 - (r-t)^2\right] = \pi t(2r-t)$ (B-22)

That gives:

$$c^2 = t(2r-t) \tag{B-23}$$

Another condition gives:

Moment of area of a circle (Eq.(13)):

$$I_x = I_0 = \frac{\pi c^4}{4} \tag{B-24}$$

Moment of area of a tube:

$$I_0 = \frac{\pi r^4}{4} - \frac{\pi (r-t)^4}{4}$$

$$\Rightarrow I_0 = \frac{\pi}{4}\left(4r^3t - 6r^2t^2 + 4rt^3 - t^4\right) \tag{B-25}$$

That gives:

$$\frac{\pi c^4}{4} = \frac{\pi}{4}\left(4r^3t - 6r^2t^2 + 4rt^3 - t^4\right)$$

$$\Rightarrow c^4 = 4r^3t - 6r^2t^2 + 4rt^3 - t^4$$

$$\Rightarrow (4t)r^3 - (6t^2)r^2 + (4t^3)r - (t^4 - c^4) = 0 \tag{B-26}$$

We can solve this cubical equation by either assuming thickness (t) is known or assuming radius (r) is given. It is assuming a given t here.

Rewrite equation (26) in the following form:

$$(4t)r^3-(6t^2)r^2+(4t^3)r-(t^4-c^4)=0$$

$$\Rightarrow r^3-\left(\frac{3}{2}t\right)r^2+t^2r-\left(\frac{t^4-c^4}{4t}\right)=0$$

$$\Rightarrow C_1r^3+C_2r^2+C_3r+C_4=0 \qquad \text{(B-27)}$$

where $C_1 = 1$, $C_2 = (-3t/2)$, $C_3 = t^2$, $C_4 = -(t^4-c^4)/(4t)$.

Eliminating the cubical equation by setting:

$$r=k-\frac{b}{3a}=k-\frac{-\frac{3t}{2}}{3}=k+\frac{t}{2} \qquad \text{(B-28)}$$

Substitute it into Eq.(27), it becomes:

$$\left(k+\frac{t}{2}\right)^3-\left(\frac{3}{2}t\right)\left(k+\frac{t}{2}\right)^2+t^2\left(k+\frac{t}{2}\right)-\left(\frac{t^4-c^4}{4t}\right)=0$$

$$\Rightarrow k^3+\left(\frac{t^2}{4}\right)k+\left(\frac{c^4}{4t}\right)=0$$

$$\Rightarrow k^3+\left(3\times\frac{t^2}{12}\right)k+\left(2\times\frac{c^4}{8t}\right)=0 \qquad \text{(B-29)}$$

Set $x=\pm\sqrt{|t^2/12|}=\pm\sqrt{t^2/12}=\left(\pm\sqrt{3}/6\right)t$, furthermore,

$$3\varphi=\cos^{-1}\left[\left(c^4/8t\right)/\left(\pm\sqrt{3}/(6t)\right)^3\right]=\cos^{-1}\left[3\sqrt{3}(c/t)^4\right]$$

Thus,

$$\varphi=\frac{1}{3}\cos^{-1}\left[3\sqrt{3}\left(\frac{c}{t}\right)^4\right] \qquad \text{(B-30)}$$

Therefore, the possible three roots of k are:

$$k_1=2x\cos(\varphi)=\frac{\pm\sqrt{3}t}{3}\cos\left[\frac{1}{3}\cos^{-1}\left(3\sqrt{3}\frac{c^4}{t^4}\right)\right]$$

$$k_2=2x\cos\left(\frac{3\pi}{2}+\varphi\right)=\frac{\pm\sqrt{3}t}{3}\cos\left[\frac{3\pi}{2}+\frac{1}{3}\cos^{-1}\left(3\sqrt{3}\frac{c^4}{t^4}\right)\right]$$

$$k_3=2x\cos\left(\frac{4\pi}{3}+\varphi\right)=\frac{\pm\sqrt{3}t}{3}\cos\left[\frac{4\pi}{3}+\frac{1}{3}\cos^{-1}\left(3\sqrt{3}\frac{c^4}{t^4}\right)\right] \qquad \text{(B-31)}$$

Because r = k + t/2, the three roots of r are shown below:

$$r_1 = k_1 + \frac{t}{2} = \frac{\pm\sqrt{3}t}{3}\cos\left[\frac{1}{3}\cos^{-1}\left(3\sqrt{3}\frac{c^4}{t^4}\right)\right] + \frac{t}{2}$$

$$r_2 = k_2 + \frac{t}{2} = \frac{\pm\sqrt{3}t}{3}\cos\left[\frac{3\pi}{2} + \frac{1}{3}\cos^{-1}\left(3\sqrt{3}\frac{c^4}{t^4}\right)\right] + \frac{t}{2}$$

$$r_3 = k_3 + \frac{t}{2} = \frac{\pm\sqrt{3}t}{3}\cos\left[\frac{4\pi}{3} + \frac{1}{3}\cos^{-1}\left(3\sqrt{3}\frac{c^4}{t^4}\right)\right] + \frac{t}{2} \qquad \text{(B-32)}$$